

of the logic tree for our local fault models is shown on Figure SBK-7; remaining steps follow from the data in Table SBK-3.

Finally, we consider the likelihood that ruptures on all the faults or combinations of faults have been simultaneous. Given the uncertainties in the dating available from the paleoseismic studies (an inherent aspect of working with infrequent surface faulting events in an arid environment), it is possible to use the rupture scenarios of S. K. Pezzopane *et al.* (USGS, written communication, 1996a) as one extreme, and independence of every paleoseismic event as the other extreme. The intimate stratigraphic association of Scenario Event U with ash, apparently derived from an eruption of the Lathrop Wells Cone, perhaps about 70 ka, suggests one possible simultaneous rupture that is tied to volcanic eruptions in the Crater Flat area. We find it unlikely that even this "ash event" represents a true simultaneous rupture: some exposures show reworked ash, whereas others seem to have direct airfall, which suggests that not all ash-filled fractures opened simultaneously; even if events are closely spaced in time sufficiently to appear simultaneous from a stratigraphic point of view, it is highly unlikely that the events were simultaneous from a seismic point of view, given numerous examples such as the Mammoth Lakes earthquakes of 1980 or the Dixie Valley and Fairview Peak earthquakes of 1954. It nonetheless is a possibility for the maximum-magnitude earthquake that has been (and could be) experienced within the site area. We apply low weighting to this possibility and tie recurrence of such an event principally to the recurrence of Crater Flat volcanism as described in the Probabilistic Volcanic Hazard Analysis (Geomatrix Consultants, written communication, 1996). We also apply an unusual recurrence curve to this event, as explained further below. Given these unique circumstances, we treat this kind of simultaneous event in the logic tree as an additional source. Thus, we add a maximum magnitude event to the data on maximum magnitude otherwise developed for the faults (independent, linked, or coalesced).

We believe that a simultaneous rupture is more likely to occur on faults that are coalesced than on faults that are linked or independent. Accordingly, our weighting of such an event differs depending on the branch of the logic tree. For the branch in which all faults sole into a detachment, we assign a weight of 0.5 to a combination of simultaneous ruptures tied principally to volcanic events in the Crater Flat area and non-simultaneous events on the faults, and a weight of 0.5 to having all events be non-simultaneous. For the model in which

all faults coalesce at depth, we apply the same weights to simultaneous and non-simultaneous events. However, for the models of linked or independent faults, we apply a weight of 0.1 to the combination of simultaneous and non-simultaneous events, with a weight of 0.9 to having all events be non-simultaneous.

2.4.2 Maximum Magnitudes

Our approach to calculating maximum magnitude for the local faults is similar to that taken for the regional faults. However, we add another branch by using stress drops to constrain average displacement, and the fault areas are more sensitive to the details of the down-dip width as estimated from fault intersection analysis and combinations of coalesced and linked faults.

We evaluated fault length based on mapped surface traces. Some teams discussed the possibility that the local faults continue south of their mapped surface traces into the subsurface beneath the Amargosa Valley (SSC Workshop 5), but we conclude that data do not support this interpretation. The Highway 95 fault provides a termination to the YM faults as well as the Bare Mountain fault. Given the lack of evidence and a model for fault termination, we see no reason to speculate that the faults extend any farther south than they are mapped at the surface. The northern extent of some faults is less certain. Faults have been mapped north of the main Yucca Mountain block into bedrock, but without Quaternary displacement. We use the maximum mapped fault length, from Simonds *et al.* (1995), and consider that these pre-Quaternary fault extensions have a lower likelihood of contributing to the maximum magnitude earthquake than do the Quaternary sections of the faults (Figure SBK-6).

Treatment of fault length for coalesced and linked faults is an important consideration. For the models in which faults sole into a detachment and for coalesced faults, we interpret the fault length as that of the longest fault involved in coalescence: the combined South Crater Flat + Windy Wash + Fatigue Wash fault for the shorter length of 27 km (wt. 0.6), and the combined Paintbrush Canyon + Stagecoach Road fault for the longer length of 35 km (wt. 0.4).

Fault coalescence in the subsurface, the maximum depth of penetration of faults into the crust, and fault area were evaluated using a combination of structure contour maps and trigonometric calculations. Structure contour maps were constructed as overlays to the Quaternary fault map of A. R. Ramelli and J. W. Bell (Nevada Bureau of Mines and Geology, written communication, 1996). The structure contour overlay maps were drawn for the local fault sources (YM faults and Bare Mountain fault), as well as for the Ghost Dance fault. Fault strike was constrained by the surface trace on the map of A. R. Ramelli and J. W. Bell (Nevada Bureau of Mines and Geology, written communication, 1996), and the angle of fault dip was constrained primarily by outcrop measurements annotated on the map of Simonds *et al.* (1995). We investigated a range of fault dips, considering the common observation that the dip angle of normal faults often is steeper at the surface than at depth. Average fault dip angles between 45 and 75 degrees were considered, with subsurface dip angles between 45 and 70 degrees considered most likely. The Bare Mountain fault was assumed to be the master structure, with other faults either intersecting one another above the Bare Mountain fault, or being truncated against the Bare Mountain fault surface at depth. We do not consider it credible that one of the YM faults truncates the Bare Mountain fault at depth. The depth and orientations of fault intersections were found either by connecting points of equal depth on structure contour maps of two fault surfaces, or by direct trigonometric calculation of the depth of intersection. The trigonometric calculation was done using the dip angle of the two faults of interest and the horizontal distance between the fault surface traces as measured normal to strike. The calculated intersection depths in combination with fault lengths were used to constrain the down-dip widths of faults to estimate area for computing the maximum earthquake magnitude. The maximum seismogenic width was limited by the intersection of a fault either with the Bare Mountain fault surface or with the base of the seismogenic crust, whichever was shallower.

The following is a summary of the weighting for down-dip width for the local faults based on a Bare Mountain/YM fault dip scenario. Using minimum dip combinations for Bare Mountain and YM faults of 45 degrees/50 degrees preferred, 60 degrees/60 degrees, and a steep limit (70 degrees/70 degrees) for both, the down-dip width in km is listed for each independent YM fault. The first dip in the (aa/bb) pair is that on the Bare Mountain fault (aa); the second is the dip on the YM fault (bb). To capture all uncertainty, the base of the

seismogenic crust is interpreted to be at 17 km. The only scenario controlled by a 17-km seismogenic thickness is the case of 70 degrees/70 degrees.

	BM/YM DIPS (°)	BM/YM DIPS (°)	BM/YM DIPS (°)
	45 /50	60 /60	70 /70
Weight	0.2	0.7	0.1
DOWN-DIP WIDTH OF FAULTS IN KM			
Paintbrush Canyon	14	17	18
Bow Ridge	14	17	18
Stagecoach Road	10	15	18
Solitario Canyon	10	14	18
Windy Wash	8	11	17
Fatigue Wash	8	11	17
N Crater Flat	6	9	13
S Crater Flat	5	6	7

These estimates of down-dip fault width are multiplied by fault lengths to compute areas of individual faults. For the coalescing faults model, we compute fault area for a simultaneous rupture by summing all the contributing fault areas; we compute fault area for non-simultaneous ruptures by considering the maximum fault area for an individual contributor to the coalescing faults (i.e., the Stagecoach Road + Paintbrush Canyon combination). A similar approach is used with the model in which faults sole into a detachment.

These estimates of down-dip width also are used to compute average slip from static stress-drop weighting to establish another estimate of maximum magnitude. Stress-drop weighting was established by taking into account the distribution of static stress drops for the normal faulting regimes (Becker and Abrahamson, 1997; GMC Workshop 3), and the stress-drop estimates for the Little Skull Mountain earthquake (Becker and Abrahamson, 1997).

Weight	0.2	0.5	0.25	0.05
σ (bars)	30	35	50	100

Stress drop is calculated from (Kanamori and Anderson, 1975)

$$\sigma = 8/(3 * \pi) * \mu * [u/ W]$$

where, $\mu = 3 \times 10^{11}$ dyne-cm (rigidity), u = average fault slip (cm), W = down-dip fault width (cm).

For the local faults, then, we use five methods to compute maximum magnitude. These are: fault length, fault area, maximum displacement from surface studies, average displacement from surface studies, and average displacement from stress-drop analysis. These are weighted for individual faults and combinations (Table SBK-3) based on availability and quality of data.

2.4.3 Recurrence

Calculation of earthquake recurrence parameters for the local faults followed the guidelines discussed for the regional fault sources. Considerably more data are available to constrain fault slip rate for the local faults than for most of the regional fault sources. In addition, we have repeat-time information available from paleoseismic trench studies for all of the local fault sources. These repeat times are defined in the field for events having different displacements, however, so they probably do not all represent the repeat time of the maximum earthquake for that source. Accordingly, we weight paleoseismic repeat-time data much lower (generally weighted 0.2 to 0.3) than slip-rate information.

Again, special consideration must be given to assessing repeat times for coalesced faults and the model of faults that sole into a detachment. In both cases, we summed slip rates computed at the surface on east-west transects across the faults (e.g., slip rate for coalesced faults = slip rate on Paintbrush Canyon + slip rate on Solitario Canyon + slip rate on Windy Wash + slip rate on North Crater Flat). We use these slip rate calculations exclusively to define recurrence for non-simultaneous ruptures for these fault models. Our model of simultaneous ruptures ties these events closely to the recurrence of volcanic eruptions in the Crater Flat tectonic domain. Thus, we weight the recurrence of simultaneous events heavily by recurrence of volcanic eruptions (0.75 weight) and less by fault slip rate (0.25 weight), regardless of fault model (same weighting for soling faults, coalesced faults, linked faults, and individual faults when they rupture simultaneously).

We weight the choice between characteristic and truncated exponential recurrence models differently for the local faults, depending on whether we consider individual faults or combinations. The Bare Mountain fault is a range-bounding fault, so we weight the characteristic model more strongly (0.6 weight). The YM faults are not, so we weight the truncated exponential model more strongly (0.7 weight). The behavior of the fault combinations is less well resolved, so we weight the two models equally.

Finally, we consider the case of simultaneous ruptures, as represented by the “ash event,” the recurrence of which we tie strongly to volcanic eruptions in the Crater Flat area. We consider these to be unusual events, whose frequency is not as much related to conventional fault models as it is tied to volcanic eruptions. Therefore, we treat these events as single contributors to moment release within the study area, reasoning that all other earthquakes are captured either by the distributions otherwise assigned to the faults or by the maximum earthquake and distribution of seismicity for the Local Zone. They are added events, which contribute only their own moment, not a full range of moment distribution as occurs with a characteristic or truncated exponential model. Thus we assign a maximum moment distribution to this kind of event, with the recurrence constrained by a combination of fault slip rate and volcanic-event rate (Table SBK-3), and the only magnitudes given by the range of the maximum magnitude distribution (i.e., all $M < M_{\max}$ give no contribution to moment for this source).

As described in Section 2.3.2 for regional faults, we assume that the characteristic and maximum moment events are uniformly distributed in the magnitude range $M_{\max} \pm 1/4$, such that the upper limit of the recurrence relationship is $M_{\max} + 1/4$. For the exponential recurrence model the upper limit is also set at $M_{\max} + 1/4$. When the overall rate of earthquake occurrence is specified by the recurrence interval of surface-rupturing earthquakes, this recurrence rate was assumed to apply to earthquakes of magnitude greater than or equal to $M_{\max} - 1/4$.

FAULT DISPLACEMENT CHARACTERIZATION

3.1 INTRODUCTION

Our characterization of fault displacement is designed to permit estimates of fault displacement potential on two general classes of faults in the Yucca Mountain Controlled Area: (1) those for which we have specific data concerning the Quaternary rupture history; and (2) those faults and fractures for which data indicate no Quaternary rupture, or for which no data on Quaternary displacement are available. The first class of faults includes the major block-bounding faults, particularly the Solitario Canyon and Bow Ridge faults, that are considered potential earthquake sources (demonstration points 1 and 2); we also include structures such as the fractures in Midway Valley that have no measurable displacement in Quaternary alluvium (demonstration point 9). The second class of faults includes intrablock faults (such as the Drill Hole Wash, Ghost Dance, Sundance, and Dune Wash faults, demonstration points 3-6) as well as small faults, shears, and fractures (demonstration points 7-8). Potential fault displacement in intact rock can be assessed using the characterizations applied to this second group.

For either class of faults, we address two questions: (1) How often might displacement events occur? and (2) How large might these events be? Responding to the first question involves assessing event frequency. Our assessment involves two approaches. In the first, frequency is estimated from analysis of fault slip rate. The second uses direct (fault- or site-specific) information on frequency of displacement or cracking events. Response to the second question involves assessing the range of displacements that might characterize the events defined during the first part of the analysis. This may include fault- or site-specific data regarding prehistoric displacement events, information on variability of displacement along a fault (which may be general or fault-specific), scaling relationships for fault displacements, and data on secondary fault ruptures.

The procedures and methods for characterizing fault displacement presumably will change with improvements in our understanding of the mechanical and statistical characteristics of

fault displacement on both individual faults and fault systems. Our approach is to use several alternative procedures for estimating the frequency and magnitude of fault displacement, which we consider in combination make the best use of available data and capture the uncertainty in characterization of fault displacement at this time. We discuss our general approaches for the two classes of faults, then apply the approaches to the demonstration points.

3.2 FAULTS HAVING DOCUMENTED QUATERNARY DISPLACEMENT

Our characterization of fault displacement potential for faults within the Controlled Area for which data on Quaternary displacement are available incorporates two approaches: one based on the frequency of earthquake occurrence, the earthquake approach; and the other based on assessments of the frequency and size of events from trenching data, the displacement approach (Figure SBK-8). The relative weights assigned to these two approaches depend on the data available for the site of interest.

3.2.1 Earthquake Approach

The earthquake approach to the assessment of fault displacement hazard considers two sources of earthquake induced displacements: principal faulting from earthquakes occurring on the feature of interest, and distributed faulting induced by earthquakes centered on other sources.

3.2.1.1 Characterization of Principal Faulting Potential. The steps involved in characterizing potential displacement due to principal faulting on a fault are shown on Figure SBK-8.

Frequency of Principal Faulting Events. Section 2.0 presents our characterization of the frequency of occurrence of earthquakes as a function of magnitude, $\lambda(m)$, on each seismic source. The frequency of displacement events, λ_{DE} at a point of interest is given by

$$\lambda_{DE} = \lambda(m) \cdot P_R(m) \cdot P(\text{intersection}) \quad (1)$$

where $P_R(m)$ is the probability that an earthquake of magnitude m will rupture the surface and $P(\text{intersection})$ is the probability that the along-strike location of the rupture will pass through

the site of interest. The probability of surface rupture is assessed using the logistic probability model presented by R.R Youngs (Appendix H, Section H.4.1) in SSC Workshop 5 based on data presented in S. K. Pezzopane and T. E. Dawson (USGS, written communication, 1996). We chose to use the assessment based on recent western Basin and Range earthquake ruptures (Figure SBK-9). The assessment of the probability that the along strike location of the rupture will pass through the site is obtained by randomizing the location of the rupture along the fault in the same manner as is done for ground motion hazard assessment.

Distribution of Principal Faulting Displacement at a Point. The probability distribution for the amount of displacement at a point is defined based on the concept presented by the ASM team in SSC Workshop 5. The first step is an estimate of the maximum displacement, MD , in the earthquake. We use the empirical relationship between MD and moment magnitude developed by Wells and Coppersmith (1994) to define a lognormal distribution for MD in each earthquake.

Given a maximum displacement, we assess the distribution for displacement at a point using normalized distributions for D/MD as a function of location along the rupture. We use two approaches, one based on the ASM evaluation of historical rupture patterns presented in Wheeler (1989) (Figure SBK-10; Appendix H, Section H.3.1) and one based on our fractal model of fault surface roughness presented in SSC Workshop 5 (Figure SBK-11; Appendix H, Section H.3.2). We give equal weight to the historical rupture and fractal interpolation approaches.

The fractal model is based on the assumption that variability in displacement along the length of a fault rupture scales with the roughness of the rupture surface. This variability is modeled using a two-dimensional fractal interpolation function in which an arbitrary displacement is located at random within the length of a synthetic rupture (length = -1 to +1). Displacement at 99 additional points are then interpolated between the initial displacement point and the end points of the rupture using fractal interpolation (Barnsley, 1988). The variability in displacement between points is controlled by the fractal dimension (Df) of the interpolation function, which is set at $Df = 1.3$, a value determined by Lee and Bruhn (1996) for natural fault surfaces with Quaternary and older rupturing history. One hundred ruptures were

simulated using the fractal interpolation algorithm of Barnsley (1988). The displacements at 100 points along the length of the simulated ruptures were then normalized to the maximum displacement in each simulated rupture, and then collected as an ensemble from which the average and variability in displacement at each point was calculated to produce the results presented in Figure SBK-11. More details of the simulation procedure are included in documentation presented by the SBK team at Workshop 5.

3.2.1.2 Characterization of Distributed Faulting Potential. The steps involved in characterizing the potential for distributed faulting from earthquakes on other sources are the same regardless of whether the fault has documented Quaternary displacement or not. These methods are discussed below in Section 3.3.1.

3.2.2 Displacement Approach

The displacement approach to the characterizing fault displacement potential combines the effects of principal and distributed faulting into a single assessment. The steps involved in this approach are shown on Figure SBK-8.

3.2.2.1 Frequency of Displacement Events. The frequency of displacement events is computed using two approaches: one involving estimates of fault slip rate and average displacement per event; and the other involving event frequency estimated from trenching data. In general, the slip-rate approach is weighted higher than the event-frequency approach for the demonstration points consistent with our weighting of these types of data in the assessment of local fault seismic sources (Table SBK-3). However, weights will differ for other faults depending on the type and quality of information available concerning their Quaternary rupture history.

Slip Rate Evaluation. Slip rate is either determined directly at the point of interest or interpolated along the strike of the fault between trenches or other survey localities, where fault offsets and the age of offset horizons are known from measurements and dating. We consider these two conditions in structuring our logic tree for fault displacement hazard (Figure SBK-8).

Detailed mapping of Quaternary geomorphic surfaces and faults, along with the large number of paleoseismic trenches excavated across Yucca Mountain faults, has yielded considerable information about slip rate, and its variability, along major faults such as the Solitario Canyon and Paintbrush Canyon faults. Thus, slip rate can be estimated directly at numerous locations. The slip rate at a point of interest can be estimated by measuring the cumulative offset of a Quaternary horizon of known age, which may be measured in a trench or on a geomorphic surface in the landscape. Slip rate (*SR*) is estimated from the equation:

$$SR = \text{Offset} / (\text{Horizon Age}) \quad (2)$$

Minimum, preferred, and maximum slip rates are calculated using the estimated range of minimum, maximum, and preferred magnitude of offset of a geologic horizon and its age. No along-strike interpolation is necessary in these cases. At demonstration point #1 on the Bow Ridge fault, for instance, slip rate can be estimated directly.

More commonly, the point of interest is located between trenches or other points along a fault where the slip rate has been calculated from site-specific geologic data. One or more methods of slip rate interpolation must be applied. We apply two methods, the first using data on Quaternary displacements along the fault of interest, the second using cumulative displacement along the fault. The slip rate at a point of interest is scaled between two points of known displacement; we use linear interpolation unless sufficient data are available to more accurately characterize the variation in displacement along strike. The first method requires data on Quaternary displacement at two points that bracket (along strike) a point of interest. For example, this approach is used for the Solitario Canyon fault at demonstration point #2, because along-strike changes in the offset of middle to late Quaternary geomorphic surfaces are known from detailed mapping and trenching (Ramelli, SSC Workshop 6). The slip rate at the point of interest is interpolated from those obtained at trench SC-T4 and the north end of Quaternary faulting using Ramelli's curve of along-strike variability in the offset of mid- to late-Quaternary geomorphic surfaces. Such an approach can be used for any point on a fault that is between two locations of known Quaternary displacement (even if one of those is a location of known zero displacement).

Along-strike variation in fault displacement also may be measured using displaced bedrock horizons of known age. Yount (SSC Workshop 6) presented curves estimating the along-strike variability in cumulative bedrock offset along both the Solitario Canyon and Bow Ridge faults, for example. We apply a linear interpolation for this method also, unless a sufficiently large data set is available to more accurately characterize the along-strike variation in fault slip.

Given an assessment of slip rate, SR on a feature, the frequency of displacement events, λ_{DE} , is given by the expression:

$$\lambda_{DE} = SR / \bar{D}_E \quad (3)$$

where \bar{D}_E is the average displacement per event. The approaches used to assess \bar{D}_E are discussed below.

Direct Evaluation of Event Frequency. Our interpretation of the frequency of events from fault trenching data includes both those events for which we have measured shear offset and fracturing events having no measured shear offset, as both kinds of events have broken the surface. The number of events divided by the age of the youngest horizon that predates the oldest faulting or fracturing event is an estimate of the frequency (number of events / annum). Event frequency is expressed as minimum, preferred, and maximum values based on the range of estimated ages of geologic horizons and uncertainty in the number of events interpreted from the trench logs. We use the compilation (Table 5.1) of S. K. Pezzopane *et al.* (USGS, written communication, 1996a) as our principal source in estimating event frequency.

Some faults have near-surface or surface fractures that developed by cracking in Quaternary soils, but across which there is no measurable shear offset to prove Quaternary surface faulting; a good example is the Midway Valley structure at demonstration point #9. These fractures may have undergone only opening or may have been sheared less than can be detected in the paleoseismic studies (we estimate up to 10 cm). Alternatively, opening-mode or mixed shear- and opening-mode cracks may have developed at or near the surface in response to shear displacement on the fault at depth. Bruhn and Schultz (1996) provided theoretical support for this kind of surface-crack development. They investigated the nature

of near-surface fracturing caused by sliding on part of a normal fault patch at depth and found that mixed opening- and shear-mode cracking is expected at or near the Earth's surface. These features could also develop during strong ground shaking, as discussed below. Thus, surface cracking could be indicative of fault displacement at depth, even at shallow crustal depths such as those at the potential repository.

The maximum frequency of occurrence of cracking events is estimated by dividing the number of cracking events by the age of the youngest soil that is affected by the oldest cracks; the minimum is estimated by dividing the number of events by the age of the oldest deposits. The amount of displacement is estimated from the thickness of calcite or silica laminae filling the cracks following each event. Data on these events is summarized by S. K. Pezzopane *et al.* (USGS, written communication, 1996a) and recorded in detailed trench logs. We assess a 50% chance that surface cracking having no measurable shear offset reflects deformation above a slip patch on the fault at depth. This implies that not all surface cracking is directly related to shearing on the fault at depth, even if the cracks are located directly on a fault that extends to the surface.

3.2.2.2 Characterization of Amount of Displacement. Characterizing the amount of fault displacement, given a displacement event, involves estimating maximum or average displacement per event on the fault. These values can be computed from paleoseismic data (preferred, given that we have data available) or from regressions of displacement versus magnitude from historical ruptures elsewhere (Wells and Coppersmith, 1994). Paleoseismic values are obtained from S. K. Pezzopane *et al.* (USGS, written communication, 1996a) and Table SBK-3; weighting is fault-specific. As with computation of slip rate, displacement data may be available at a particular site, or it may have to be interpolated from nearby locations along the fault. Again, we use linear interpolation, and we assign greatest weighting to Quaternary displacement data.

Three approaches are used to compute the average displacement at the point of interest, two based on empirical relationships between rupture length and maximum and average displacements. Each of these, in turn, is used to characterize the variability in displacement per event.

Paleoseismic Estimates of Average Displacement. We calculate the variability of displacement about an assessment of the average displacement from paleoseismic data through three steps. Step 1: For each trench for which we have three or more offset measurements, compute the average slip, U_{ap} .

$$U_{ap} = 1/n \sum U_i \quad (4)$$

where U_i is a single event fault slip (offset) at a site with three or more offsets, and n is the number of measurements at the site. This assessment is then used as an estimate of the average displacement per event, \bar{D}_E . Step 2: Divide each offset measurement (U_i) by U_{ap} . Step 3: Accumulate the U/U_{ap} samples from all trenches on all local faults, except the Rock Valley and Bare Mountain faults in Table 5.1 of S. K. Pezzopane *et al.* (USGS, written communication, 1996a). This provides an estimate of $P(U/U_{ap})$, the probability density function of a displacement U given an average displacement U_{ap} at a site. This approach is applicable directly at trench sites where at least three events have been recorded, and we interpolate between known points to calculate $P(U/U_{ap})$ when the site of interest is not at a trench location. Figure SBK-13 shows the resulting data and the fitted gamma distribution (Appendix H, Section H.2.2) used to characterize the probability distribution for U/U_{ap} . The data for this distribution is listed in Table SBK-6.

Empirical Estimates of Average Displacement. We apply a slightly different approach to estimate the distribution of displacement events about the average slip from the Wells and Coppersmith (1994) empirical relationships between rupture length and average displacement. Here, our approach involves four steps. Step 1: Determine the maximum, preferred, and minimum fault lengths for all local faults with trench data for Quaternary offset (Table 5.1 of S. K. Pezzopane *et al.*, USGS, written communication, 1996a), except the Rock Valley and Bare Mountain faults. We use the values we assessed in the seismic source characterization (Table SBK-3). Step 2: Calculate the average slip, U_a for each fault:

$$\log(U_a) = -1.99 + 1.24 \log(FL) \quad (5)$$

where FL is the fault length used to estimate the maximum magnitude earthquake in Section 3.0. This assessment is then used as an estimate of the average displacement per event, \bar{D}_E . Equation (5) is from Table C2 of Wells and Coppersmith (1994). Step 3: Divide the offset measurement U_i from each trench on a fault by U_a for that fault. Do this for each local fault except the Rock Valley and Bare Mountain faults listed in Table 5.1 of S. K. Pezzopane *et al.* (USGS, written communication, 1996a). Step 4: Plot the frequency histogram of U/U_a as an estimator of $P(U/U_a)$. Figure SBK-13 shows the resulting data and the fitted gamma distribution (Appendix H, Section H.2.3) used to characterize the probability distribution for U/U_a . The data for this distribution is listed in Table SBK-6.

Empirical Estimates of Maximum Displacement. The alternative is to compute U_m from the Wells and Coppersmith (1994) regression for maximum displacement from fault length:

$$\log(U_m) = -1.98 + 1.51(FL) \quad (6)$$

where appropriate ranges of fault length are obtained from Table SBK-3. The estimate of average displacement per event, \bar{D}_E , is set equal to $0.69 \times U_m$. We divide each offset measurement (U_i) from the trenches on each Yucca Mountain fault by U_m for that fault. The result is a frequency histogram of U/U_m as an estimator of $P(U/U_m)$, the probability distribution of displacement U given U_m for a site. Figure SBK-14 shows the resulting data and the fitted gamma distribution (Appendix H, Section H.2.4) used to characterize the probability distribution for U/U_m . The data for this distribution is listed in Table SBK-6.

In each case we compute a cumulative probability density function from the integrals of the probability density functions. The results are expressed as the probability of exceeding a normalized displacement if fault rupture occurs at a site of interest.

3.3 FAULTS WITHOUT DOCUMENTED QUATERNARY DISPLACEMENT

Many faults in the Controlled Area lack evidence for Quaternary displacement because they are inactive, have exceedingly long recurrence intervals, are located in areas that lack Quaternary cover, or are embedded in the rock mass beneath the surface. Our approach to characterize potential displacement on these faults follows the same principles as described

above, using either an earthquake approach to estimate the frequency of induced slip events or the displacement approach using direct assessment of slip rate and event size based on data for the feature. However, these are modified to account for the types of data available for the characterization. The generalized logic tree for this class of faults is diagrammed on Figure SBK-15.

3.3.1 Earthquake Approach for Distributed Faulting

The steps involved are assessment of the probability that slip can occur, evaluation of the frequency of distributed ruptures, and evaluation of the distribution of displacements.

3.3.1.1 Fault Orientation Weighting. Maps of distributed ruptures formed during historical earthquakes and nuclear test blasts (Covington, 1987; S. K. Pezzopane and T. E. Dawson, USGS, written communication, 1996), and simple rock mechanics theory (e.g., Ferrill *et al.*, 1996a), suggest that the likelihood of fault activation is a strong function of the orientation (strike and dip) of a fault surface with respect to the principal stresses. We develop an orientation index for evaluating the likelihood of fault activation. This index is based either on stress ratios between a most favorably oriented reference fault and the fault of interest, or by comparison to the orientations of distributed rupturing generated by historical, surface faulting earthquakes (based on diagrams in S. K. Pezzopane *et al.*, USGS, written communication, 1996a). By most favorably oriented fault, we mean that fault which would have the greatest slip tendency, or ratio of shear to normal traction, in the ambient stress field within the Controlled Area.

Use of Fault Slip Tendency. The orientation (strike and dip) of a fault surface relative to the contemporary stress field is an important measure of the likelihood of fault activation (Ferrill *et al.*, 1996a). Faults most likely to be active and slip in the contemporary stress field have the largest ratio of shear (T_s) to normal stress (T_n), which defines their slip tendency. Faults having lower shear-to-normal stress ratios are less likely to be active and slip as distributed or secondary ruptures under dynamic and static stress perturbations caused by an earthquake in the surrounding area. We extend this analysis by defining the fault activation factor (AF) as the ratio of the slip tendency on the fault of interest to that on the most favorably oriented fault in the contemporary stress field. The activation factor (AF) will range between 1.0 and 0. AF is a weight that reduces the expectation of failure on less favorably oriented faults.

The shear stress state on a fault or fracture is defined as:

$$T_s = \text{magnitude } (T - T_n) \quad (7)$$

where T is the traction vector across the fault of interest induced by the ambient stress tensor, T_n is the normal stress acting across the fault surface, and the bracketed term implies vector subtraction. We assume that the orientation of the fault is known to within ± 10 degrees, an angular variation that captures uncertainty in measurement by the geologist or mapper, and accounts for most natural undulations of the fault surfaces. Traction vector components of T and T_n are found using standard vector and tensor operations:

$$T_i = S_{ij} n_j \quad \text{and} \quad T_n = [S_{ij} n_i n_j] n_i \quad (8)$$

where $\mathbf{n} = \langle n_1, n_2, n_3 \rangle$ is the unit vector parallel to the pole of the fault surface, S is the stress tensor, and summation is implied over repeated indices in the equations (Einstein Summation Convention).

The ambient stress in the ESF was determined by hydrofracture measurements in Testhole ESF-AOD-HDFR#1 at a depth of 244 m (Sandia National Laboratories, written communication, 1997). The three principal stresses are: $S_v = 4.69$ MPa, vertical; $SH = 2.9 \pm 0.4$ MPa, N15°±14°E; and $Sh = 1.7 \pm 0.1$ MPa, N75°±14°W, where S_v is the vertical compressive stress, SH is the maximum horizontal compressive stress, and Sh is the minimum horizontal compressive stress. The ESF stress tensor may originate partly by tectonic and partly by topographically induced loading. Regardless of its origin, this stress tensor indicates a normal faulting stress regime in the ESF facility, with vertical maximum compressive stress, and least horizontal compressive stress oriented approximately normal to the block-bounding faults. Notably, the orientation and magnitude of the stress tensor are compatible with other hydrofracture measurements in the Yucca Mountain block and at the Nevada Test Site, which indicate a normal faulting regime and similar horizontal stress orientations to depths of approximately 1 km (e.g. Stock and Healy, 1988).

We conclude that the most favorably oriented fault dips between 60 and 65 degrees and strikes parallel to SH. The ratio $|T_s/T_n|$ on this fault is 0.54. We use this value to normalize the ratio $|T_s/T_n|$ on faults of interest that have different orientations. The ratio of the orientation of the fault of interest to the most favorably oriented fault defines the *AF* factor, which we multiply by the slip rate or event frequency to compute a revised rate or frequency.

This method neglects the role of fault interactions, which may rotate and concentrate the local stress field to cause slip on adjacent faults that are not favorably oriented for failure in the ambient stress field. We acknowledge this limitation, but we consider it of secondary importance in the evaluation of displacement hazard.

Use of Orientation Histogram. An activation factor (weight) can also be derived from empirical data on the pattern of distributed rupturing generated during historical earthquakes (S. K. Pezzopane and T. E. Dawson, USGS, written communication, 1996). This method requires construction of an azimuth (fault trend) frequency distribution of secondary ruptures generated during historical earthquakes (Appendix H, Section H.4.3; S. K. Pezzopane and T. E. Dawson, USGS, written communication, 1996; diagram presented by Pezzopane, SSC Workshop 4) and following nuclear test blasts at the Nevada Test Site (Covington, 1987). The objective is to estimate the chance that secondary rupturing will occur on faults orientated at various angles to the primary rupture zone. We expect secondary rupturing to be most common on faults that parallel the primary rupture, and least common on other faults. The underlying physical principle is that secondary rupturing is most likely on those faults favorably oriented for failure under the ambient stress field, and that other, less favorably oriented faults are less likely to rupture. Visual inspection of rupture maps in S. K. Pezzopane and T. E. Dawson's (USGS, written communication, 1996) compilation shows that secondary ruptures are concentrated along the azimuth of the primary rupture trace in most earthquakes, and that the frequency and length of secondary rupturing decrease significantly for other orientations.

3.3.1.2 Frequency of Distributed Faulting Events. Section 2.0 presents our characterization of the frequency of occurrence of earthquakes as a function of magnitude,

$\lambda_n(m)$, on each seismic source, n . The frequency of distributed faulting ruptures, λ_{DE} , is computed by the relationship

$$\lambda_{DE} = \lambda_n(m)P_n(\text{Slip|Event}) \quad (9)$$

where $P_n(\text{Slip|Event})$ is the probability that an earthquake on source n will induce slip on the feature of interest. We employ two approaches to characterize the frequency of events by earthquake triggering (Figure SBK-15). The first approach uses the earthquake recurrence on independent seismic sources, along with empirical functional relationships for distributed ruptures on hanging and foot wall (S. K. Pezzopane and T. E. Dawson, USGS, written communication, 1996; Pezzopane, SSC Workshops 2 and 3; R.R. Youngs, SSC Workshop 6). The second approach uses empirical observations of secondary fracturing and faulting in underground workings caused by strong ground shaking (Brady, 1990).

Historical Rupture Approach. The probability that a secondary or distributed displacement event will occur on a fault away from the seismic source is computed based on distance from the source (Appendix H, Section H.4.2). Pezzopane (SSC Workshop 3) showed the relationship between width of secondary or distributed rupture zone and earthquake magnitude derived from the S. K. Pezzopane and T. E. Dawson (USGS, written communication, 1996) database of historical Basin and Range earthquakes. R.R. Youngs (SSC Workshop 6) showed the frequency of occurrence of displacement events with distance from the fault as a function of magnitude in both hanging-wall and foot wall positions. Figure SBK-16 shows the resulting relationship for the probability that distributed rupture will occur at a point as a function of earthquake magnitude, distance to rupture, and location in the hanging wall and foot wall. For earthquakes occurring in the local areal source, we consider that it is equally likely the point of interest lies in the hanging wall or the foot wall. We assign a weight of 0.5 to this approach.

Ground Shaking Approach. This approach makes use of peak particle velocity (PPV) induced by strong ground motion and transient seismic strain (Hanks and McGuire, 1981; McGarr, 1984) to estimate the probability of triggering displacement on faults and fractures in the Yucca Mountain block. The method is based on observations of damage in underground tunnels and openings (Brady, 1990), and is only applied if the point under

consideration is located within an underground excavation (See Excavated Fault, or Excavation Site decision columns in Figures SBK-9 and SBK-17).

The approach is applicable for evaluating displacement on fractures that are either located adjacent to, or intersect, an underground working. Rock excavations create stress concentrations that can either destabilize or stabilize faults and joints in the vicinity of an underground excavation. Displacements may occur, but the likelihood depends on the geometry of the excavation, the orientation of the fractures, and the ambient principal stresses (Brady, 1990; Galybin, 1997). The approach presented here reflects our evaluation that, although it is important to incorporate the effects of strong ground motion on fault displacement hazard, techniques for implementing such an analysis are not well established.

The annual probability of exceedance of a specified peak particle velocity (PPV) at the surface is a ground motion parameter that is calculated as part of the PSHA analysis. $F(PPV)$ is the annual frequency of exceedance of a PPV at the surface above a point of interest. This is computed directly from the PSHA parameters. We define $P(\text{Damage}|PPV)$ as the probability that joint or fault movement (damage) will occur in a subsurface excavation given a specified PPV. The function is based on the correlation between observed damage in underground excavations in jointed rock, and the PPV measured at the surface (Brady, 1990). Figure SBK-17 shows our evaluation of the probability function $P(\text{Damage}|PPV)$. We weight this approach 0.5.

3.3.1.3 Distribution of Distributed Faulting Displacement at a Point. We lack information about average or maximum displacement during individual rupture events on faults that lack Quaternary displacement. However, cumulative (late Cenozoic) displacement generally is known on faults for which we can measure offset of marker horizons in excavations or at the surface.

Our preferred approach for estimating displacement variability on a fault where only cumulative slip is known involves comparing the cumulative slip on the fault of interest with the cumulative slips on all Yucca Mountain faults. First, we use the maximum, preferred, and minimum estimates of cumulative fault displacement, D_m , for each Yucca Mountain fault (principally from Simonds *et al.*, 1995). For each trench site on the Yucca Mountain faults,

we divide the single-event displacement by the total to develop a frequency histogram of U/D_m (see Table SBK-7), which specifies a probability density function $P(U/D_m)$ (Appendix H, Section H.3.2; U/D_m , Figure SBK-18). The cumulative slip at the site or fault of interest is then multiplied by this function to obtain the distribution of single-event displacements for the fault of interest.

3.3.2 Displacement Approach for Distributed Faulting

The steps involved are assessment of the probability that slip can occur, evaluation of the frequency of displacement events, and evaluation of the distribution of displacements.

3.3.2.1 Frequency of Displacement Events. The frequency of displacement events is evaluated using Equation (3). This assessment requires estimating the slip rate and average displacement per event.

Evaluation of Slip Rate. In the absence of data to characterize the Quaternary slip history of a fault, our use of slip rate relies on long-term, fault-specific slip data and/or on scaling of slip on one fault based on slip rates for better-studied faults in the Yucca Mountain area. We describe first the geohistorical approach, which is our preferred method because it takes into account the history of slip on a particular fault (although the weighting varies from point to point). Then we describe the fault scaling approach.

Geohistorical Method. This approach provides estimates of fault slip rate based on the cumulative displacement of a horizon of known age. The approach, which was outlined in detail by the DFS Team during SSC Workshop 5, involves not only the assessment of total displacement at a point on the fault, but also weighting of three models of slip history. The approach is applicable only to those points for which total displacement can be measured.

In the first model, we compute an average long-term slip rate. Displacement of the Tiva Canyon tuff (Ttc), with an estimated age of 12.5 Ma, is used to determine the long-term slip rate. In this model we assume that slip has been uniform during the past 12.5 Ma. Given the arguments summarized below that slip has not been uniform in the Yucca Mountain area during the past 12.5 Ma, we assign a weight of 0.1 to slip rates calculated using this model.

The second model assumes a change in slip rate at the close of tuff deposition. Fridrich (1997) suggests that approximately 80 percent of the post-Tiva Canyon tuff displacement on faults in the Yucca Mountain area occurred prior to deposition of the Rainier Mesa tuff (Trm) at 11.6 Ma. With this model, we calculate slip rates by dividing 20 percent of the post-Ttc displacement by 11.6 Ma. Here we assume that slip has been uniform during the past 11.6 Ma, although it was much more rapid from 12.5 to 11.6 Ma. We consider that this model accounts for the geologic evidence for changes in late Cenozoic slip better than the first model, so we weight it higher (0.3).

The third model is based on geologic observations and interpretation by Day *et al.* (USGS, written communication, 1996e, Fig. 2-10) that the rate of crustal extension in the region encompassing Yucca Mountain has continued to decrease since the middle Miocene. The late Miocene slip rate is calculated by dividing 80 percent of the post-Tiva Canyon displacement by the estimated age difference between the Rainier Mesa and Tiva Canyon tuffs (about 900 ka). Then we compute the Quaternary slip rate by multiplying this late Miocene rate by a reduction factor of 0.021 ± 0.018 , which is the ratio of Quaternary to late Miocene extension estimated by Day *et al.* (USGS, written communication, 1996e). This model most fully incorporates evidence for the changes in late Cenozoic slip history; thus we weight it the highest of the three methods for computing Quaternary slip rate from long-term slip (0.6). We note that an estimate of a long-term slip rate can be defined in principle by dividing the age of any geologic horizon into the cumulative fault offset of that horizon, so one is not restricted to offsets of the Tiva Canyon or Rainier Mesa tuff horizons. However, the displacements of Ttc or Trm are the most common measurements available on the Yucca Mountain faults.

Fault Scaling Methods. Fault scaling methods are based on the observation that the slip rates on two different faults scale with their relative surface areas (Cowie and Scholz, 1992b). That is, the larger fault presumably has the higher slip rate. If fault area is not known, then ratios of cumulative displacement or fault length may be substituted for surface area based on the scaling relationships between cumulative fault displacement and fault length, and between fault length and fault surface area (Walsh and Watterson, 1987, 1992; Cowie and Scholz, 1992a, b; Clark and Cox, 1996). Because cumulative displacement either is known or can be estimated from geologic mapping on block-bounding faults at Yucca Mountain, and

this is the most likely data available for fractures and shears mapped in the subsurface, we give highest weight to the use of the cumulative displacement ratio (however, weighting varies with each case). The displacement ratio method proposed here is supported by both observational (Nicol *et al.*, 1997) and mechanical modeling (P.A. Cowie, Lamont-Doherty, written communication, 1998) studies which indicate that the slip rates of normal faults with larger cumulative displacement are consistently greater than those of smaller faults with less cumulative displacement in the same region. Nicol *et al.*'s (1997) study is based on observations of normal faulting from six rift basins located in different parts of the world, and is applicable to terrains like those in the Controlled Area. We therefore consider the slip rates of two faults to be proportional to the ratio of their cumulative displacement:

$$Sr_i = [Dcum_i / Dcum_r] \times SR_r \quad (10)$$

where *Dcum* is cumulative displacement and *SR* is slip rate. Index "i" refers to the fault of interest, and index "r" refers to a fault with known slip rate. One or more of the block-bounding faults at Yucca Mountain with known *SR_r* may be used as the reference fault. If more than one fault is used to calibrate slip rate, then the slip rate for the reference fault must be expressed as an average value, and the reference cumulative displacement must also be averaged over the reference faults. The fault of interest may be located in the repository block or elsewhere in the Controlled Area; it has known cumulative displacement at one or more points but no definitive geologic evidence for Quaternary slip rate.

Average Displacement Per Event. We use three probability distributions ($P(U/D_m)$, $P(U/U_a)$, and $P(U/U_m)$) for displacement per event at points on faults where both fault length and cumulative displacement are known (Figure SBK-15, displacement logic tree branch). However, for those points where only cumulative fault displacement is known we use just one function, $P(U/D_m)$.

3.3.2.2 Distribution of Distributed Faulting Displacement. The distribution function described in Section 3.3.1.3 and shown on Figure SBK-18 is used to characterize the distribution of displacements in faulting events.

4.0 REFERENCES

- Anderson, L.W., and Klinger, R.E., 1996, The Beatty scarp in Nye County, Nevada—an important Late Quaternary morphologic datum: *Bulletin of the Seismological Society of America*, v. 86, p. 1650-1654.
- Anderson, R.E., Bucknam, R.C., Crone, A.J., Haller, K.M., Machette, M.N., Personius, S.F., Barnhard, T.P., Cecil, M.J., and Dart, R.L., 1995a, Characterization of Quaternary and suspected Quaternary faults, regional studies, Nevada and California: U.S. Geological Survey Open-File Report 95-599, 56 p. plus app.
- Anderson, R.E., Crone, A.J., Machette, M.N., Bradley, L.A., and Diehl, S.F., 1995b, Characterization of Quaternary and suspected Quaternary faults, Amargosa area, Nevada and California: U.S. Geological Survey Open-File Report 95-613, 41 p. plus appendices.
- Argus, D.F., and Gordon, R.G., 1991, No-net-rotation model of current plate velocities incorporating plate motion model NUVEL-1: *Geophysical Research Letters*, v. 18, p. 2038-2042.
- Barnsley, M.F., 1988, *Fractals Everywhere*: Boston, Academic Press, 394 p.
- Beanland, S., and Clark, M.M., 1994, The Owens Valley fault zone, eastern California, and surface faulting associated with the 1872 earthquake: *U.S. Geological Survey Bulletin* 1982, 29 p.
- Becker, A., and Abrahamson, N., 1997, Stress drops in normal faulting earthquakes [abs.]: *Seismological Research Letters*, v. 68, p. 322.
- Berrill, J.B., and Davis, R.D., 1980, Maximum entropy and the magnitude distribution: *Bulletin of the Seismological Society of America*, v. 70, p. 1823-1831.
- Brady, B.H., 1990, Dynamic performance and design of underground excavations in jointed rock, *in* Brummer, R. ed., *Static and Dynamic Considerations in Rock Engineering*: Rotterdam, A.A. Balkema, p. 1-11.
- Brocher, T.M., Hart, P.E., Hunter, C.W., and Langenheim, V.E., 1996, Hybrid-source reflection profiling across Yucca Mountain, Nevada: regional lines 2 and 3: U.S. Geological Survey Open-File Report 96-28, 110 p.

- Bruhn, R.L., and Schultz, R.A., 1996, Geometry and slip distribution in normal fault systems; implications for mechanics and fault-related hazards: *Journal of Geophysical Research*, v. 101, p. 3401-3412.
- Burchfiel, B.C., Hodges, D.V., and Royden, L.M., 1987, Geology of Panamint Valley-Saline Valley pull apart system, California; palinspastic evidence for low-angle geometry of a Neogene range-bounding fault: *Journal of Geophysical Research*, v. 92, p. 10,422-10,426.
- Carr, W. J., 1984, Regional structural setting of Yucca Mountain, Southwestern Nevada, and late Cenozoic rates of tectonic activity in part of the Southwestern Great Basin, Nevada and California: U. S. Geological Survey Open-File Report 84-854, 114 p.
- Carr, W. J., 1990, Styles of extension in the Nevada Test Site region, Southern Walker Lane Belt; An integration of volcano-tectonic and detachment fault models, in Wernicke, B.P., ed., *Basin and Range Extensional Tectonics near the Latitude of Las Vegas, Nevada*: Geological Society of America Memoir 176, p. 283-303.
- Clark, R.M., and Cox, S.J.D., 1996, A modern regression approach to determining fault displacement-length scaling relationships: *Journal of Structural Geology*, v. 16, p. 147-152.
- Covington, H.R., 1987, Map showing surface features induced by underground nuclear explosions at Pahute Mesa, Nevada Test Site, Nye County, Nevada, April 1976 through November 1983: U.S. Geological Survey Miscellaneous Investigations Series Map I-1872, scale 1:48,000.
- Cowie, P.A., and Scholz, C.H., 1992a, Physical explanation for the displacement - length relationship of faults using a post-yield fracture mechanics model: *Journal of Structural Geology*, v. 14, p. 1133-1148.
- Cowie, P.A., and Scholz, C.H., 1992b, Displacement-length scaling relationship for faults: data synthesis and discussion: *Journal of Structural Geology*, v. 14, p. 1149-1156.
- DeMets, C., Gordon, R.G., Argus, D.F. and Stein, S., 1990, Current plate motions: *Geophysical Journal International*, v. 101, p. 425-478.
- dePolo, C.M., 1994, The maximum background earthquake in the Basin and Range: *Bulletin of the Seismological Society of America*, v. 84, p. 466-472.
- Dixon, T.H., Robaudo, S., Lee, J., and Reheis, M., 1995, Constraints on present-day Basin and Range deformation from space geodesy: *Tectonics*, v. 14, p. 755-772.

- Dokka, R.K., and Travis, C.J., 1990, Role of the Eastern California shear zone in accommodating Pacific-North American plate motion: *Geophysical Research Letters*, v. 17, p. 1323-1326.
- Doser, D.I., 1986, Earthquake processes in the Rainbow Mountain-Fairview Peak-Dixie Valley, Nevada, region (1954-1959): *Journal of Geophysical Research*, v. 91, p. 12,572-12,586.
- Doser, D.I., 1988, Source parameters of earthquakes in the Nevada seismic zone (1915-1943): *Journal of Geophysical Research*, v. 93, p. 15,001-15,016.
- Doser, D.L., and Smith, R.B., 1989, An assessment of source parameters of earthquakes in the Cordillera of the western United States: *Bulletin of the Seismological Society of America*, v. 79, p. 1383-1409.
- Ferrill, D.A., Stirewalt, G.L., Henderson, D.B., Stamatakos, J.A., Morris, A.P., Spivey, K.H., and Wernicke, B.P., 1996a, Faulting in the Yucca Mountain region: NUREG/CR-6401, CNWRA 95-017, variously paginated.
- Ferrill, D.A., Stamatakos, J.A., Jones, S.M., Rahe, B., McKague, H.L., Martin, R.H., and Morris, A.P., 1996b, Quaternary slip history of the Bare Mountain fault (Nevada) from the morphology and distribution of alluvial fan deposits: *Geology*, v. 24, p. 559-562.
- Fridrich, C.J., 1997, Tectonic evolution of the Crater Flat basin, in Wright, L., and Troxel, B., eds., *Cenozoic Basins of the Death Valley Region: Geological Society of America Special Paper* (in press).
- Frizzell, V.A. Jr., and Shulters, J., 1990, Geologic map of the Nevada Test Site, southern Nevada: U.S. Geological Survey Miscellaneous Investigations Series Map I-2046, scale 1:100,000.
- Galybin, A.N., 1997, A model of mining induced fault sliding: *Proceedings of the 36th U.S. Rock Mechanics Symposium*, Columbia University, June 29 - July 2.
- Hanks, T.C., and McGuire, R.K., 1981, The character of high frequency strong ground motion: *Bulletin of the Seismological Society of America*, v. 71, p. 2071-2095.

- Hardyman, R.F., and Oldow, J.S., 1991, Tertiary tectonic framework and Cenozoic history of the central Walker Lane, Nevada, in Raines, G.L., Lisle, R.E., Schafer, R.W., and Wilkinson, W.H., eds, *Geology and Ore Deposits of the Great Basin: Geological Society of Nevada Symposium Proceedings*, v. 1, p. 279-301.
- Harmsen, S.C., 1993, Preliminary seismicity and focal mechanisms for the southern Great Basin of Nevada and California-January 1992 through September 1992: U.S. Geological Survey Open-File Report 93-369, 213 p.
- Hemphill-Haley, M.A., and Weldon, R.J. II, 1996, Estimating prehistoric earthquake magnitude from point displacements instead of surface rupture length [abs.]: *EOS, Transactions of the American Geophysical Union*, v. 77, no. 46 supplement, p. F512.
- Humphreys, E.D., and Weldon, R.J., 1994, Deformation across the western United States: a local estimate of Pacific-North America transform deformation: *Journal of Geophysical Research*, v. 99, p. 19,975-20,010.
- Jackson, J.A., and White, N.J., 1989, Normal faulting in the upper continental crust: observations from regions of active extension: *Journal of Structural Geology*, v. 11, p. 15-36.
- Jennings, C.W., 1994, Fault activity map of California and adjacent areas with locations and ages of recent volcanic eruptions: California Division of Mines and Geology, California Geologic Data Map Series, Map No. 6, scale 1:750,000.
- Kanamori, H., and Anderson, D.L., 1975, Theoretical basis of some empirical relations in seismology: *Bulletin of the Seismological Society of America*, v. 65, p. 1073-1095.
- Langenheim, V.E., Kirchoff-Stein, K.S., and Oliver, H.W., 1993, Geophysical investigations of buried volcanic centers near Yucca Mountain, southwestern Nevada, in *Fourth International Conference on High-Level Radioactive Waste Management: La Grange Park, Illinois, American Nuclear Society*, p. 1840-1846.
- Lee, J-J., and Bruhn, R.L., 1996, Characterization of the structural anisotropy of normal fault surfaces: *Journal of Structural Geology*, 18, p. 1043-1059.
- Lienkaemper, J.J., Pezzopane, S.K., Clark, M., and Rymer, M.J., 1987, Fault fractures formed in association with the 1986 Chalfant Valley, California, earthquake sequence; preliminary report: *Bulletin of the Seismological Society of America*, v. 77, p. 297-305.

- Loper, S., Pasyanos, M., Dreger, D., and Romanowicz, B., 1993, Broadband source study of the 1993 Eureka Valley, California, earthquake sequence [abs.]: EOS, Transactions of the American Geophysical Union, v. 74, no. 43 supplement, p. 397.
- Lubetkin, L.D.C., and Clark, M., 1988, Late Quaternary activity along the Lone Pine fault, eastern California: Geological Society of America Bulletin, v. 100, p. 755-766.
- Massonnet, D., and Feigl, F.L., 1995, Satellite radar interferometric map of the coseismic deformation field of the M 6.1 Eureka Valley, California earthquake of May 17, 1993: Geophysical Research Letters, v. 22, p. 1541-1544.
- McGarr, A., 1984, Some applications of seismic source mechanism studies to assessing underground hazard, in Gay, N.C., and Wainwright, eds., Proceedings of the First International Congress on Rock Bursts and Seismicity in Mines: South African Institute of Mining and Metallurgy, Johannesburg, p. 198-208.
- Meremonte, M. E., Gomberg, J., and Cranswick, E., 1995, Constraints on the 29 June 1992 Little Skull Mountain sequence provided by robust hypocentral estimates: Bulletin of the Seismological Society of America, v. 85, p. 1039-1049.
- Minster, J.B., and Jordan, T.H., 1987, Vector constraints on western U.S. deformation from space geodesy, neotectonics and plate motions: Journal of Geophysical Research, v. 92, p. 4798-4804.
- Nicol, A., Walsh, J.J., Waterson, J., and Underhill, J., 1997, Displacement rates of normal faults. Nature (in press).
- Parsons, T., and Thompson, G.A., 1991a, Coupled processes of normal faulting and dike intrusion in tectonically extended regions [abs.]: Seismological Research Letters, v. 62, p. 26.
- Parsons, T., and Thompson, G.A., 1991b, The role of magma overpressure in suppressing earthquakes and topography: worldwide examples: Science, v. 253, p. 1399-1402.
- Peltzer, G., and Rosen, P., 1995, Surface displacement of the 17 May 1993 Eureka Valley, California earthquake observed by SAR interferometry: Science, v. 268, p. 1333-1336.
- Piety, L.A., 1995, Compilation of known and suspected Quaternary faults within 100 km of Yucca Mountain, Nevada and California: U.S. Geological Survey Open-File Report 94-112, 404 p.

- Ponce, D.A., 1993, Geophysical investigations of concealed faults near Yucca Mountain, southwest Nevada, *in* High Level Radioactive Waste Management: Proceedings, Fourth Annual International Conference, v. 1, p. 168-174.
- Reheis, M.C, and Dixon, T.H., 1996, Kinematics of the Eastern California shear zone: evidence for slip transfer from Owens and Saline Valley fault zones to Fish Lake Valley fault zone: *Geology*, v. 24, 339-342.
- Reheis, M.C., and Sawyer, T.L., 1997, Late Cenozoic history and slip rates of the Fish Lake Valley, Emigrant Peak, and Deep Springs fault zones, Nevada and California: *Geological Society of America Bulletin*, v. 109, p. 280-299.
- Richard, S.M. ed., 1992, Deformation associated with the Neogene, Eastern California shear zone, southeastern California and southwestern Arizona: Proceedings, San Bernardino County Museum Association, Special Publication 92-1, 78 p.
- Rogers, A.M., Harmsen, S.C., Corbett, E.J., Priestly, K.F. and dePolo, D., 1991, The seismicity of Nevada and some adjacent parts of the Great Basin, in Slemmons, D.B., Engdahl, E.R., Zoback, M.D., and Blackwell, D.D., eds., *Neotectonics of North America: Geological Society of America, Decade Map Volume 1*, p. 153-184.
- Rogers, A. M., Harmsen, S.C., and Meremonte, M.E., 1987, Evaluation of the seismicity of the Southern Great Basin and its relationship to the tectonic framework of the region: U.S. Geological Survey Open-File Report 87-408.
- Savage, J.C., Lisowski, M., and Prescott, W.H., 1990, An apparent shear zone trending north-northwest across the Mojave Desert into Owens Valley, California: *Geophysical Research Letters*, v. 17, p. 2113-2136.
- Schwartz, D.P., and Coppersmith, K.J., 1984, Fault behavior and characteristic earthquakes: examples from the Wasatch and San Andreas faults: *Journal of Geophysical Research*, v. 89, p. 5681-5698.
- Scott, R.B., 1990, Tectonic setting of Yucca Mountain, southwest Nevada, in Wernicke, B.P., ed., *Basin and Range Extensional Tectonics Near the Latitude of Las Vegas, Nevada: Geological Society of America Memoir 176*, p. 251-282.
- Shields, G., Smith, K.D., and Brune, J.N., 1995, Source parameters of a sequence of very shallow earthquakes in the Rock Valley fault zone, southern Nevada Test Site [abs.]: EOS, *Transactions of the American Geophysical Union*, v. 76, p. F426.

- Simonds, W.F., Whitney, J.W., Fox, K., Ramelli, A., Yount, J., Carr, M., Menges, C.M., Dickerson, R., and Scott, R.B., 1995, Map of fault activity of the Yucca Mountain area, Nye County, Nevada: U.S. Geological Survey Miscellaneous Investigations Series Map I-2520, scale 1:24,000.
- Smith, K.D., and Brune, J.N., 1997, A sequence of very shallow earthquakes in the Rock Valley fault zone, southern Nevada Test Site: U.S. Geological Survey Circular on Yucca Mountain Tectonics (in press).
- Smith, K.D., and Priestley, K.F., 1997, The 1986 Chalfant, California earthquake sequence, earthquake relocations and source parameters: *Bulletin of the Seismological Society of America* (in press).
- Smith, R.B., and Sbar, M.L., 1974, Contemporary tectonics and seismicity of the western United States with emphasis on the Intermountain seismic belt: *Geological Society of America Bulletin*, v. 85, p. 1205-1218.
- Smith, R.P., Jackson, S.M., and Hackett, W.R., 1996, Paleoseismology and seismic hazards evaluations in extensional volcanic terrains: *Journal of Geophysical Research*, v. 101, p. 6277-6292.
- Stamatakos, J.A., Connor, C.B., and Martin, R.H., 1997, Quaternary basin evolution and basaltic volcanism of Crater Flat, Nevada from detailed ground magnetic surveys of the Little Cones: *Journal of Geology*, v. 105, p. 319-330.
- Stewart, J.H., 1978, Basin-range structure in western North America: a review, in Smith, R.B., and Eaton, G.P., eds., *Cenozoic Tectonics and Regional Geophysics of the Western Cordillera*: Geological Society of America Memoir 152, p. 1-31.
- Stewart, J.H., 1988, Tectonics of the Walker Lane belt, western Great Basin--Mesozoic and Cenozoic deformation in a zone of hear, in Ernst, W.G., ed., *Metamorphism and Crustal Evolution of the Western United States*, Rubey Volume VII: Englewood Cliffs, NJ, Prentice Hall, p. 683-713.
- Stock, J.M., and Healy, J.H., 1988, Stress field at Yucca Mountain, Nevada: U.S. Geological Survey Bulletin 1790, p. 87-93.
- Veneziano, D. and van Dyck, J., 1985, Statistical discrimination of "aftershocks" and their contribution to seismic hazard, Appendix A-4, in *Seismic Hazard Methodology for Nuclear Facilities in the Eastern United States*: EPRI Research Project Number P101-29, p. A121-A186.

- Walsh, J.J., and Waterson, J., 1987, Distribution of cumulative displacement and of seismic slip on a single normal fault surface: *Journal of Structural Geology*, v. 9, p. 1039-1046.
- Walsh, J.J., and Waterson, J., 1992, Populations of faults and fault displacements and their effects on estimates of fault related regional extension: *Journal of Structural Geology*, v. 14, p. 701-712.
- Ward, S.H., 1990, Pacific-North America plate motions: new results from very long baseline interferometry: *Journal of Geophysical Research*, v. 95, p. 21,965-21,981.
- Wells, D.L., and Coppersmith, K.J., 1994, New empirical relationships among magnitude, rupture length, rupture width, rupture area, and surface displacement: *Bulletin of the Seismological Society of America*, v. 84, p. 974-1002.
- Wernicke, B., 1995, Low-angle normal faults and seismicity: a review: *Journal of Geophysical Research*, v. 100, p. 20,159-20,174.
- Wheeler, R.L., 1989, Persistent segment boundaries on basin-range normal faults, *in* Schwartz, D.P. and Sibson, R.H., eds., *Fault segmentation and controls of rupture initiation and termination*: U.S. Geological Survey Open-File Report 89-315, p.432-444.
- Wiechert, D.H., 1980, Estimation of the earthquake recurrence parameters for unequal observation periods for different magnitudes: *Bulletin of the Seismological Society of America*, v. 70, p. 1337-1346.
- Wright, L., 1976, Late Cenozoic fault patterns and stress fields in the Great Basin and westward displacement of the Sierra Nevada block: *Geology*, v. 4, p. 489-494.
- Wright, L.A., 1989, Overview of the role of strike-slip and normal faulting in the Neogene history of the region northeast of Death Valley, California-Nevada, in Ellis, M.A., ed., *Later Tertiary Evolution of the Southern Great Basin*: Nevada Bureau of Mines and Geology Open File 89-1, p. 1-11.
- Youngs, R.R., and Coppersmith, K.J., 1985, Implications of fault slip rates and earthquake recurrence models to probabilistic seismic hazard estimates: *Bulletin of the Seismological Society of America*, v. 75, p. 939-964.

Youngs, R.R., Swan, F.H., Power, M.S., Schwartz, D.P., and Green, R.K., 1987, Probabilistic analysis of earthquake ground shaking hazard along the Wasatch Front, Utah: U.S. Geological Survey Open-File Report 87-585, v. II, p. M1-M110.

Zhang, P., Ellis, M., Slemmons, D.B., and Mao, F., 1990, Right-lateral displacements and the Holocene slip rate associated with prehistoric earthquakes along the southern Panamint Valley fault zone; implications for southern Basin and Range tectonics and coastal California deformation: *Journal of Geophysical Research*, v. 95, p. 4857-4872.

**TABLE SBK-1
REGIONAL FAULT SOURCES**

Fault Name	Ind. Source	Type and Dip Direction	Maximum Magnitude Approach				Recurrence Approach			Recurrence Model		
			Length (km)	Area	Max. Offset (m)	Av. Offset (m)	Long-term Slip Rate (m/kyr)	Quat Slip Rate (m/kyr)	Interval (kyr)			
Amargosa River	Y (0.8)	RL (0.6)	(0.35)	(0.35)	(0.3)			(0.9)	(0.1)	C (0.4)		
	N (0.2)	N (0.4)	12 (0.7)		2.5 (0.2)			0.02 (0.5)			10 (1.0)	TE (0.6)
		East (1.0)	15 (0.3)		1.6 (0.8)			0.03 (0.5)				
Ash Meadows	Y (0.8)	N (1.0)	(0.35)	(0.35)	(0.3)		(0.1) 0.016 (1.0)	(0.9)		C (0.6)		
	N (0.2)		30 (0.3)		1.4 (0.2)			0.01 (0.2)			TE (0.4)	
		West (1.0)	40 (0.6)		1.8 (0.8)			0.04 (0.7)				
			100 (0.1)			0.1 (0.1)						
Belted Range	Y (0.9)	N (1.0)	(0.25)	(0.25)	(0.3)	(0.2) 0.8 (1.0)	(0.2) .005 (1.0)	(0.8)		C (0.6)		
	N (0.1)		22 (0.4)		1.0 (1.0)			0.01 (0.1)			TE (0.4)	
		West (1.0)	38 (0.2)					0.09 (0.7)				
			50 (0.4)			0.2 (0.2)						
Buried Hills – Emigrant Valley South	Y (0.01)	N (1.0)	(0.5)	(0.5)				(1.0)		C (0.6)		
	N (0.99)		51 (0.8)					0.01 (0.5)			TE (0.4)	
		West (1.0)	57 (0.2)					0.001 (0.5)				

**TABLE SBK-1
REGIONAL FAULT SOURCES
(Continued)**

Fault Name	Ind. Source	Type and Dip Direction	Maximum Magnitude Approach				Recurrence Approach			Recurrence Model			
			Length (km)	Area	Max. Offset (m)	Av. Offset (m)	Long-term Slip Rate (m/kyr)	Quat Slip Rate (m/kyr)	Interval (kyr)				
Southern Death Valley – Death Valley – Furnace Creek – Fish Lake Valley	Y (0.01) N (0.99)	RL (1.0)	(0.25)	(0.25)		(0.5)		(0.8)	(0.2)	C (0.9) TE (0.1)			
		West (1.0)	340 (1.0)			2.5 (0.3)		4.0 (0.4)	0.40 (0.5)				
						3.5 (0.3)		5.0 (0.4)	0.80 (0.5)				
					4.5 (0.4)		8.0 (0.2)						
Death Valley – Southern Death Valley	Y (0.05) N (0.95)	N (0.2)	(0.15)	(0.15)		(0.7)	(0.2)	(0.4)	(0.4)	C (0.9) TE (0.1)			
		RL (0.8)	115 (0.7)			2.5 (0.5)		1.5 (0.2)	0.50 (0.2)				
		West (1.0)	140 (0.3)			3.5 (0.5)		3.0 (0.5)	0.70 (0.3)				
							5.0 (0.4)	1.00 (0.3)					
								1.30 (0.2)					
Furnace Creek – Fish Lake Valley	Y (0.05) N (0.95)	RL (1.0)	(0.2)	(0.2)	(0.2)	(0.4)	(0.8)	(0.2)		C (0.9) TE (0.1)			
		West (1.0)	230 (0.5)		3.0 (0.5)						2.5 (0.1)	2.0 (0.1)	0.60 (0.4)
			240 (0.5)		6.0 (0.5)						4.5 (0.9)	4.0 (0.4)	0.80 (0.2)
							8.0 (0.4)	1.70 (0.4)					
							10.0 (0.1)						
Fish Lake Valley	Y (0.94) N (0.95)	RL (1.0)	(0.5)	(0.5)			(0.4)	(0.6)		C (0.9) TE (0.1)			
		West (1.0)	50 (0.4)									.30 (0.3)	2 (0.2)
			75 (0.6)									.50 (0.7)	3 (0.5)
								4 (0.3)					

**TABLE SBK-1
REGIONAL FAULT SOURCES
(Continued)**

Fault Name	Ind. Source	Type and Dip Direction	Maximum Magnitude Approach				Recurrence Approach			Recurrence Model					
			Length (km)	Area	Max. Offset (m)	Av. Offset (m)	Long-term Slip Rate (m/kyr)	Quat Slip Rate (m/kyr)	Interval (kyr)						
Southern Death Valley	Y. (0.94) N (0.06)	RL (1.0)	(0.5)	(0.5)				(0.8)	(0.2)		C (0.9) TE (0.1)				
			45 (0.2)					.2.0 (0.5)				0.3 (1.0)			
		West (1.0)	75 (0.7)					.3.0 (0.5)							
			85 (0.1)												
Death Valley	Y. (0.94) N (0.06)	N (0.5)	(0.35)	(0.35)				(0.3)	(0.6)	(0.4)	C (0.9) TE (0.1)				
			45 (0.4)					2.5 (0.5)				1.5 (0.2)	0.5 (0.2)		
		Obl (0.5)	51 (0.2)					3.5 (0.5)				3.0 (0.4)	0.7 (0.3)		
		West (1.0)	68 (0.4)									5.0 (0.3)	1.0 (0.3)		
							7.0 (0.1)	1.3 (0.2)							
Furnace Creek	Y. (0.94) N (0.06)	RL (1.0)	(0.2)	(0.4)	(0.2)			(0.1)	(0.6)	(0.3)	C (0.9) TE (0.1)				
			105 (0.7)					6.0 (1.0)				4.5 (1.0)	4.0 (0.2)	4.0 (0.4)	0.60 (0.5)
		West (1.0)	115 (0.1)										8.0 (0.4)	8.0 (0.5)	0.80 (0.5)
			160 (0.2)										10.0 (0.4)	10.0 (0.1)	
Kawich Range	Y (0.04) N (0.6)	N (1.0)	(0.35)	(0.35)	(0.3)			(1.0)	(1.0)		C (0.6) TE (0.4)				
			74 (0.1)					1.5 (1.0)				0.01 (0.3)			
		West (1.0)	78 (0.3)									0.002 (0.7)			
			84 (0.6)												

**TABLE SBK-1
REGIONAL FAULT SOURCES
(Continued)**

Fault Name	Ind. Source	Type and Dip Direction	Maximum Magnitude Approach				Recurrence Approach			Recurrence Model		
			Length (km)	Area	Max. Offset (m)	Av. Offset (m)	Long-term Slip Rate (m/kyr)	Quat Slip Rate (m/kyr)	Interval (kyr)			
Pahrump	Y (0.9)	Obl (0.8)	(0.45)	(0.45)	(0.1)		(0.8) (RL)	(0.2) (V)		C (0.4)		
	N (0.1)	RL (0.2)	18.5 (0.33)		0.7 (1.0)		.11 (0.5)	0.009 (0.5)		TE (0.6)		
		West (1.0)	50 (0.33)				.19 (0.5)	0.02 (0.5)				
Rock Valley	Y (1.0)	LL-N (0.3)	(0.2)	(0.2)	(0.3)	(0.3)		(0.8)	(0.2)	C (0.4)		
		LL (0.7)	19 (0.1)		5.2 (0.2)			1.7 (0.5)	0.003 (0.1)		6 (0.1)	TE (0.6)
		SE (1.0)	32 (0.5)		5.7 (0.8)			3.9 (0.5)	0.02 (0.8)		12 (0.2)	
			65 (0.4)				0.05 (0.1)	20 (0.2)				
			100 (0.5)									
Sarcobatus Flat	Y (0.01)	N (1.0)	(0.5)	(0.5)				(1.0)		C (0.4)		
	N (0.99)	West (1.0)	27 (0.2)		49 (0.8)			0.01 (0.1)		TE (0.6)		
								0.001 (0.6)				
								0.0001 (0.3)				
West Pintwater Range	Y (0.5)	N (1.0)	(0.5)	(0.5)				(1.0)		C (0.6)		
	N (0.5)	West (1.0)	60 (0.3)		82 (0.7)			0.01 (0.6)		TE (0.4)		
								0.001 (0.4)				

TABLE SBK-1
REGIONAL FAULT SOURCES
(Continued)

Fault Name	Ind. Source	Type and Dip Direction	Maximum Magnitude Approach				Recurrence Approach			Recurrence Model				
			Length (km)	Area	Max. Offset (m)	Av. Offset (m)	Long-term Slip Rate (m/kyr)	Quat Slip Rate (m/kyr)	Interval (kyr)					
West Spring Mountains	Y (0.9)	N (1.0)	(0.3)	(0.3)		(0.4)		(0.7)	(0.3)	C (0.6)				
	N (0.1)		30 (0.2)								1.7 (0.5)	0.02 (0.5)	28 (0.2)	TE (0.4)
		West (1.0)	47 (0.5)								2.0 (0.5)	0.07 (0.5)	120 (0.8)	
			54 (0.3)											
Yucca	Y (0.9)	N (0.8)	(0.5)	(0.5)			(0.2)	(0.8)		C (0.4)				
	N (0.1)	Obl (0.2)	20 (0.2)								.003 (0.5)	0.03 (0.20)	TE (0.6)	
			32 (0.5)								.007 (0.5)	0.09 (0.79)		
		East (1.0)	45 (0.3)				0.5 (0.01)							

Notes and Sources - Table SBK-1:

Each column contains a weighting in parenthesis (**bold**) for that variable within the overall grouping (e.g., weight of 0.3 for fault length as an estimator for maximum magnitude) as well as weightings of individual values for that variable (e.g., 60-km length weighted 0.3; 82-km length weighted 0.7). Ind. Source: likelihood that fault behaves as an independent source, generating a maximum magnitude earthquake that is larger than that of regional seismic source in which it is located. Type: RL - right lateral; LL - left lateral; Obl - oblique; N - normal. Area: computed from down-dip width of fault (fault dip and maximum seismogenic depth) times length; down-dip width depends on fault type, as noted in text. Seismogenic depth derived from regional source zone in which fault is embedded. Interval: average time between surface rupture events. Recurrence Model: shape of recurrence curve; C - characteristic; TE - truncated exponential.

Amargosa River Anderson *et al.*, 1995b; Piety, 1995. Discontinuous strike-slip fault; fault length of 12 km from Anderson *et al.*, 15 km from Piety. 100-ka scarps according to Anderson *et al.*; single-event ruptures interpreted from their scarp data. Slip Rate from 2.5 to 3 m offset in ca. 100 ka as best data.

TABLE SBK-1
REGIONAL FAULT SOURCES
(Continued)

Notes and Sources - Table SBK-1 (Continued):

- Ash Meadows** Anderson *et al.*, 1995b; Piety, 1995; Carr, 1990; regional gravity data. Discontinuous normal fault zone, up to 8 km wide. Longest length is obtained by including the so-called "gravity fault" recognizable in regional gravity gradient data along the east side of Fortymile Wash in Jackass Flat. Rock Valley fault, however, may terminate active fault zone at north, cutting off connection to "gravity fault." We consider this the more likely case, given lack of surface expression for "gravity fault," especially compared to expression of Ash Meadows fault in Amargosa Valley. Likely age of youngest event varies substantially along mapped fault traces; probably a segmented fault, but insufficient data to constrain segments.
- Belted Range** Piety, 1995; Anderson *et al.*, 1995a. Relatively short length (21 km according to Anderson and others) has Quaternary offset; however, maximum length set as equal to mapped fault length, which is uncertain depending on source. Limited evidence for Quaternary slip leads to conclusion that earthquakes above those defined for regional source zone are very unlikely on this fault. Slip rate estimated by using 11.3 m in about 50 ka from scarp morphology reported by Anderson and others
- Buried Hills-Emigrant Valley South** S. K. Pezzopane, USGS, written communication, 1996; Piety, 1995. Possible fault combination; neither fault zone considered capable of producing larger earthquake than regional maximum magnitude. Slip rate based on comparison with other Basin-Range faults, thus has low certainty. No actual evidence that these faults have ruptured together; thus low weighting as independent source.
- Combined Southern Death Valley – Death Valley - Furnace Creek - Fish Lake Valley** Jennings, 1994; R. E. Klinger and L. A. Piety, USBR, written communication, 1996; Piety, 1995; Reheis and Sawyer, 1997. Formed by combining all four faults. Total length measured from Jennings map. Average offset taken from data compiled by R. E. Klinger and L. A. Piety, USBR, written communication, 1996. Slip rate based on best constrained slip rates for the four constituent faults. Treats Death Valley fault as a pull-apart along the shear zone. Little likelihood that all faults rupture together, given size of pull-apart basin and discontinuous traces.
- Combined Death Valley and Southern Death Valley** Piety, 1995; R. E. Klinger and L. A. Piety, USBR, written communication, 1996; Jennings, 1994. Rupture length reported as 45 to 60 km, although total length is 115 km if both faults are considered together. Note that Southern Death Valley fault is strike-slip, Death Valley fault normal (pull-apart). Long-term rate for Southern Death Valley, Quaternary rate for Death Valley.
- Combined Furnace Creek-Fish Lake Valley** Reheis and Sawyer, 1997; Piety, 1995; R. E. Klinger and L. A. Piety, USBR, written communication, 1996; Jennings, 1994. Some chance that Furnace Creek and Fish Lake Valley faults are continuous and can rupture together, within uncertainties of the data. However, available data are insufficient to prove (within overlaps on dating) that paleoseismic events could have been simultaneous on the two faults. Note that restraining bend between them has no Holocene slip.
- Fish Lake Valley** Reheis and Sawyer, 1997; Piety, 1995; Jennings, 1994. Northern termination of fault poorly shown on maps of Jennings or Reheis and Sawyer, producing uncertainty in maximum fault length. Slip rate data well constrained by Reheis and Sawyer.
- Southern Death Valley** Piety, 1995; Jennings, 1994. Southern extent of fault uncertain. Most likely southern termination at Garlock fault. Late Quaternary slip rate poorly constrained.
- Death Valley** R. E. Klinger and L. A. Piety, USBR, written communication, 1996; Jennings, 1994; Piety, 1995. Shorter fault length based on older scarps in northern third of fault, suggesting rupture length less than total fault length.
- Furnace Creek** Piety, 1995; R. E. Klinger and L. A. Piety, USBR, written communication, 1996; Jennings, 1994. Maximum surface rupture length reported as 105 km by Klinger and Piety, so this is considered most likely maximum rupture length. Fault shown by Jennings possibly continuing as much as 20 km farther southeast into Amargosa Valley; however, no evidence for this continuation, and remainder of southern Furnace Creek fault is well expressed along the range front. Thus we consider any greater length to the fault exceedingly unlikely, and it is given zero weight.

TABLE SBK-1
REGIONAL FAULT SOURCES
(Continued)

Notes and Sources - Table SBK-1 (Continued):

- Kawich Range** S. K. Pezzopane, USGS, written communication, 1996, Piety, 1995; Anderson *et al.*, 1995a. Same as Kawich Range West fault zone of Anderson and others. Only a short section (3.6 to 7.4 km) is indicated by Anderson and others to have Quaternary slip; were this the entire source, it would produce earthquakes no larger than those accounted for in the regional source zone. Assessment is based on assuming entire fault could break in a single event, which is extremely unlikely, given evidence this apparently has not happened in Quaternary. Anderson and others argue that slip rate must be very low given lack of recurrent Quaternary slip and embayed range front. Most likely slip rate from approximately 2 m slip in alluvium of Quaternary age, possibly 1 Ma.
- Pahrump** Piety, 1995; Anderson *et al.*, 1995b. Likely length 50 to 70 km; Quaternary activity may be only along 18.5 km. Maximum vertical offset 5 m on late Quaternary deposits; no constraints on Quaternary right-lateral displacement rate.
- Rock Valley** Piety, 1995; Anderson *et al.*, 1995b; J. A. Coe *et al.*, USGS, written communication, 1996; unpubl preliminary TL ages from Mahan, 2/20/97. Main fault zone 32 km long, SS; youngest event post 2.45 ka at one site, >10 cm; prior event > 20km rupture ca. 7.2 ka. 14.2 m slip in that and two prior events from trench data constrain offset per event and Quaternary slip rate. Offsets of 3.2, 5.2, and 5.7 m if horiz:vert ratio remains constant. Maximum length taken by including southwest extension as mapped by Anderson and others, others; however, this section may be older than main Rock Valley fault zone, so is weighted less as defining maximum length.
- Sarcobatus Flat** Anderson *et al.*, 1995a; Piety, 1995. Almost no evidence for any Quaternary displacement according to Anderson and others, so slip rate must be extremely low. Rate constrained by similar low slip-rate faults in regional and local area.
- West Pintwater Range** Piety, 1995. Longer fault length includes North Desert Range fault. Apparently there is a lack of repeated Quaternary displacement. Slip rate constrained by comparisons with other regional and local faults.
- West Spring Mountains** Piety, 1995; Anderson *et al.*, 1995a. More than 20 m late Quaternary displacement. Possibly 12 m on 120-ka surface. Length uncertain principally based on how far south past range front fault is continued, as well as northern termination. Maximum length includes all of range front to north and a southern termination at the Pahrump fault. Minimum distance based on Anderson and others' mapping of scarps.
- Yucca** Piety, 1995. Scarp at least 20 km long; longer lengths from combining with other faults to the north, despite lack of evidence for linked ruptures. Fault shows explosion-related offsets; also reported to be youngest prehistoric scarp in test site region, as cited by Piety. 0.3-0.6 km total displacement post tuff 11 to 8.5 Ma; Quaternary slip rates computed assuming 15 m slip in middle to late Quaternary, as summarized by Piety, and the slight chance that historical explosion-related ruptures are releasing tectonic strain.

TABLE SBK-2
OTHER REGIONAL FAULTS
 (Page 1 of 3)

FAULT NAME	SOURCES	NOTES
Area Three	W. R. Keefer and S. K. Pezzopane, USGS, written communication, 1996; Piety, 1995	Within regional source magnitudes
Bullfrog Hills	W. R. Keefer and S. K. Pezzopane, USGS, written communication, 1996; Piety, 1995	No convincing Q displ
Cane Spring	W. R. Keefer and S. K. Pezzopane, USGS, written communication, 1996; Piety, 1995	No convincing Q displ
Carpetbag	W. R. Keefer and S. K. Pezzopane, USGS, written communication, 1996; Piety, 1995	Largely concealed; no convincing late Q displacement
Checkpoint Pass	W. R. Keefer and S. K. Pezzopane, USGS, written communication, 1996; Piety, 1995	Little if any Quat offset proven
Crossgrain Valley	W. R. Keefer and S. K. Pezzopane, USGS, written communication, 1996; Piety, 1995	Little data on age; prob. Q scarps along 20% of mapped fault; within regional source magnitudes
Eleana Range	W. R. Keefer and S. K. Pezzopane, USGS, written communication, 1996; Piety, 1995	6-9 km likely length, but not all late Q; within regional source magnitudes
Emigrant Valley North	W. R. Keefer and S. K. Pezzopane, USGS, written communication, 1996; Piety, 1995	Within regional source magnitudes
Grapevine	W. R. Keefer and S. K. Pezzopane, USGS, written communication, 1996; Piety, 1995	Within regional source magnitudes
Hunter Mtn-Panamint Valley	Piety, 1995	Not a linked structure
Hunter Mtn	Piety, 1995	Within regional source magnitudes
Kawich Valley	W. R. Keefer and S. K. Pezzopane, USGS, written communication, 1996; Piety, 1995	Not likely middle-late Q displ

**TABLE SBK-2
OTHER REGIONAL FAULTS
(Page 2 of 3)**

FAULT NAME	SOURCES	NOTES
Keane Wonder	Piety, 1995; Anderson <i>et al.</i> , 1995a	Not likely middle-late Q displ; within regional source magnitudes
Mercury Ridge	W. R. Keefer and S. K. Pezzopane, USGS, written communication, 1996; Piety, 1995	Within regional source magnitudes
Mine Mountain	W. R. Keefer and S. K. Pezzopane, USGS, written communication, 1996; Piety, 1995	Not likely middle-late Q displ
North Desert Range	W. R. Keefer and S. K. Pezzopane, USGS, written communication, 1996; Piety, 1995	Within regional source magnitudes
Oak Spring Butte	W. R. Keefer and S. K. Pezzopane, USGS, written communication, 1996; Piety, 1995	Combined with Yucca fault
Oasis Valley	Piety, 1995; Anderson <i>et al.</i> , 1995a	Not likely middle-late Q displ
Pahute Mesa	W. R. Keefer and S.K. Pezzopane, USGS, written communication, 1996; Piety, 1995	Not likely middle-late Q displ; within regional source magnitudes
Panamint Valley	Piety, 1995	Paleoseismic event 25-30 km long, so within regional source magnitudes
Plutonium Valley	W. R. Keefer and S. K. Pezzopane, USGS, written communication, 1996; Piety, 1995	Within regional source magnitudes
Ranger Mountains	W. R. Keefer and S. K. Pezzopane, USGS, written communication, 1996; Piety, 1995	Within regional source magnitudes
Rocket Wash-Beatty Wash	Anderson <i>et al.</i> , 1995b; Anderson and Klinger, 1996; Piety, 1995	Not a fault
South Ridge	W. R. Keefer and S. K. Pezzopane, USGS, written communication, 1996; Piety, 1995	Within regional source magnitudes
Spotted Range	W. R. Keefer and S. K. Pezzopane, USGS, written communication, 1996; Piety, 1995	Within regional source magnitudes

TABLE SBK-2
OTHER REGIONAL FAULTS
 (Page 3 of 3)

FAULT NAME	SOURCES	NOTES
Tolicha Peak	Anderson <i>et al.</i> , 1995a; W. R. Keefer and S. K. Pezzopane, USGS, written communication, 1996; Piety, 1995	Within regional source magnitudes
Wahmonie	W. R. Keefer and S. K. Pezzopane, USGS, written communication, 1996; Piety, 1995	Within regional source magnitudes
West Specter Range	Anderson <i>et al.</i> , 1996b	Within regional source magnitudes
Yucca Lake	W. R. Keefer and S. K. Pezzopane, USGS, written communication, 1996; Piety, 1995	Within regional source magnitudes

Note - Table SBK-2:

“Within regional source magnitudes” indicates that maximum magnitude on this fault would be within the range of magnitudes incorporated into the regional source zone of which this fault is a part.

**TABLE SBK-3
LOCAL FAULTS**

Fault Name	Ind. Source	Type	Maximum Magnitude Approach					Recurrence Approach			Recurrence Model	
			Length (km)	Area	Max Offset (m)	Av Offset (m)	Offset from Stress Drop	Long-term Slip Rate (m/kyr)	Quat Slip Rate (m/kyr)	Interval (kyr)		
Hwy. 95 fault (0.8 likelihood of existence)	Y (0.4)	LL (0.5)	(0.5)	(0.5)					(1.0)			C (0.1)
	N (0.6)	N (0.5)	30 0.5						0.002 0.9			TE (0.9)
			49 0.5						0.02 0.1			
Bare Mountain	Y (1.0)	N (1.0)	(0.2)	(0.5)	(0.3)				(0.05)	(0.65)	(0.3)	C (0.6)
			15.5 0.1		0.80 0.2			0.13 0.1	0.01 0.7	20 0.05	TE (0.4)	
			20 0.5		1.50 0.8			0.20 0.6	0.02 0.3	40 0.05		
			23 0.4				0.24 0.3		100 0.45	200 0.45		
South Crater Flat		N-LL (1.0)	(0.2)	(0.4)	(0.1)	(0.1)	(0.2)		(0.7)	(0.3)	C (0.3)	
			6.1 0.5		0.20 0.5	0.05 0.3		0.001 0.1	60 0.7	TE (0.7)		
			8.2 0.3		0.50 0.5	0.10 0.6		0.002 0.8	70 0.2			
			10 0.2			0.20 0.1		0.003 0.1	180 0.1			
North Crater Flat		N (0.5) Obl (0.5)	(0.2)	(0.5)	(0.1)		(0.2)		(0.7)	(0.3)	C (0.3)	
			10 0.3		0.40 0.4			0.002 0.5	120 0.5	TE (0.7)		
			13.3 0.7		0.60 0.6			0.003 0.5	160 0.5			
Windy Wash		N-LL (1.0)	(0.2)	(0.4)	(0.2)	(0.1)	(0.1)	(0.1)	(0.7)	(0.2)	C (0.3)	
			25 0.2		0.96 0.5	0.30 0.5		0.025 0.2	0.01 0.2	35 0.1	TE (0.7)	
			27 0.5		0.98 0.5	0.50 0.5		0.027 0.8	0.011 0.6	40 0.4		
			28 0.3					0.016 0.2	45 0.4	100 0.1		
Fatigue Wash		N (0.7) Obl (0.3)	(0.2)	(0.4)	(0.1)	(0.1)	(0.2)		(0.7)	(0.3)	C (0.3)	
			7.5 0.2		0.50 0.9	0.25 0.2		0.002 0.2	50 0.05	TE (0.7)		
			12.5 0.5		1.50 0.1	0.30 0.4		0.009 0.8	120 0.1			
			18.5 0.3			0.50 0.4			185 0.7	250 0.15		
Solitario Canyon		N-LL (1.0)	(0.2)	(0.5)	(0.2)		(0.1)	(0.05)	(0.75)	(0.2)	C (0.3)	
			13 0.2		1.10 0.1			0.002 0.5	0.007 0.2	40 0.3	TE (0.7)	
			18 0.8		1.20 0.6			0.003 0.5	0.01 0.6	60 0.3		
				1.30 0.3			0.02 0.2	100 0.1	180 0.3			

**TABLE SBK-3
LOCAL FAULTS
(Continued)**

Fault Name	Ind. Source	Type	Maximum Magnitude Approach					Recurrence Approach			Recurrence Model
			Length (km)	Area	Max Offset (m)	Av Offset (m)	Offset from Stress Drop	Long-term Slip Rate (m/kyr)	Quat Slip Rate (m/kyr)	Interval (kyr)	
Iron Ridge	Y (0.1)	N (1.0)	(0.3)	(0.5)	(0.1)		(0.1)		(1.0)		C (0.3)
	N (0.9)		7.2 0.8		1.00 0.7			0.002 0.5		TE (0.7)	
			8.5 0.2		1.30 0.3			0.004 0.5			
Bow Ridge	Y (0.4)	N (0.5)	(0.2)	(0.6)	(0.1)		(0.1)		(0.7)	(0.3)	C (0.3)
	N (0.6)	Obl (0.5)	6.7 0.7		0.40 0.2			0.002 0.2	40 0.05	TE (0.7)	
			12.2 0.3		0.45 0.6			0.003 0.6	70 0.1		
					0.80 0.2			0.007 0.2	100 0.35 140 0.35 215 0.1 350 0.05		
Paintbrush Canyon		N-LL (1.0)	(0.2)	(0.4)	(0.2)	(0.1)	(0.1)		(0.7)	(0.3)	C (0.3)
			12 0.5		1.42 0.1	0.20 0.1		0.002 0.1	20 0.01	TE (0.7)	
			18 0.2		1.67 0.7	0.45 0.5		0.007 0.3	50 0.19		
			23 0.3		2.05 0.19	0.5 0.4		0.015 0.5	65 0.2		
					2.57 0.01			0.02 0.09	100 0.3 115 0.2 270 0.1		
Stagecoach Road		N-LL (1.0)	(0.2)	(0.4)	(0.2)	(0.1)	(0.1)		(0.7)	(0.3)	C (0.3)
			8 0.7		0.5 0.15	0.40 0.7		0.006 0.1	5 0.05	TE (0.7)	
			12 0.3		0.67 0.8	0.60 0.3		0.03 0.4	10 0.2		
					0.99 0.05			0.05 0.4 0.07 0.1	35 0.5 50 0.2 75 0.05		

**TABLE SBK-3
LOCAL FAULTS
(Continued)**

Fault Name	Ind. Source	Type	Maximum Magnitude Approach					Recurrence Approach				Recurrence Model			
			Length (km)		Area	Max Offset (m)		Av Offset (m)	Offset from Stress Drop	Long-term Slip Rate (m/kyr)				Interval (kyr)	
Paintbrush Canyon + Stagecoach Road + Bow Ridge		N-LL (1.0)	(0.1)	(0.6)	(0.2)		(0.1)		(0.8)	(0.2)		C (0.5) TE (0.5)			
			23 0.7										0.79 0.29	0.015 0.2	10 0.05
			34 0.3										0.84 0.5	0.03 0.4	20 0.2
													1.0 0.2	0.05 0.4	40 0.6
			1.4 0.01							45 0.1					
			75 0.05												
So. Crater Flat + Windy Wash + Fatigue Wash		N-LL (1.0)	(0.1)	(0.6)	(0.1)		(0.1)		(0.8)	(0.2)		C (0.5) TE (0.5)			
			25.5 0.3										0.50 0.3	0.30 0.5	50 0.2
			27.2 0.4										0.98 0.7	0.50 0.5	185 0.8
			28.3 0.3												
Solitario Canyon + Iron Ridge		N-LL (1.0)	(0.2)	(0.5)	(0.2)		(0.1)		(1.0)			C (0.5) TE (0.5)			
			13 0.2										1.10 0.1	0.009 0.2	
			18 0.8										1.20 0.6	0.012 0.3	
													1.30 0.3	0.014 0.4	
			0.024 0.2												
Simultaneous Rupture of Linked Faults		N-LL (1.0)	(0.1)	(0.6)	(0.3)				(1.0)			C (0.5) TE (0.5)			
			82 0.8										2.50 0.5	0.04 0.2	
			95 0.2										3.30 0.5	0.06 0.6	
			0.09 0.2												
Coalesced Faults		N-LL (1.0)	(0.1)	(0.6)	(0.3)				(0.25 to 1.0)	(0 to 0.75)		Max Moment 1.0 for volcanic otherwise C 0.5 TE 0.5			
			27 0.6										2.50 0.5	0.04 0.2	Same as
			34 0.4										3.30 0.5	0.06 0.6	volcanic eruption
										freq.					

**TABLE SBK-3
LOCAL FAULTS
(Continued)**

Notes and Sources - Table SBK-3 (Continued):

Each column contains a weighting in parenthesis (**bold**) for that variable within the overall grouping, as well as weightings of individual values for that variable. Both Hwy. 95 fault and Bare Mountain fault are treated as independent sources in analysis. Other local faults can rupture in various combinations, as detailed in text. Unless otherwise noted, maximum displacements obtained from trench data; average displacement used when at least four points available for a single event along strike of the fault, from trench data and/or mapping. Southern termination of each fault taken from A. R. Ramelli and J. W. Bell, Nevada Bureau of Mines and Geology, written communication, 1996, except for Hwy. 95 fault, which may truncate all of the others considered here.

Hwy. 95 fault Data interpreted from Memorandum by D.B. Slemmons, 3 February 1997. Likelihood of existence 0.8; if it exists, likelihood it ruptures as an independent seismogenic structure 0.5 (lacking any definitive evidence of offset in the Quaternary, yet there are sufficient indicators of possible activity to convince us we can't favor one conclusion over the other). Arguments in favor of existence and activity: apparent uplift of bedrock across feature, truncation of faults of Crater Flat/Yucca Mountain block, irregular subdued scarps as described by Slemmons, left-lateral deflection of gravity gradient at south end of Bare Mountain fault plus deflection of subsurface horizons as reported by Slemmons, April 1997 SSC Workshop. Arguments against existence and activity: irregular subdued scarps along regional gradient suggest fluvial activity.

Bare Mountain fault Sources of data: L. W. Anderson and R. E. Klinger, USBR, written communication, 1996b; Piety, 1995; Ferrill *et al.*, 1996a, b; S. K. Pezzopane *et al.*, 1996a; A. R. Ramelli and J. W. Bell, Nevada Bureau of Mines and Geology, written communication, 1996. Length of fault confined to that mapped by previous workers at surface along Bare Mountain. Although a gravity gradient is approximately aligned with Bare Mountain fault to south, no Quaternary faulting is associated with it, so we do not include it. There may be some secondary rupture on Yucca Mountain faults associated with primary events on the Bare Mountain fault, based on Pezzopane and others' compilation; however, no evidence of simultaneous ruptures, and the "ash event" is not recorded in Bare Mtn. rupture stratigraphy; thus we consider this an independent structure. Displacement data based on assuming that Anderson and Klinger's single late Quaternary event is in fact two events. Long-term slip rate from 2 to 3 km; total displacement in 15 Ma.

South Crater Flat fault Sources of data: A. R. Ramelli and J. W. Bell, Nevada Bureau of Mines and Geology, written communication, 1996; E. M. Taylor, USGS, written communication, 1996; Simonds *et al.*, 1995; S. K. Pezzopane *et al.*, USGS, written communication, 1996a. Three-dimensional fault geometry consistent with possible linkage to Windy Wash fault. Late Quaternary slip rate estimated from total displacement from trenches divided by age of offset deposits.

North Crater Flat fault Sources of data: A. R. Ramelli and J. W. Bell, Nevada Bureau of Mines and Geology, written communication, 1996; J. A. Coe *et al.*, USGS, written communication, 1996; Simonds *et al.*, 1995; S. K. Pezzopane *et al.*, 1996a. Three-dimensional fault geometry consistent with lack of connection to South Crater Flat fault. Late Quaternary slip rate estimated from displacement in trenches, although ages of offset deposits not well constrained.

Windy Wash fault Sources of data: A. R. Ramelli and J. W. Bell, Nevada Bureau of Mines and Geology, written communication, 1996; J. W. Whitney *et al.*, USGS, written communication, 1996b; Simonds *et al.*, 1995; S. K. Pezzopane *et al.*, USGS, written communication, 1996a. Northern extension of fault from Simonds and others; however, northernmost portion of fault has no convincing evidence of Quaternary displacement, so given lower weighting. Slip rate estimated from trench data.

**TABLE SBK-3
LOCAL FAULTS
(Continued)**

Notes and Sources - Table SBK-3 (Continued):

- Fatigue Wash fault** Sources of data: A. R. Ramelli and J. W. Bell, Nevada Bureau of Mines and Geology, written communication, 1996; Coe *et al.*, USGS, written communication, 1996; Simonds *et al.*, 1995; S. K. Pezzopane *et al.*, 1996a. Most likely geometry is splaying from Windy Wash fault at both north and south; second possible geometry is that Fatigue Wash fault continues north, parallel to Windy Wash fault. All Fatigue Wash paleoseismic events are permissibly same timing as some of the Windy Wash events, although equally well they could be independent earthquakes. Slip rate estimated from trench data.
- Solitario Canyon fault** Sources of data: A. R. Ramelli and J. W. Bell, Nevada Bureau of Mines and Geology, written communication, 1996; A. R. Ramelli *et al.*, Nevada Bureau of Mines and Geology, written communication, 1996; Simonds *et al.*, 1995; W.C. Day *et al.*, USGS, written communication, 1996a; S. K. Pezzopane *et al.*, USGS, written communication, 1996a. Fault mapped in detail by Simonds and others and Day and others, yielding little uncertainty on fault length. Surface breakage events are extremely variable in displacement, including minor cracking events as well as a major displacement (the maximum event noted in table) as part of the "ash event." It is likely that at least some of the surface breaks are secondary in nature. South end of fault could link with Stagecoach Road fault, although we have not addressed this possibility explicitly in our analysis. Slip rate estimated from trench data.
- Iron Ridge fault** Sources of data: A. R. Ramelli and J. W. Bell, Nevada Bureau of Mines and Geology, written communication, 1996; A. R. Ramelli, *et al.*, Nevada Bureau of Mines and Geology, written communication, 1996; Simonds *et al.*, 1995; S. K. Pezzopane *et al.*, USGS, written communication, 1996a. Given geometry and timing of rupture event, it is very unlikely that this structure ruptures independently of the Solitario Canyon fault. Slip rate estimated from trench data.
- Bow Ridge fault** Sources of data: A. R. Ramelli and J. W. Bell, Nevada Bureau of Mines and Geology, written communication, 1996; E. M. Taylor *et al.*, USGS, written communication, 1996b; C. M. Menges and J. W. Whitney, USGS, written communication, 1996b; Simonds *et al.*, 1995; S. K. Pezzopane *et al.*, USGS, written communication, 1996a. Fault may link north end of Solitario Canyon fault with Paintbrush Canyon fault, although the most likely geometry is as a splay of the Paintbrush Canyon fault. Given this geometry and the short length of the fault, we consider it less likely to behave as an independent seismogenic structure than to slip in response to other faults. Northern continuation of fault uncertain; we used the Pagany Wash fault mapped by Simonds and others as the most likely continuation, although given the lack of Quaternary displacement on this structure it is considered a less likely geometry than the Bow Ridge fault as shown by Ramelli and Bell. Slip rate based on trench data; complicated options for return periods based on uncertainties in dating from trench studies and variability in repeat times of events inferred from the trenches.
- Paintbrush Canyon fault** Sources of data: A. R. Ramelli and J. W. Bell, Nevada Bureau of Mines and Geology, written communication, 1996; C. M. Menges and J. W. Whitney, 1996; Simonds *et al.*, 1995; Frizzell and Shulters, 1990; S. K. Pezzopane *et al.*, USGS, written communication, 1996a. Northern extent of fault from Frizzell and Shulters map; however, no evidence of Quaternary slip along north half of fault, so given lower weight in assessment of length. Slip rate and displacement data obtained principally from Busted Butte paleoseismic data.
- Stagecoach Road fault** Sources of data: A. R. Ramelli and J. W. Bell, Nevada Bureau of Mines and Geology, written communication, 1996; C. M. Menges and J. W. Whitney, USGS, written communication, 1996b; Simonds *et al.*, 1995; S. K. Pezzopane *et al.*, USGS, written communication, 1996a. Connection between Stagecoach Road fault and Paintbrush Canyon fault is uncertain, and we interpret the Stagecoach Road fault *sensu stricto* to extend as shown by Simonds and others. Displacement, slip rate, and repeat-time data all obtained from trench studies.

**TABLE SBK-3
LOCAL FAULTS
(Continued)**

Notes and Sources - Table SBK-3 (Continued):

Linked faults As discussed in text, we consider one set of models in which four "block-bounding" faults behave as either independent structures or rupture simultaneously. The former case involves three linked structures--Paintbrush Canyon + Stagecoach Road + Bow Ridge; South Crater Flat + Windy Wash + Fatigue Wash; and Solitario Canyon + Iron Ridge--along with the North Crater Flat fault. Fault lengths for each linked system are estimated by taking the longest along-strike fault zone; parallel and branch faults that are part of a linked system do not contribute to fault length. Maximum displacement and slip rate data are obtained from any part of the total linked fault system, using data from events that are in common for any given set of faults as summarized by S. K. Pezzopane *et al.*, USGS, written communication, 1996a. The latter case assumes that all linked faults may have ruptured simultaneously during one or more surface faulting events. The principal example of this is the "ash event." For this scenario, the fault length is the sum of the various linked faults, and the maximum displacement is estimated from the maximum displacement on each constituent linked fault. The return time of the event can be estimated either from the sum of the slip rates on each fault, or (given the unique nature of the "ash event" and its apparent tie to volcanism) from the frequency of occurrence of volcanic eruptions in the Crater Flat area.

Coalesced faults As discussed in text, we consider a set of models in which all of the YM faults (excluding Hwy. 95 and Bare Mountain) coalesce at depth. Should all these faults rupture at the surface in a single event, as may have been the case for the "ash event," the fault length would be that of the longest ("master") fault, in this case the Paintbrush Canyon-Stagecoach Road linked fault or the Solitario Canyon-Iron Ridge linked fault. An alternative is that during any given event on a master fault at depth, any combination of the surface faults may rupture, depending on the pathway the rupture takes between the hypocenter and the surface. Recurrence estimate for the former case is tied strongly to volcanic eruption frequency (0.75 likelihood); recurrence for the latter case is tied exclusively to the summed slip rates determined from the surface faults.

TABLE SBK-4
FAULT DISPLACEMENT HAZARD CHARACTERIZATION DATA, POINTS 1, 2, AND 9

Point	Slip Rate (mm/yr) weight 0.8			Event Frequency weight 0.2		Displacement (m)			
	Site-Specific	Interpolated Quaternary	Interpolated Cumulative	Paleoseismic Data	EQ Recur.	Uave Paleo	Uave W&C	Umax Paleo	Umax W&C
1 (Bow Ridge fault)	1.0 wt. 0.002, 0.2 wt. 0.003, 0.6 wt. 0.007, 0.2 wt.			0.5 wt. Details in Table SBK-3	0.5 wt.	0.4 wt. 0.06, 0.2wt 0.27, 0.6wt 0.55, 0.2wt	0.1 wt	0.4 wt Table SBK-3	0.1 wt
2 (Solitario Canyon fault)		1.0 wt 0.0006 to 0.00355 (see notes)		0.5 wt. 4 events 0.5 wt 3 events 0.5 wt	0.5 wt.	0.25 wt.	0.25 wt	0.25 wt 0.3, 0.4, 0.6	0.25 wt
9 (Midway Valley fractures)	1.0 wt. 0.0, 0.2 wt. 6.6×10^{-5} , 0.4 1.4×10^{-4} , 0.4			Event frequency not used for point 9			0.3 wt.	0.4 wt. 0.05, .8 0, 0.2	0.3 wt.

Notes, Table SBK-4

EQ Recur.: earthquake recurrence distribution computed in ground shaking hazard analysis for SBK Team; **Uave Paleo:** average displacement per rupture event from paleoseismic data; **Uave W&C:** average displacement computed from Wells and Coppersmith regression; **Umax Paleo:** maximum displacement from trench-specific data; **Umax W&C:** maximum displacement computed from Wells and Coppersmith regression.

Bow Ridge fault: Slip rate approach given 0.7 weight for computation of occurrence frequency, event frequency approach given 0.3 weight. Site-specific data from Trench 14D, as compiled by S. K. Pezzopane *et al.*, USGS, written communication, 1996a.

Solitario Canyon fault: Slip rate approach given 0.7 weight for computation of occurrence; event frequency approach given 0.3 weight. Slip rate calculated by interpolating slip rate from known point, Trench 4, along strike; demonstration point is between this trench and a point of known zero displacement (Ramelli, SSC Workshop 6). Slip rate at Trench 4, based on data from A. R. Ramelli *et al.*, USGS, written communication, 1996: 0.0012 (0.2 wt.), 0.0024 (0.3 wt.), 0.004 (0.2 wt.), 0.0053 (0.3 wt.). Reduction factor, computed based on distance between points and uncertainty in interpolation: 0.67 (0.2 wt.), 0.59 (0.6 wt.), 0.5 (0.2 wt.). Final slip-rate results: 0.0006 (0.04 wt.), 0.00071 (0.12 wt.), 0.0084 (0.04 wt.), 0.0012 (0.06 wt.), 0.00142 (0.18 wt.), 0.00161 (0.06 wt.), 0.002 (0.04 wt.), 0.00236 (0.12 wt.), 0.00265 (0.06 wt.) 0.00268 (0.04 wt.), 0.00313 (0.18 wt.), and 0.00355 (0.06 wt.). Data on paleoseismic event frequency from

TABLE SBK-4
FAULT DISPLACEMENT HAZARD CHARACTERIZATION DATA, POINTS 1, 2, AND 9
(Continued)

A. R. Ramelli *et al.*, USGS, written communication, 1996: 4 events in 150 ka (0.2 wt.), 200 ka (0.6 wt.), or 250 ka (0.2 wt.) is assigned weight of 0.5; 3 events in same time periods assigned weight of 0.5. Average and maximum displacements computed by interpolating between Trench SCF-T4 and zero displacement point, the position of which was shown by Ramelli (SSC Workshop 6). Displacement values for U_{ave} are dependent on number of events (3 or 4) assumed to have occurred. For 4 events

Notes, Table SBK-4 (cont.)

(weight 0.5), U_{ave} weighted 0.075 m (0.2 wt.), 0.1375 m (0.6 wt.), and 0.2 m (0.2 wt.). For 3 events (weight 0.5), U_{ave} weighted 0.1 m (0.2 wt.), 0.183 m (0.6 wt.), and 0.267 m (0.2 wt.). U_{max} is not sensitive to number of events.

Midway Valley fractures: Data from Swan, SSC Workshop 3. Event frequency constrained only by slip rate. Fractures on the Exile Hill fault have maximum net displacement of 5 cm in deposits 350-760 ka in age, producing extremely low slip rates. Yet the displacement may be zero. Displacement amount constrained using maximum slip of 5 cm for fractures. Fault length 0.4 km for computation of maximum and average displacement from Wells and Coppersmith regressions.

**TABLE SBK-5
FAULT DISPLACEMENT HAZARD CHARACTERIZATION DATA, POINTS 3-8**

Point	Slip Rate (mm/yr) 0.8 weight		Event Frequency 0.2 weight		Activation Factor	
	Geologic History	Fault Parameter	Distributed Rupture	PPV Frequency	Slip Tendency	Angular Histogram
3 (Drill Hole Wash)	0.75 wt. <u>Model 1 (0.1)</u> 0.0041 (0.2) 0.0033 (0.6) 0.0025 (0.2) <u>Model 2 (0.3)</u> 0.0009 (0.2) 0.0007 (0.6) 0.0005 (0.2) <u>Model 3 (0.6)</u> 0.0009 (0.2) 0.0007 (0.6) 0.0006 (0.2)	0.25 wt. 0.0036 (0.2) 0.0009 (0.6) 0.0004 (0.2)	0.5 wt.	0.5 wt.	(0.4 wt.) 0.6 (0.1 weight) 0.5 (0.8) 0.4 (0.1)	(0.6 wt.)
4 (Ghost Dance fault)	0.75 wt. <u>Model 1 (0.1)</u> 0.0029 (0.2) 0.0025 (0.6) 0.0021 (0.2) <u>Model 2 (0.3)</u> 0.0006 (0.2) 0.0005 (0.6) 0.0004 (0.2) <u>Model 3 (0.6)</u> 0.0007 (0.2) 0.0006 (0.6) 0.0005 (0.2)	0.25 wt. 0.0026 (0.2) 0.00072 (0.6) 0.00034 (0.2)	0.5 wt.	0.5 wt.	(0.4 wt.) 0.8 (0.1) 0.7 (0.8) 0.3 (0.1)	(0.6 wt.)
5 (Sundance fault)	0.75 wt. <u>Model 1 (0.1)</u> 0.0017 (0.2) 0.0013 (0.6)	0.25 wt. 0.0014 (0.2) 0.00036 (0.6) 0.00008 (0.2)	1.0 wt.		(0.4 wt.) 0.6 (0.1) 0.56 (0.8) 0.48 (0.1)	(0.6 wt.)

TABLE SBK-5
FAULT DISPLACEMENT HAZARD CHARACTERIZATION DATA, POINTS 3-8
(Continued)

Point	Slip Rate (mm/yr) 0.8 weight		Event Frequency 0.2 weight		Activation Factor	
	Geologic History	Fault Parameter	Distributed Rupture	PPV Frequency	Slip Tendency	Angular Histogram
	0.0005 (0.2) <u>Model 2 (0.3)</u> 0.0003 (0.2) 0.0003 (0.6) 0.0001 (0.2) <u>Model 3 (0.6)</u> 0.0004 (0.2) 0.0003 (0.6) 0.0001 (0.2)					
6 (west of Dune Wash fault)	0.75 wt. <u>Model 1 (0.1)</u> 0.0017 (0.2) 0.0009 (0.6) 0.00017 (0.2) <u>Model 2 (0.3)</u> 0.00035 (0.2) 0.00019 (0.6) 0.00003 (0.2) <u>Model 3 (0.6)</u> 0.00037 (0.2) 0.00021 (0.4) 0.00004 (0.2)	0.25 wt. 0.0014 (0.2) 0.00027 (0.6) 0.000026 (0.2)	0.5 wt.	0.5 wt.	1.0 (1.0 weight)	(not implemented)
7a Fault (2 m)	0.75 wt. <u>Model 1 (0.1)</u> 1.7e-4 (1.0) <u>Model 2 (0.3)</u> 5.2e-5 (1.0)	0.25 wt. 1.4e-4 (0.2) 4.8e-5 (0.6) 2.6e-5 (0.2)	0.5 wt.	0.5 wt.	1.0 (1.0 weight)	(not implemented)

TABLE SBK-5
FAULT DISPLACEMENT HAZARD CHARACTERIZATION DATA, POINTS 3-8
(Continued)

Point	Slip Rate (mm/yr) 0.8 weight		Event Frequency 0.2 weight		Activation Factor	
	Geologic History	Fault Parameter	Distributed Rupture	PPV Frequency	Slip Tendency	Angular Histogram
	<u>Model 3 (0.6)</u> 5.2e-5 (1.0)					
7b Shear (10 cm)	0.75 wt. <u>Model 1 (0.1)</u> 8e-6 (1.0) <u>Model 2 (0.3)</u> 2e-6 (1.0) <u>Model 3 (0.6)</u> 2e-6 (1.0)	0.25 wt. 7.0e-6 (0.2) 2.4e-6 (0.6) 1.3e-6 (0.2)	0.5 wt.	0.5 wt.	1.0 (1.0 weight)	(not implemented)
7c Fracture (<10 cm)	0.75 wt. [uniform between 0 & maximum of 7b]	0.25 wt. [uniform between 0 & maximum of 7b]	0.5 wt.	0.5 wt.	1.0 (1.0 weight)	(not implemented)
7d Intact Rock	notes below					
8a Fault (2 m)	0.75 wt. <u>Model 1 (0.1)</u> 1.7e-4 (1.0) <u>Model 2 (0.3)</u> 5.2e-5 (1.0) <u>Model 3 (0.6)</u> 5.2e-5 (1.0)	0.25 wt. 1.4e-4 (0.2) 4.8e-5 (0.6) 2.6e-5 (0.2)	0.5 wt.	0.5 wt.	1.0 (1.0 weight)	(not implemented)
8 bShear (10 cm)	0.75 wt. <u>Model 1 (0.1)</u> 8e-6 (1.0) <u>Model 2 (0.3)</u> 2e-6 (1.0)	0.25 wt. 7.0e-6 (0.2) 2.4e-6 (0.6) 1.3e-6 (0.2)	0.5 wt.	0.5 wt.	1.0 (1.0 weight)	(not implemented)

TABLE SBK-5
FAULT DISPLACEMENT HAZARD CHARACTERIZATION DATA, POINTS 3-8
(Continued)

Point	Slip Rate (mm/yr) 0.8 weight		Event Frequency 0.2 weight		Activation Factor	
	Geologic History	Fault Parameter	Distributed Rupture	PPV Frequency	Slip Tendency	Angular Histogram
	Model 3 (0.6) 2e-6 (1.0)					
8c Fracture (<10 cm)	0.75 wt. [uniform between 0 & maximum of 7b]	0.25 wt. [uniform between 0 & maximum of 7b]	0.5 wt.	0,1 overall	1.0 (1.0 weight)	(not implemented)
8d Intact Rock	see notes below					

Notes, Table SBK-5:

Fault Parameter Method: Total displacement and slip rate of the Bow Ridge fault are the reference parameters for this trial set of calculations. We could use an average of the Solitario Canyon and Bow Ridge fault parameters, but the slip rates of the two faults are similar, and Bow Ridge fault slip rate is well defined by trench #4 near the entrance to the repository ESF. Bow Ridge fault displacement is estimated as 100 m minimum, 125 m preferred value, and 150 m maximum value based on Day *et al.* (USGS, written communication, 1996b) and our judgement of maximum error in estimating total slip from mapping. Slip rate estimates for the Bow Ridge fault and weights are given in Table SBK-4. We report three estimated slip rates for the fault parameter method which are the preferred, the most minimum and most maximum values estimated using all combinations of the reference fault (Bow Ridge fault) parameters (displacement and slip rate) and subject fault parameters (displacement). Application of displacement variability (probability) functions is described in Section 3.3.4.

Drill Hole Wash Fault: Slip rate methods - Geologic History weighted 0.6, Model 1,2 & 3 as described in manuscript. Fault Parameter method weighted 0.2, Event Frequency - Distributed Rupture method weighted 0.1, Peak Particle Velocity method weighted 0.1). Fault parameter slip rates found by ratio of maximum estimated displacement on Drill Hole Wash to Bow Ridge Fault. Displacement estimates are (30 m, 40m, 50 m) from Day *et al.*, 1996. Stress activation factor computed using ESF stress tensor and orientation of Drill Hole Wash fault reported by Day *et al.* (USGS, written communication, 1996b). Fault pole trends 045°, plunges 05° with an assumed variation of ± 10° in both trend and plunge.

Ghost Dance Fault: Slip rate methods - Geologic History weighted 0.6, Model 1,2 & 3 as described in manuscript. Fault Parameter method weighted 0.2, Event Frequency - Distributed Rupture method weighted 0.1, Peak Particle Velocity (PPV) method weighted 0.1. Fault parameter slip rates found by ratio of maximum estimated displacement on Ghost Dance to Bow Ridge Fault. Displacement estimates are (25 m, 30 m, 35 m) from Day *et al.* USGS, written communication, 1996b).

TABLE SBK-5
FAULT DISPLACEMENT HAZARD CHARACTERIZATION DATA, POINTS 3-8
(Continued)

Stress activation factor computed using ESF stress tensor and orientation of Ghost Dance fault reported by Day *et al.* (USGS, written communication, 1996b). Fault pole trends 090°, plunges 15° with an assumed variation of $\pm 10^\circ$ in both trend and plunge.

Sun Dance Fault: Slip rate methods - Geologic History weighted 0.6, with application of Models 1, 2 & 3 as described in manuscript. Fault Parameter method weighted 0.2. Event Frequency - Distributed Rupture method weighted 0.2. Fault parameter slip rates found by ratio of maximum estimated displacement on Sun Dance to Bow Ridge Fault multiplied. Displacement estimates are (6 m, 15 m, 20 m) from Day *et al.* (USGS, written communication, 1996b). Stress activation factor computed using ESF stress tensor and orientation of Sun Dance fault reported by Day *et al.* (USGS, written communication, 1996b). Fault pole trends 050°, plunges 00° with an assumed variation of $\pm 10^\circ$ in both trend and plunge.

Point 6 west of Dune Wash: The amount of displacement on this fault is assumed to be between 2 and 20 meters. We assume a minimum of 2 m, a maximum of 20 m and a preferred value of 11 m (the average of the minimum and maximum displacement estimates for this type of intrablock fault (SSC Facilitation Team memo of January 16, 1997 entitled 'Fault Displacement Hazard Guidance). Geohistory (0.6), Fault Parameter (0.2), Distributed Rupture (0.1) and Peak Particle Velocity (PPV) (0.1) methods are all implemented with appropriate weighting in closed brackets (wt).

Points 7 and 8: Value of 10 cm slip is used for both geohistory and fault parameter methods. No fault orientation is specified, so we assume that slip tendency is 1.0. Slip of less than 10 cm is not specified, so we assume that slip rates are less than those calculated using the geohistory and fault parameter methods for slip of 10 cm. Geohistory (0.6), Fault Parameter (0.2), Distributed Rupture (0.1) and Peak Particle Velocity (PPV) (0.1) methods are all implemented with appropriate weighting in ().

Intact Rock: We use an event frequency approach by assuming that the annual probability of fracturing is less than $1 / (\text{age of intact rock})$. Consider an unfractured wall of Tiva Canyon Tuff in the repository. The chance of fracturing is less than $1 / (1.2e7 \text{ years}) = 8.3e-8 \text{ yr}^{-1}$. We assume that if new fracturing does occur, the maximum amount of shear offset will be less than 10 cm, and use the event frequency displacement variability function $P(U/Dm)$ to estimate the probability of the amount of slip.

**TABLE SBK-6
TRENCHING DATA USED TO DEVELOP DISTRIBUTIONS FOR DISPLACEMENT PER EVENT**

Fault	Trench	Event	U (cm)			U/Uap*			U/Ua**			U/Um***		
			min.	pref.	max.	min	pref.	max	min	pref	max	min.	pref	max
Bow Ridge	T-14D	Z	1	1	5	0.19	0.06	0.12	0.092	0.092	0.220	0.054	0.054	0.109
		Z	15	44	80	2.86	2.44	1.88	1.386	4.066	3.516	0.810	2.377	1.749
		Y	4	13	45	0.76	0.72	1.06	0.370	1.201	1.978	0.216	0.702	0.984
		X	1	14	40	0.19	0.78	0.94	0.092	1.294	1.758	0.054	0.756	0.874
N. Crater Flat	CFFT2-a	Z	1	3	5	0.04	0.10	0.15	0.056	0.114	0.190	0.030	0.055	0.092
		Y	1	5	5	0.04	0.17	0.15	0.056	0.190	0.190	0.030	0.092	0.092
		X	35	40	45	1.38	1.35	1.36	1.968	1.522	1.713	1.033	0.734	0.826
		W	45	50	55	1.77	1.69	1.67	2.531	1.903	2.093	1.328	0.917	1.009
		V	45	50	55	1.77	1.69	1.67	2.531	1.903	2.093	1.328	0.917	1.009
S. Crater Flat	CFFT1	Z	7.5	8	10				0.795	0.575	0.562	0.479	0.319	0.295
		Y	7.5	10	10				0.795	0.719	0.562	0.479	0.398	0.295
	CFFT1-a	Z	2	18	18	0.25	1.13	0.83	0.212	1.295	1.012	0.128	0.717	0.531
		Y	5	10	15	0.63	0.63	0.69	0.530	0.719	0.844	0.319	0.398	0.443
		X	17	20	32	2.13	1.25	1.47	1.801	1.438	1.799	1.085	0.796	0.944
Fatigue Wash	CF-1	Z	0	1	5	0.00	0.02	0.10	0.000	0.043	0.131	0.000	0.021	0.058
		Y	15	25	35	0.37	0.54	0.67	1.205	1.066	0.918	0.684	0.527	0.408
		X	100	105	110	2.44	2.27	2.11	8.034	4.477	2.885	4.557	2.212	1.282
		W	49	54	59	1.20	1.17	1.13	3.937	2.303	1.547	2.233	1.138	0.688
Iron Ridge	SCF-T2	Z	1	5	10	0.02	0.08	0.13	0.085	0.423	0.688	0.048	0.242	0.377
		Y	50	70	90	1.17	1.14	1.13	4.225	5.916	6.191	2.423	3.393	3.395
		X	70	100	130	1.64	1.63	1.63	5.916	8.451	8.943	3.393	4.846	4.904
		W	50	70	90	1.17	1.14	1.13	4.225	5.916	6.191	2.423	3.393	3.395
Stagecoach Rd	SCR-T1	Z	40	40	82	1.51	0.89	1.01	2.966	2.966	3.678	1.653	1.653	1.838
		Y	28	42	70	1.06	0.93	0.86	2.076	3.115	3.140	1.157	1.736	1.569
		X	14	47	99	0.53	1.04	1.22	1.038	3.486	4.441	0.579	1.943	2.219

TABLE SBK-6
TRENCHING DATA USED TO DEVELOP DISTRIBUTIONS FOR DISPLACEMENT PER EVENT
(Continued)

Fault	Trench	Event	U (cm)			U/Uap*			U/Ua**			U/Um***		
			min.	pref.	max.	min	pref.	max	min	pref	max	min.	pref	max
		W	24	51	74	0.91	1.13	0.91	1.780	3.782	3.319	0.992	2.108	1.658
	SCR-T3	Z	25	43	66	1.04	0.76	0.84	1.854	3.189	2.960	1.033	1.777	1.479
		Y	20	59	77	0.83	1.04	0.98	1.483	4.375	3.454	0.827	2.439	1.726
		X	25	57	84	1.04	1.01	1.07	1.854	4.227	3.768	1.033	2.356	1.882
		W	26	67	87	1.08	1.19	1.11	1.928	4.969	3.902	1.075	2.770	1.950
Solitario Cyn	SCFT-1	Z	1	10	20				0.041	0.249	0.498	0.020	0.109	0.219
		Y	10	70	90				0.406	1.742	2.240	0.199	0.765	0.984
	SCFT-3	Z	1	10	20				0.041	0.249	0.498	0.020	0.109	0.219
		W	20	35	50				0.812	0.871	1.244	0.397	0.383	0.547
	SCFT-T4	Z	1	5	20	0.10	0.27	0.67	0.041	0.124	0.498	0.020	0.055	0.219
		Y	20	30	40	1.94	1.64	1.33	0.812	0.747	0.995	0.397	0.328	0.437
		W	10	20	30	0.97	1.09	1.00	0.406	0.498	0.747	0.199	0.219	0.328
	SCFT-8	Z	5	10	20	0.13	0.19	0.30	0.203	0.249	0.498	0.099	0.109	0.219
		Y	100	120	140	2.58	2.29	2.07	4.062	2.986	3.484	1.986	1.312	1.531
		X	20	30	40	0.52	0.57	0.59	0.812	0.747	0.995	0.397	0.328	0.437
		W	30	50	70	0.77	0.95	1.04	1.219	1.244	1.742	0.596	0.547	0.765
Paint Brush C.	Trench A-1	Z	5	6	10	0.43	0.35	0.41	0.224	0.157	0.200	0.112	0.070	0.084
		Y	29	39	49	2.48	2.25	2.01	1.301	1.023	0.981	0.650	0.455	0.411
		X	1	7	14	0.09	0.40	0.58	0.045	0.184	0.280	0.022	0.082	0.117
		W	100						4.486	0.000	0.000	2.241	0.000	0.000
	Trench BB4	Z	1	44	72	0.03	0.49	0.47	0.045	1.154	1.441	0.022	0.513	0.604
		Y	16	28	56	0.49	0.31	0.36	0.718	0.734	1.121	0.359	0.326	0.470
		X	35	47	69	1.07	0.52	0.45	1.570	1.233	1.381	0.784	0.548	0.579

TABLE SBK-6
TRENCHING DATA USED TO DEVELOP DISTRIBUTIONS FOR DISPLACEMENT PER EVENT
(Continued)

Fault	Trench	Event	U (cm)			U/Uap*			U/Ua**			U/Um***		
			min.	pref.	max.	min	pref.	max	min	pref	max	min.	pref	max
		W	88	167	205	2.70	1.86	1.33	3.947	4.379	4.104	1.972	1.947	1.720
		V	1	142	222	0.03	1.59	1.44	0.045	3.724	4.444	0.022	1.655	1.863
		U	12	105	257	0.37	1.17	1.66	0.538	2.754	5.145	0.269	1.224	2.156
		T	75	94	201	2.30	1.05	1.30	3.364	2.465	4.024	1.681	1.096	1.687
	MWV-T4	Z	15	20	25	0.53	0.36	0.26	0.673	0.524	0.500	0.336	0.233	0.210
		Y	44	62	77	1.56	1.13	0.80	1.974	1.626	1.542	0.986	0.723	0.646
		X	53	98	143	1.88	1.78	1.49	2.377	2.570	2.863	1.188	1.142	1.200
		W	1	40	140	0.04	0.73	1.45	0.045	1.049	2.803	0.022	0.466	1.175
Windy Wash	T-CF2	Z	1	4	10	0.03	0.10	0.20	0.018	0.066	0.157	0.007	0.026	0.062
		Y	14	20	24	0.44	0.51	0.47	0.253	0.328	0.376	0.104	0.132	0.150
		X	20	23	30	0.63	0.58	0.59	0.361	0.377	0.471	0.148	0.151	0.187
		W	18	20	25	0.56	0.51	0.49	0.325	0.328	0.392	0.133	0.132	0.156
		V	70	73	83	2.19	1.85	1.62	1.264	1.198	1.302	0.518	0.481	0.517
		U	30	45	60	0.94	1.14	1.17	0.542	0.738	0.941	0.222	0.296	0.374
		T	38	50	78	1.19	1.27	1.52	0.686	0.821	1.224	0.281	0.329	0.486
		S	65	80	100	2.03	2.03	1.95	1.173	1.313	1.569	0.481	0.527	0.623
		Z	1	4	10	0.03	0.11	0.23	0.018	0.066	0.157	0.007	0.026	0.062
		Y	8	12	18	0.28	0.34	0.41	0.144	0.197	0.282	0.059	0.079	0.112
		X	45	50	53	1.56	1.43	1.22	0.812	0.821	0.831	0.333	0.329	0.330
		W	38	42	52	1.32	1.20	1.20	0.686	0.689	0.816	0.281	0.277	0.324
		V	24	28	30	0.83	0.80	0.69	0.433	0.459	0.471	0.178	0.184	0.187
		U	15	19	24	0.52	0.54	0.55	0.271	0.312	0.376	0.111	0.125	0.150
		T	55	60	65	1.90	1.71	1.50	0.993	0.985	1.020	0.407	0.395	0.405
		S	45	65	95	1.56	1.86	2.19	0.812	1.067	1.490	0.333	0.428	0.592
	TCF-3	Z	4	6	10	0.27	0.29	0.34	0.072	0.098	0.157	0.030	0.040	0.062
		Y	10	20	32	0.68	0.96	1.10	0.181	0.328	0.502	0.074	0.132	0.199

TABLE SBK-6
TRENCHING DATA USED TO DEVELOP DISTRIBUTIONS FOR DISPLACEMENT PER EVENT
(Continued)

Fault	Trench	Event	U (cm)			U/Uap*			U/Ua**			U/Um***		
			min.	pref.	max.	min	pref.	max	min	pref	max	min.	pref	max
		X	33	42	54	2.24	2.02	1.86	0.596	0.689	0.847	0.244	0.277	0.337
		W	12	15	20	0.81	0.72	0.69	0.217	0.246	0.314	0.089	0.099	0.125
		Z	1	4	6	0.03	0.10	0.12	0.018	0.066	0.094	0.007	0.026	0.037
		Y	25	33	42	0.82	0.83	0.87	0.451	0.542	0.659	0.185	0.217	0.262
		X	71	87	96	2.33	2.19	1.98	1.282	1.428	1.506	0.525	0.573	0.598
		W	25	35	50	0.82	0.88	1.03	0.451	0.574	0.784	0.185	0.231	0.312
	T?	Z	1	3	6	0.03	0.07	0.12	0.018	0.049	0.094	0.007	0.020	0.037
		Y	25	35	45	0.72	0.83	0.91	0.451	0.574	0.706	0.185	0.231	0.281
		X	78	88	98	2.25	2.10	1.97	1.408	1.444	1.537	0.577	0.580	0.611

Notes

* Uap is the average of measurements for fault. Minimum, preferred, and maximum values are obtained by averaging min., pref., and max. columns, respectively for U.

** Ua is computed using minimum, preferred, and maximum lengths of faults from Table SBK-3 and relationship

$$\log(Ua) = -1.99 + 1.24 \times \log(L)$$

*** Um is computed using minimum, preferred, and maximum lengths of faults from Table SBK-3 and relationship

$$\log(Ua) = -1.98 + 1.51 \times \log(L)$$

TABLE SBK-7
DATA USED TO DEVELOP DISTRIBUTION FOR U/D_m

Fault	Trench	Displacement, U (cm)	Cumulative Displacement D _m (cm)	U/D _m	
Solitario Canyon	SCF-T1	10	45313	2.21E-04	
		70		1.54E-03	
	SCF-T3	10		2.21E-04	
		80		1.77E-03	
	SCF-T4	35		7.72E-04	
		5		1.10E-04	
		30		6.62E-04	
		20		4.41E-04	
	SCF-T8	10		2.21E-04	
		120		2.65E-03	
30		6.62E-04			
50		1.10E-03			
Bow Ridge	Trench 14D	44	7500	5.87E-03	
		13		1.73E-03	
		14		1.87E-03	
Paintbrush	Trench A1	6	35000	1.71E-04	
		39		1.11E-03	
		7		2.00E-04	
		BB-4		44	1.26E-03
	28			8.00E-04	
	47			1.34E-03	
	MWV-T4			167	4.77E-03
				142	4.06E-03
				105	3.00E-03
				94	2.69E-03
20			5.71E-04		
62			1.77E-03		
Stagecoach Road	SCR-T1	98	25625	2.80E-03	
		40		1.14E-03	
		40		1.56E-03	
		42		1.64E-03	
	SCR-T3	47		1.83E-03	
		51		1.99E-03	
		43		1.68E-03	
		59		2.30E-03	
Windy Wash	CF-2nwall	57	20000	2.22E-03	
		67		2.61E-03	
		4		2.00E-04	
		20		1.00E-03	
		23		1.15E-03	
		20		1.00E-03	
	CF-2swall	73		3.65E-03	
		45		2.25E-03	
		50		2.50E-03	
		80		4.00E-03	
		4	2.00E-04		
		12	6.00E-04		
		50	2.50E-03		

TABLE SBK-7
DATA USED TO DEVELOP DISTRIBUTION FOR U/D_m
(Continued)

Fault	Trench	Displacement, U (cm)	Cumulative Displacement D _m (cm)	U/D _m
		42		2.10E-03
		28		1.40E-03
		19		9.50E-04
		60		3.00E-03
		65		3.25E-03
	CF-3nwall	4		2.00E-04
		33		1.65E-03
		87		4.35E-03
		35		1.75E-03
	CF-3swall	3		1.50E-04
		35		1.75E-03
		88		4.40E-03

<i>Tectonic Model</i>	<i>Specific Models</i>	<i>Quaternary Dike Injection affects rates?</i>
-----------------------	------------------------	---

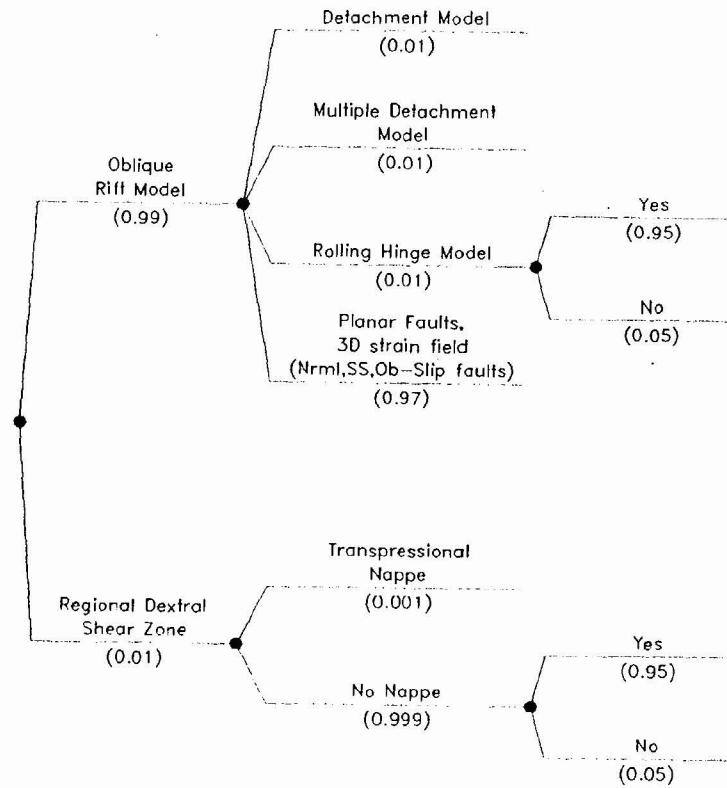


Figure SBK-1

Logic tree for tectonic models

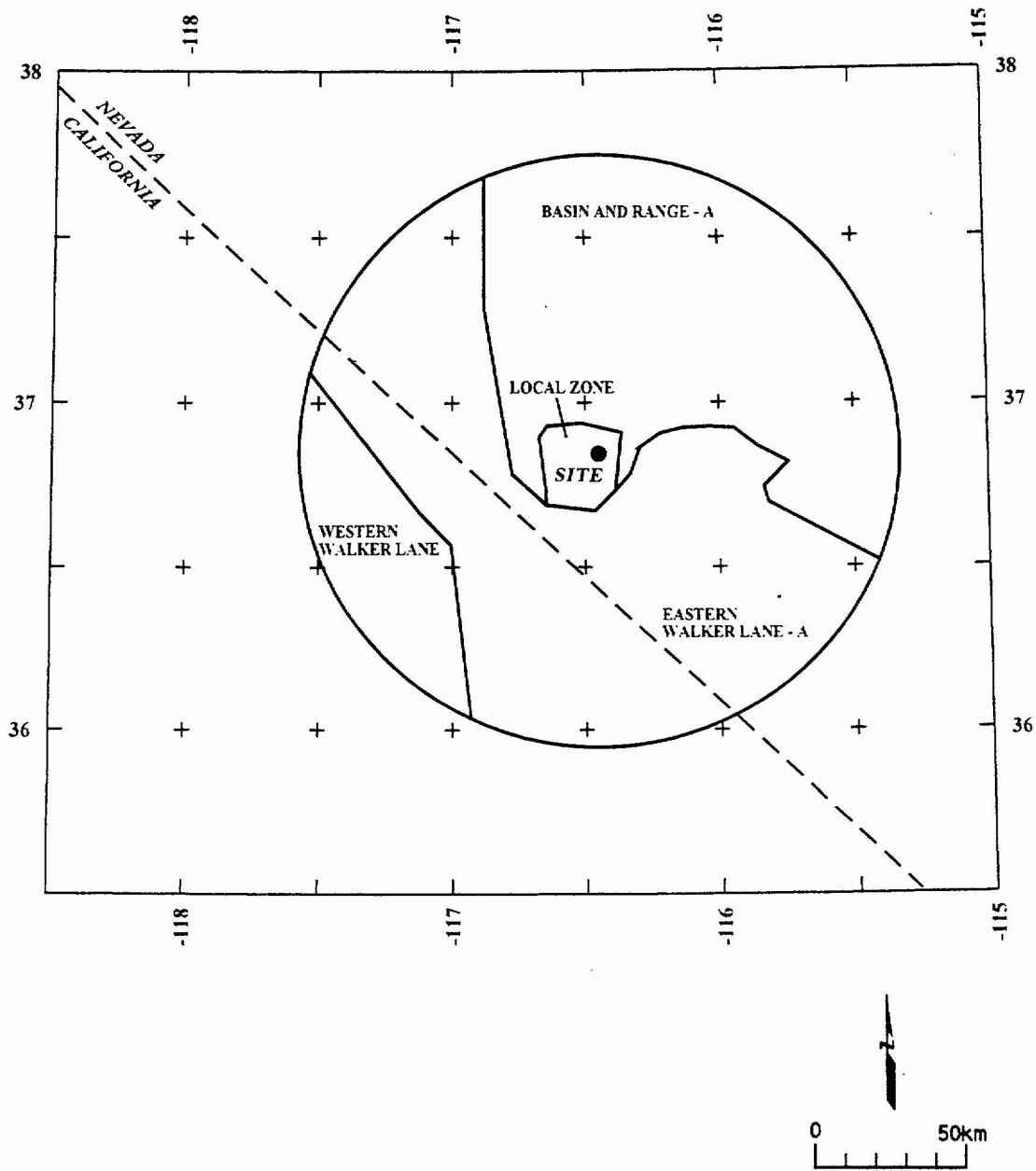


Figure SBK-2 Map showing boundaries of seismic source zones, Model A.

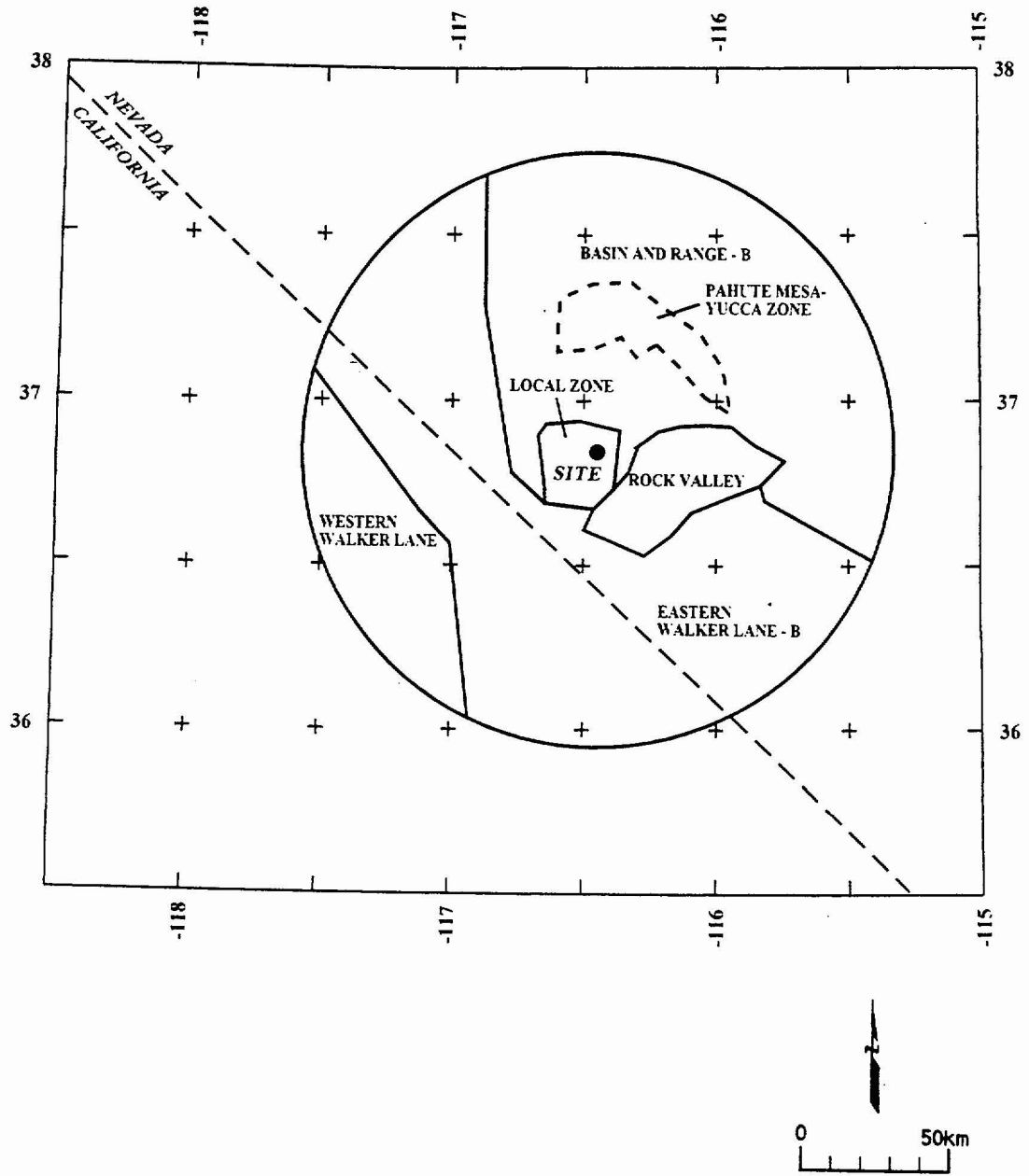


Figure SBK-3 Map showing the boundaries of seismic source zones, Model B.

Source Model	Source	Earthquake Catalog	Maximum Magnitude	Adjustment For NTS
--------------	--------	--------------------	-------------------	--------------------

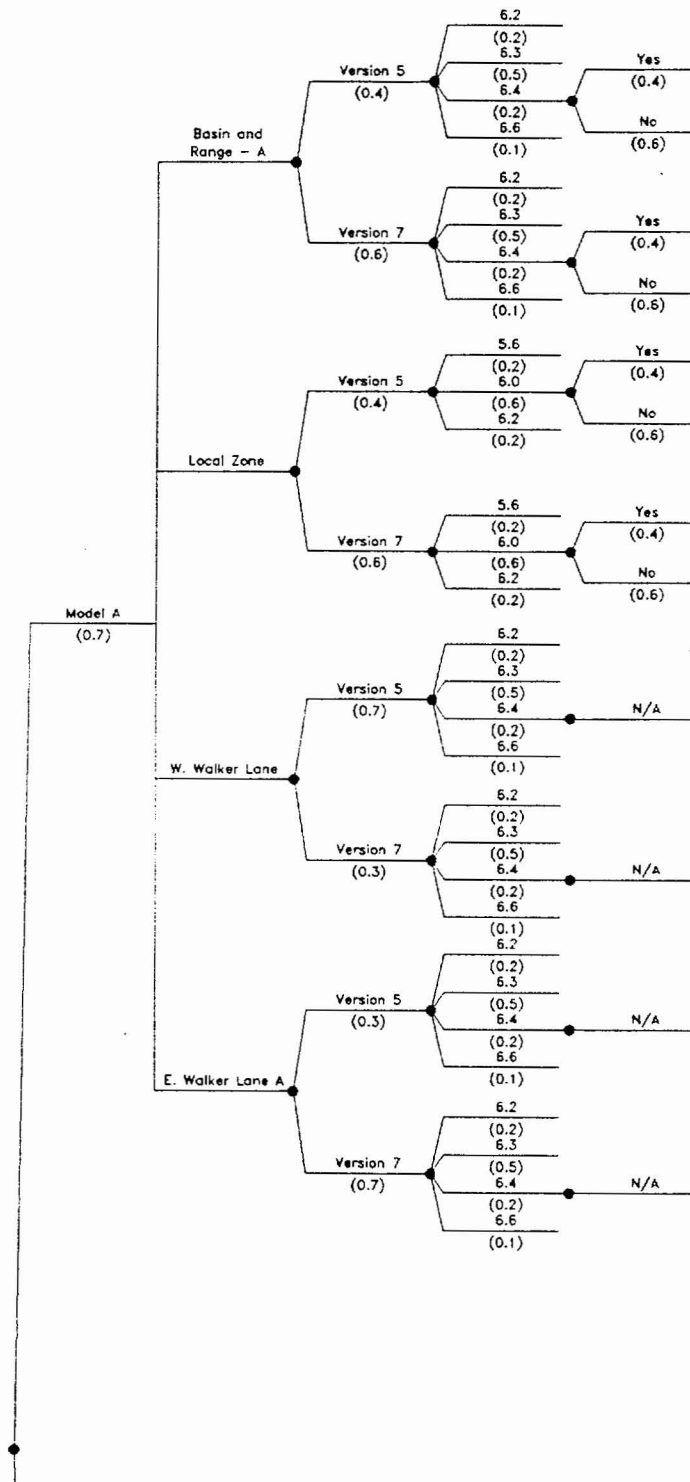


Figure SBK-4 Logic tree for characterizing areal source zones

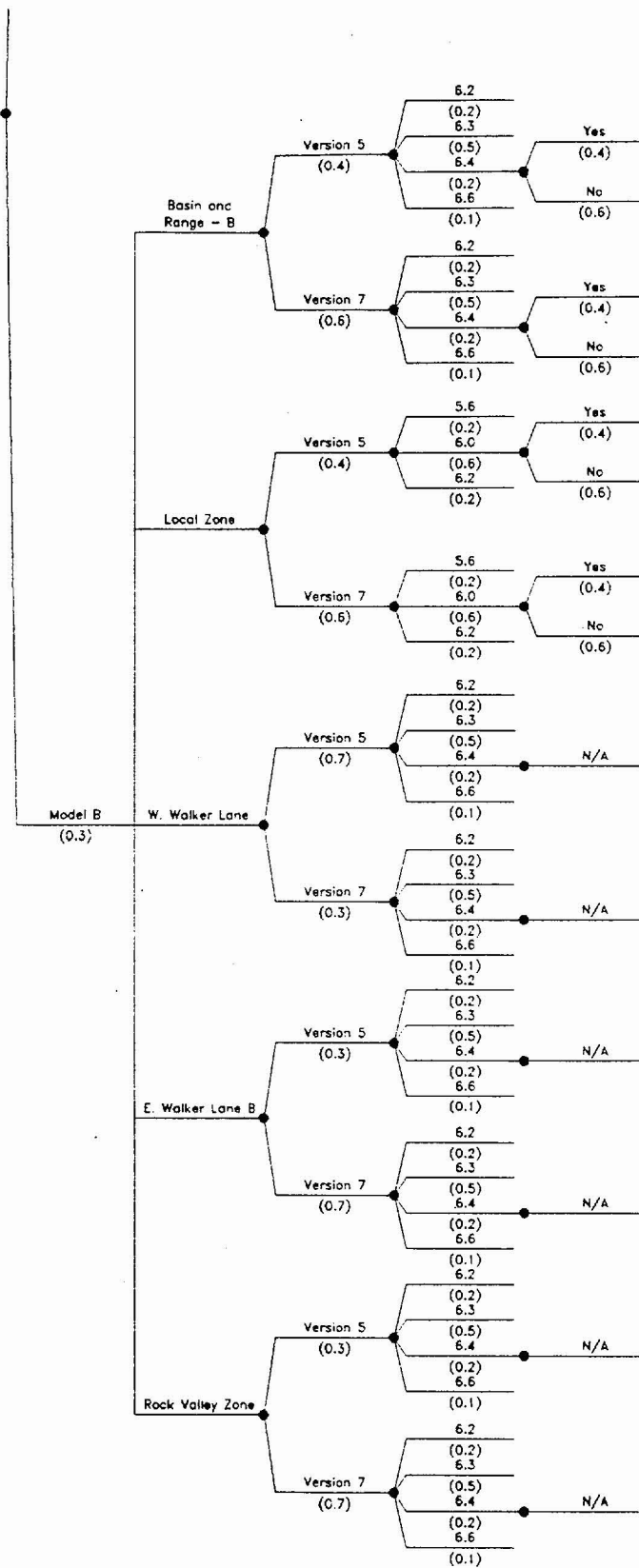
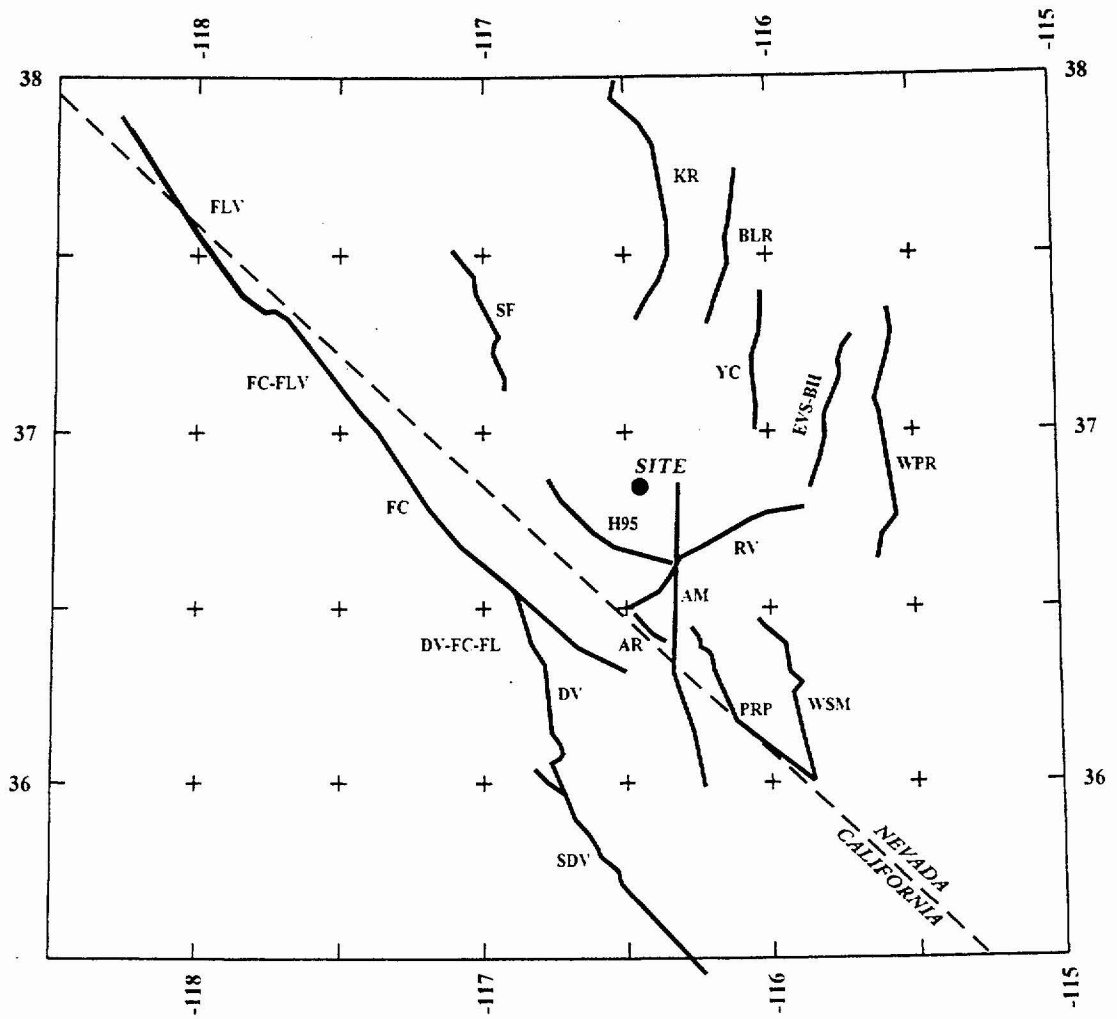


Figure SBK-4 (Cont'd.) Logic tree for characterizing areal source zones



NOTE: Fault names are listed in Table SBK-1

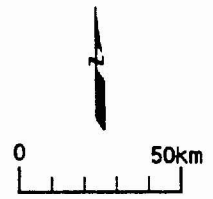


Figure SBK-5 Map showing regional faults included in the seismic source model

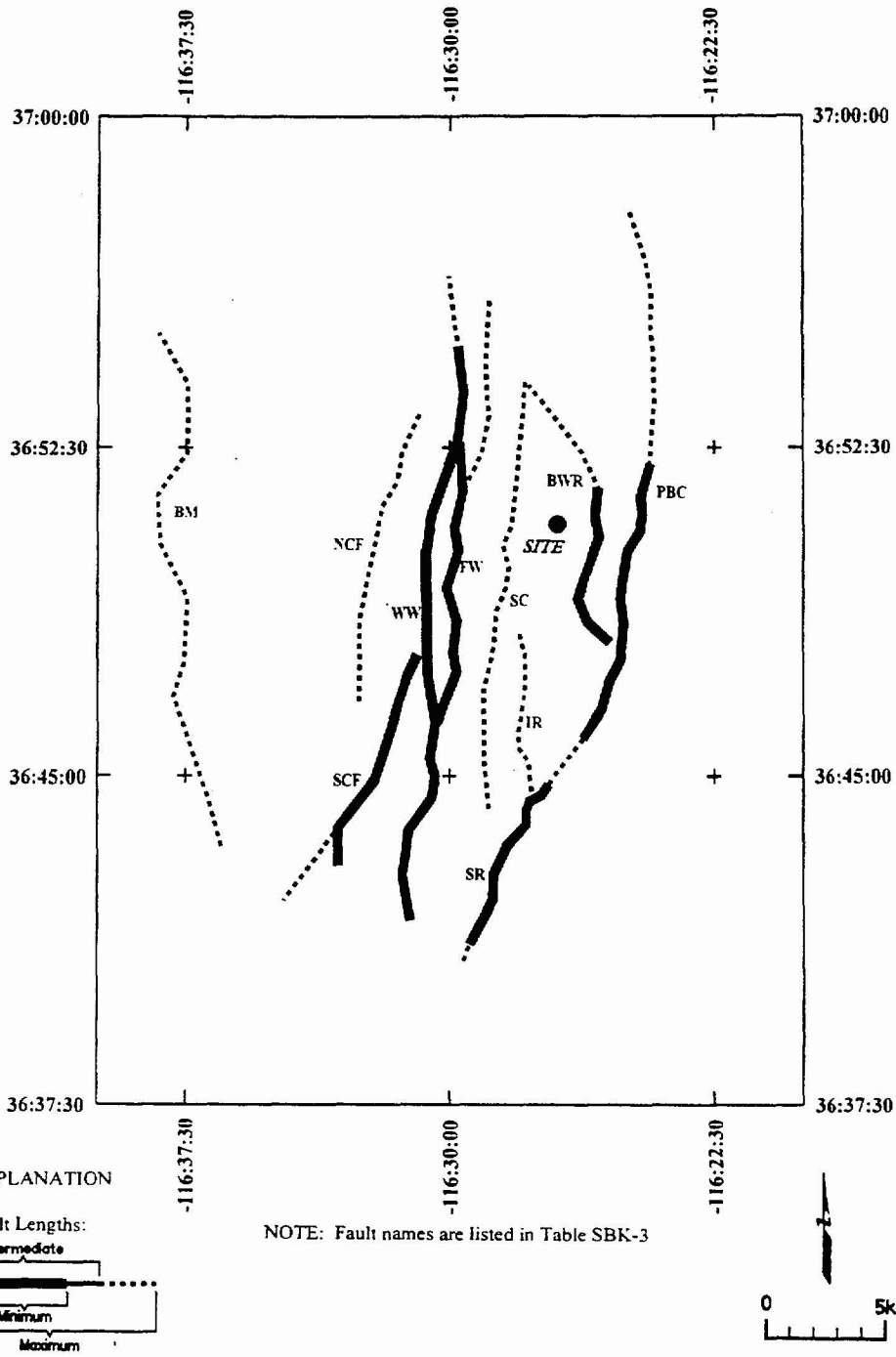


Figure SBK-6 Map showing local fault sources included in the seismic source model

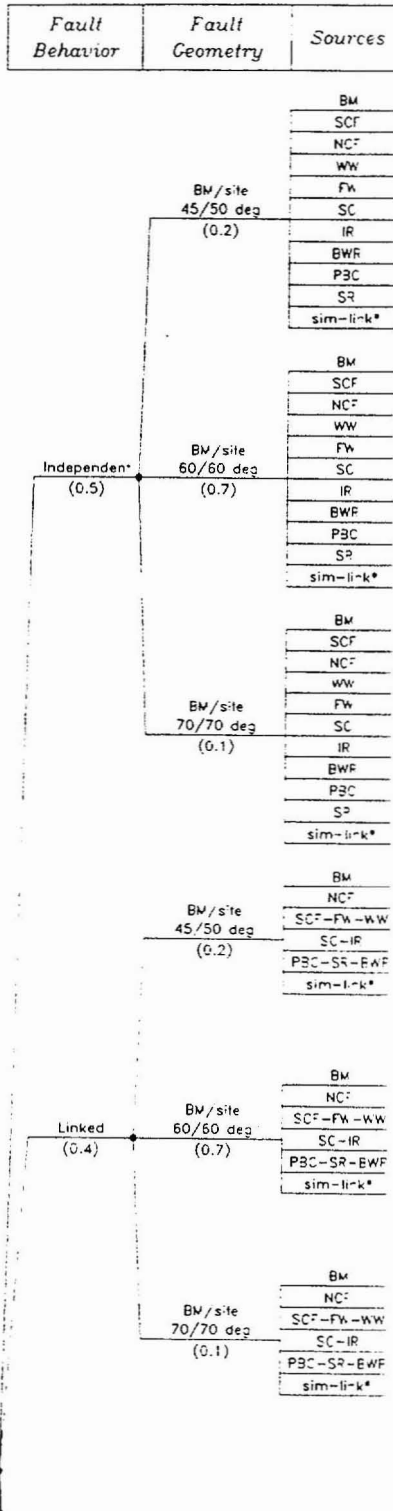
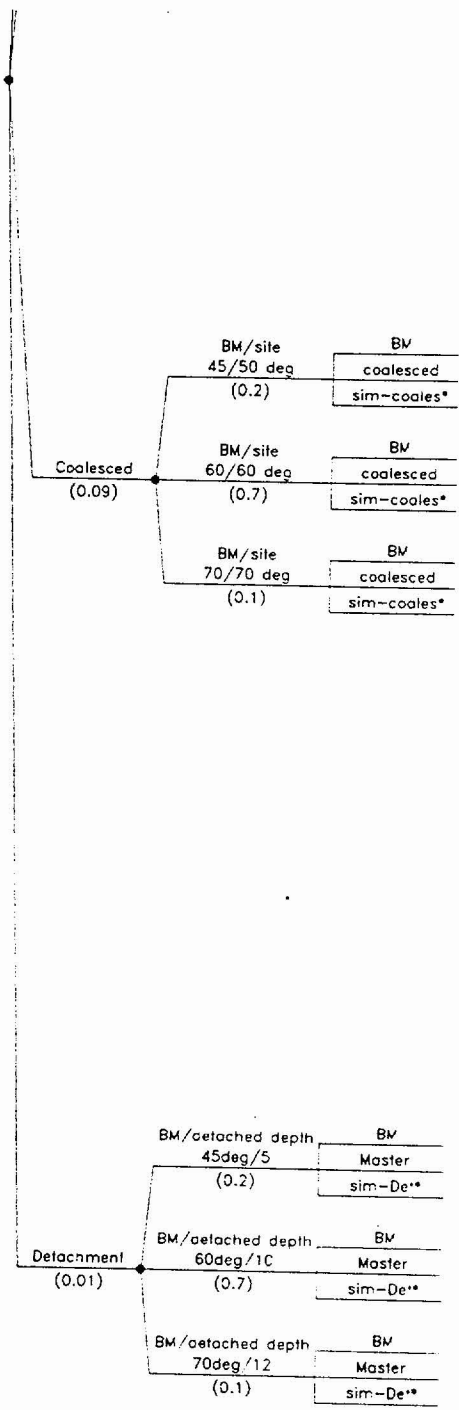


Figure SBK 7 Logic tree for local faults



* sim-link, sim-coales and sim-det are synchronous rupture scenarios that act as additional sources of large events

Figure SBK 7 (Cont'd.) Logic tree for local faults

<i>Approach</i>	<i>Hazard Source</i>	<i>Excavated Fault</i>	<i>Event Frequency</i>	<i>Event Size Measure</i>	<i>Displacement Distribution</i>
-----------------	----------------------	------------------------	------------------------	---------------------------	----------------------------------

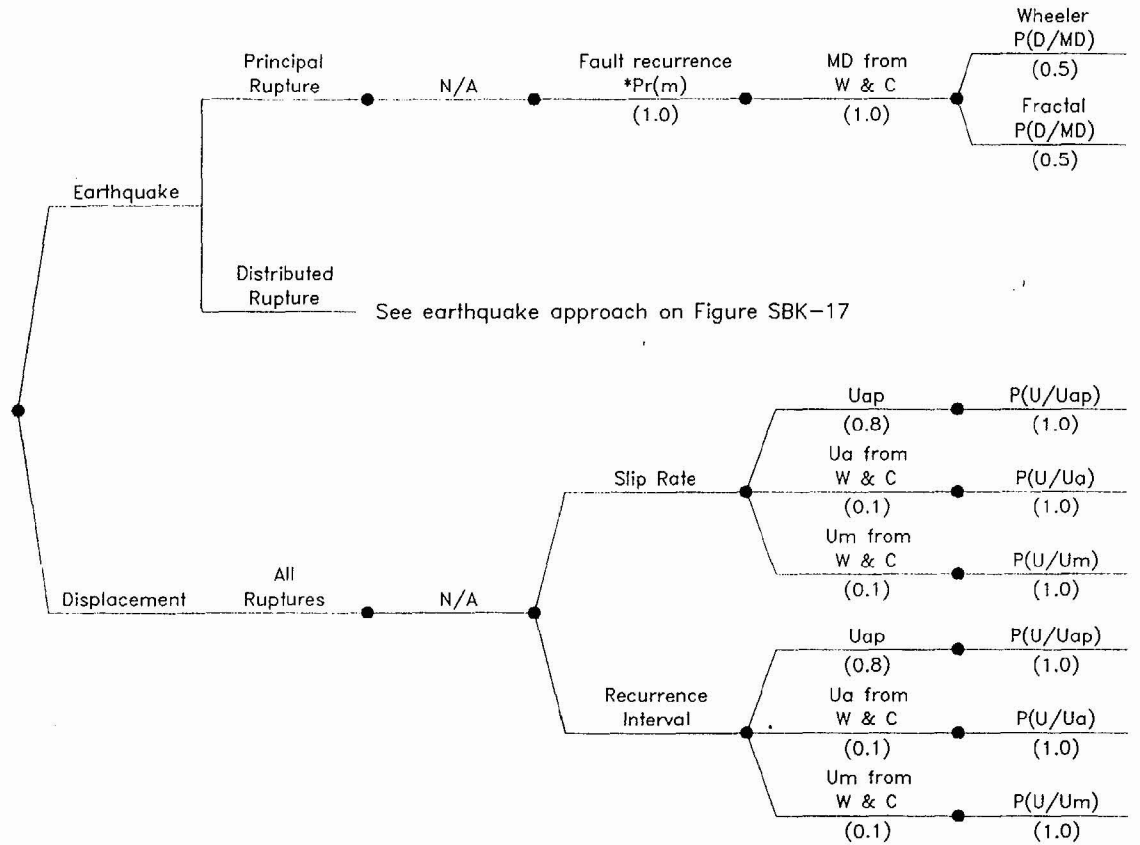


Figure SBK-8 Logic tree to characterize site with Quaternary displacement

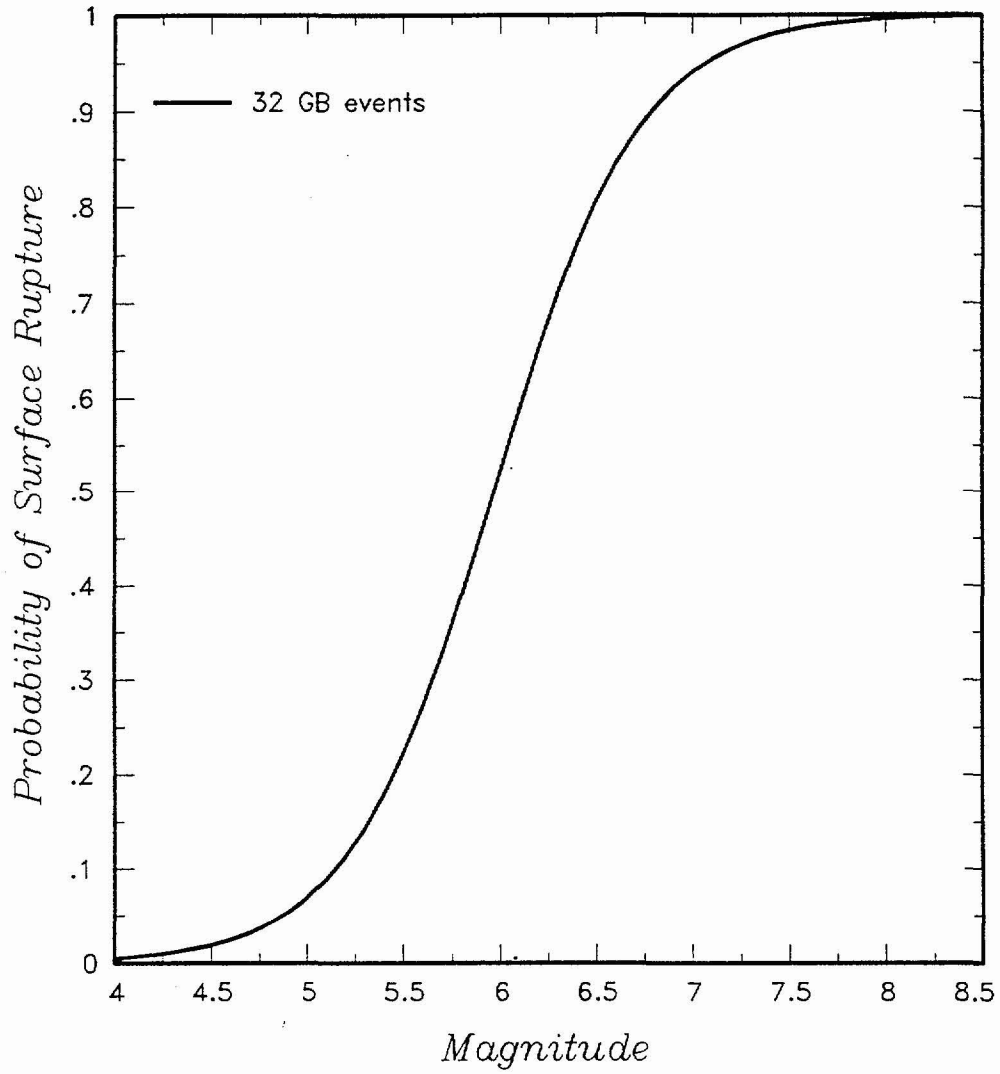


Figure SBK-9 Probability of surface rupture versus magnitude computed from data presented in S.K. Pezzopane and T.E. Dawson (USGS, written communication, 1996)

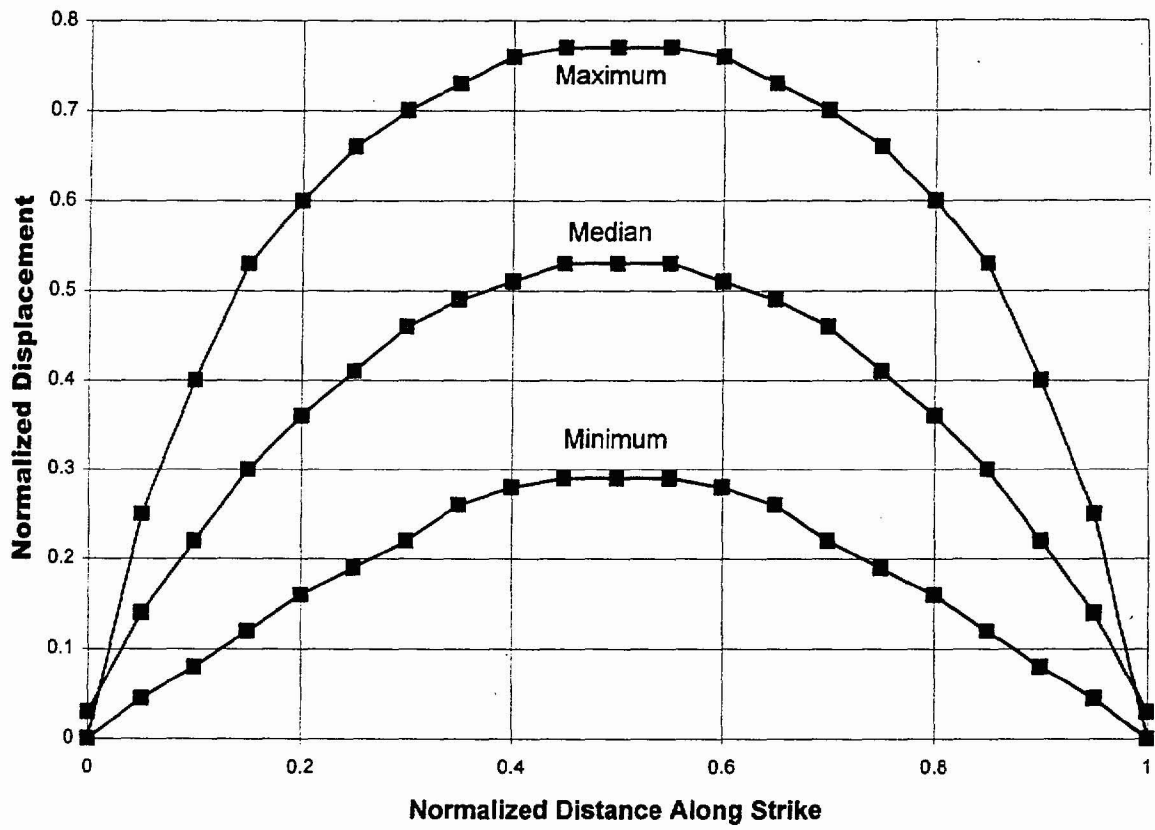


Figure SBK-10 Normalized slip along strike from five normal fault ruptures developed by ASM team from data in Wheeler (1989)

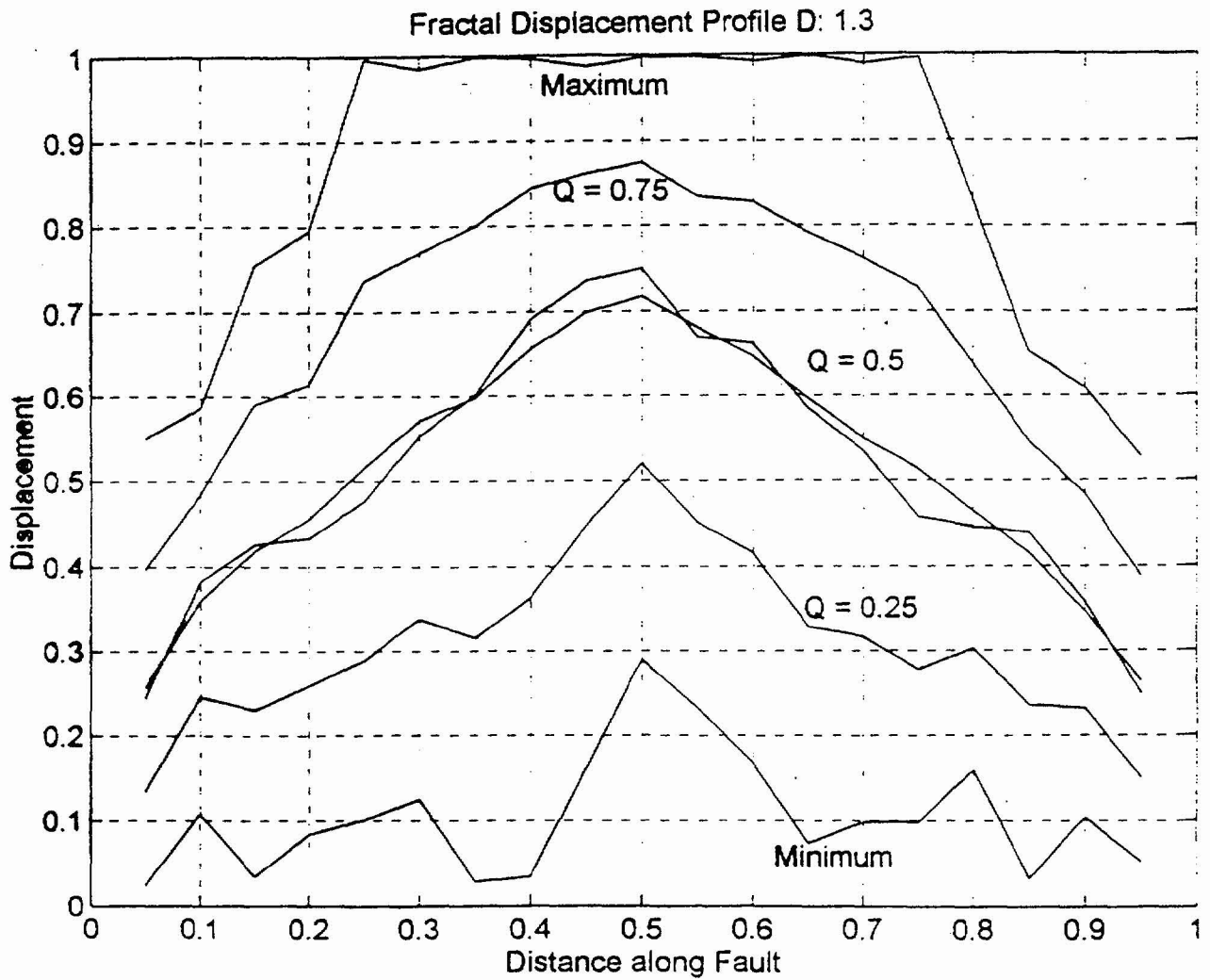


Figure SBK-11 Fractal displacement profiles developed by R. Bruhn (SBK) to predict distribution for the ratio of displacement at a point to the maximum displacement in an earthquake

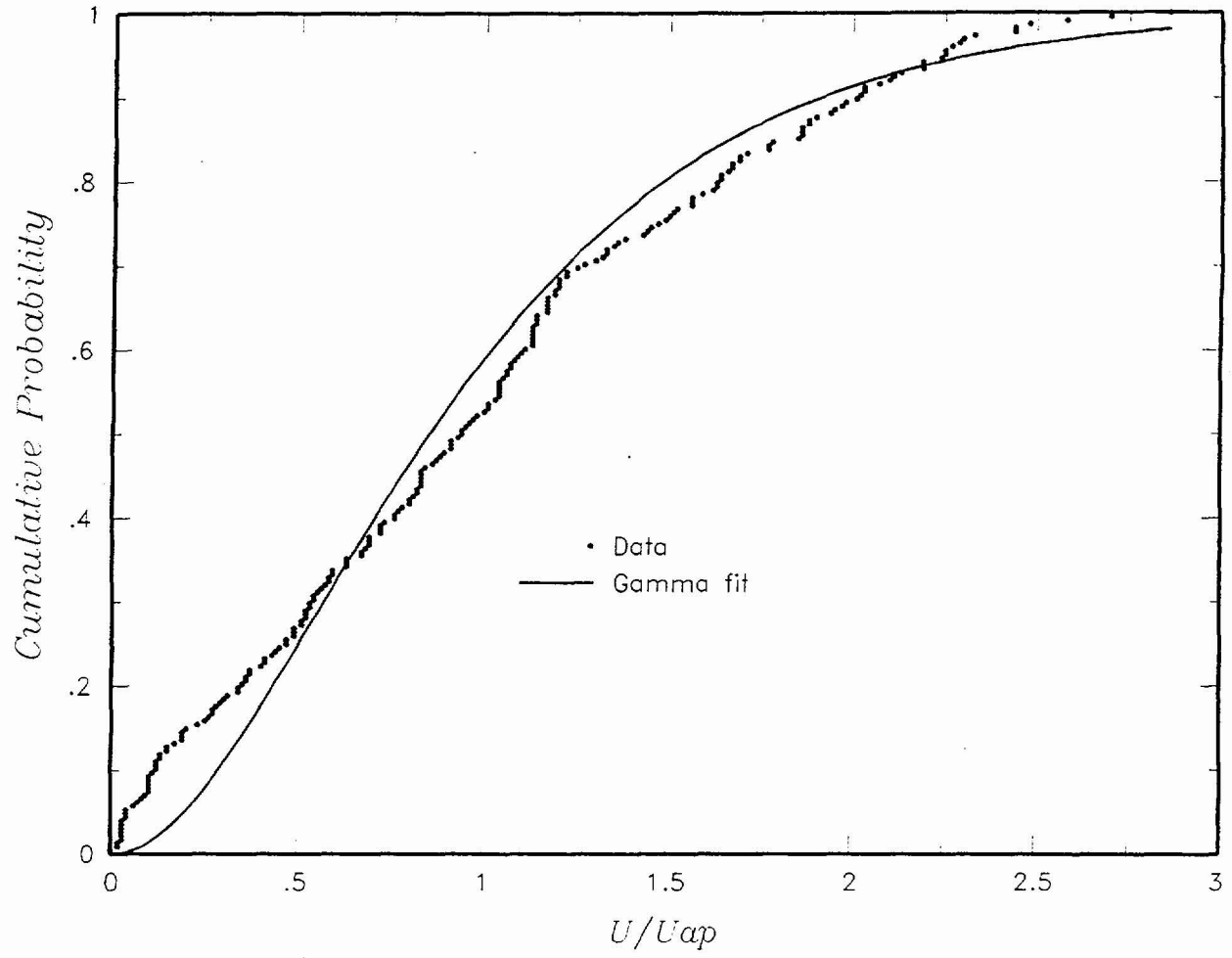


Figure SBK-12 Distribution of U/Uap

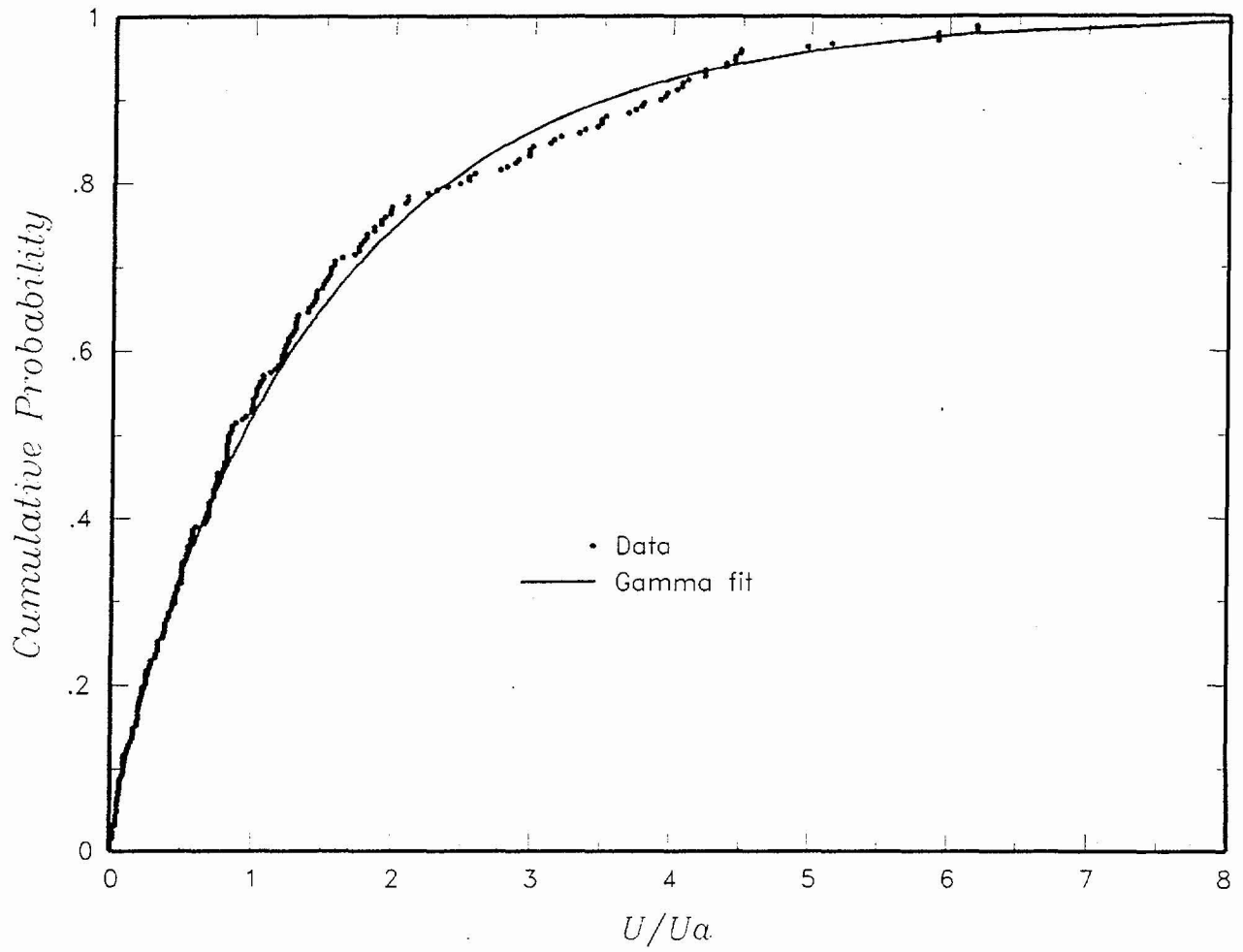


Figure SBK-13 Distribution of $U/U\alpha$

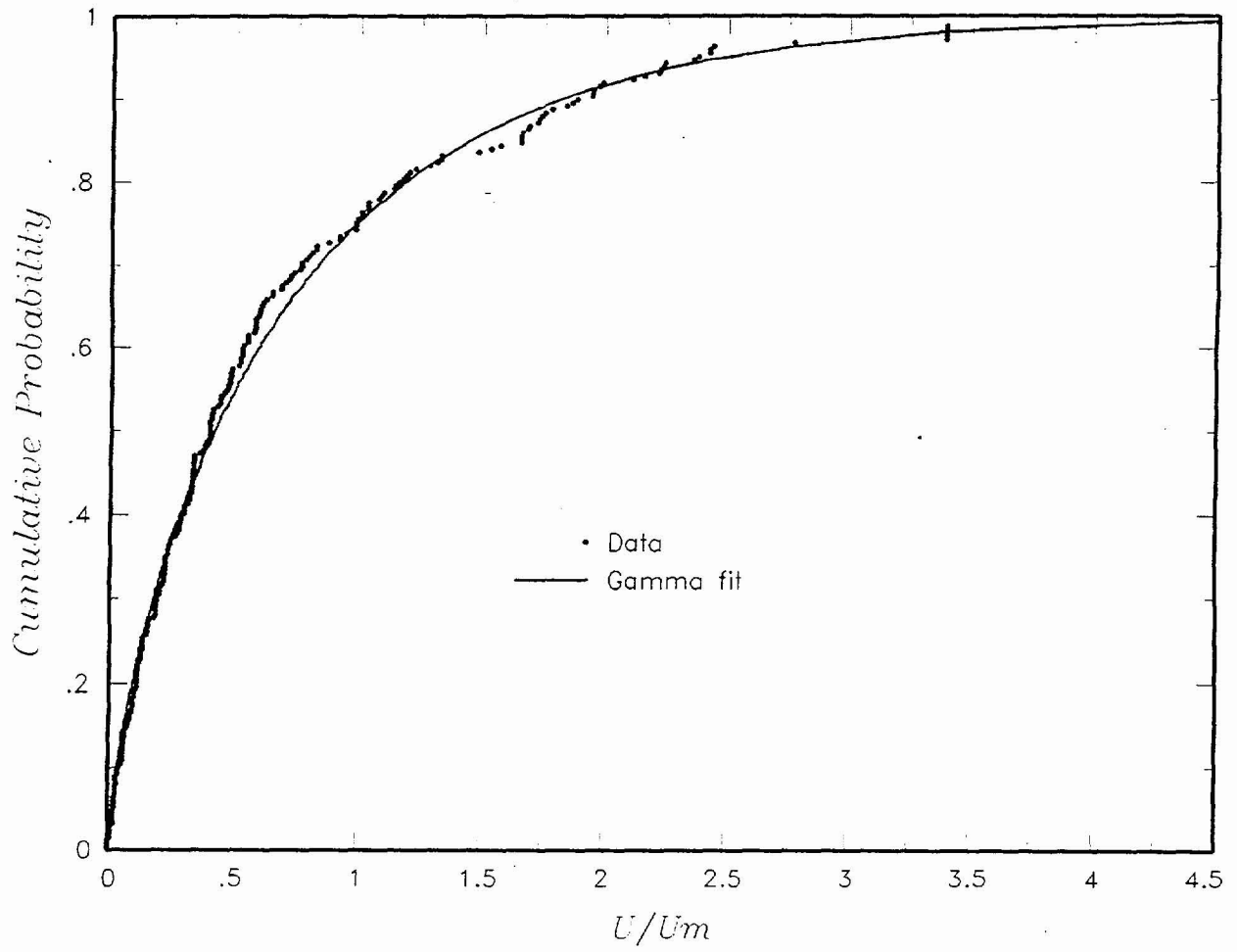


Figure SBK-14 Distribution of U/Um

<i>Approach</i>	<i>Fault Orientation Factor</i>	<i>Excavation Site</i>	<i>Frequency of Rupture</i>	<i>Slip Rate</i>	<i>Event Size Measure</i>	<i>Displacement Distribution</i>
-----------------	---------------------------------	------------------------	-----------------------------	------------------	---------------------------	----------------------------------

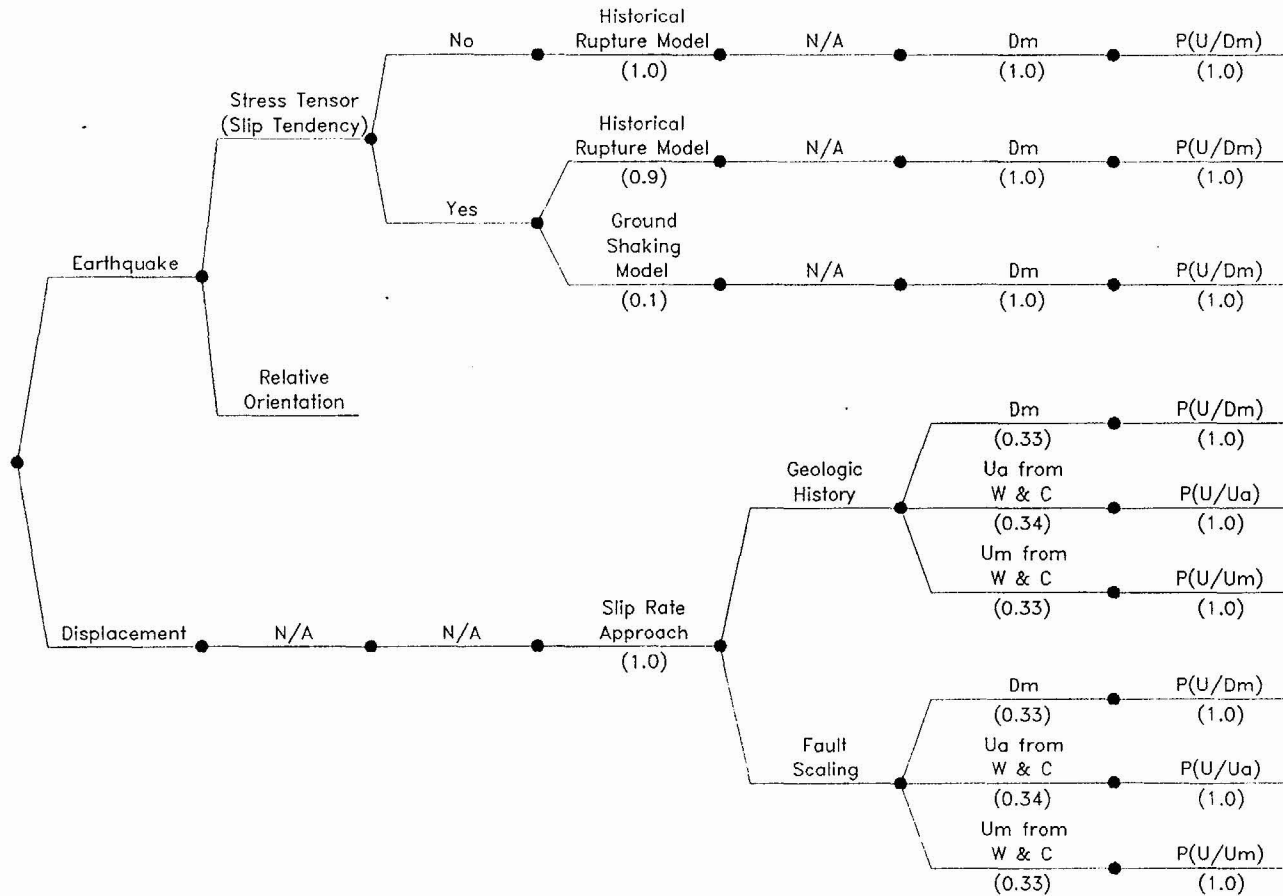


Figure SBK-15 Logic tree to characterize sites without Quaternary displacement

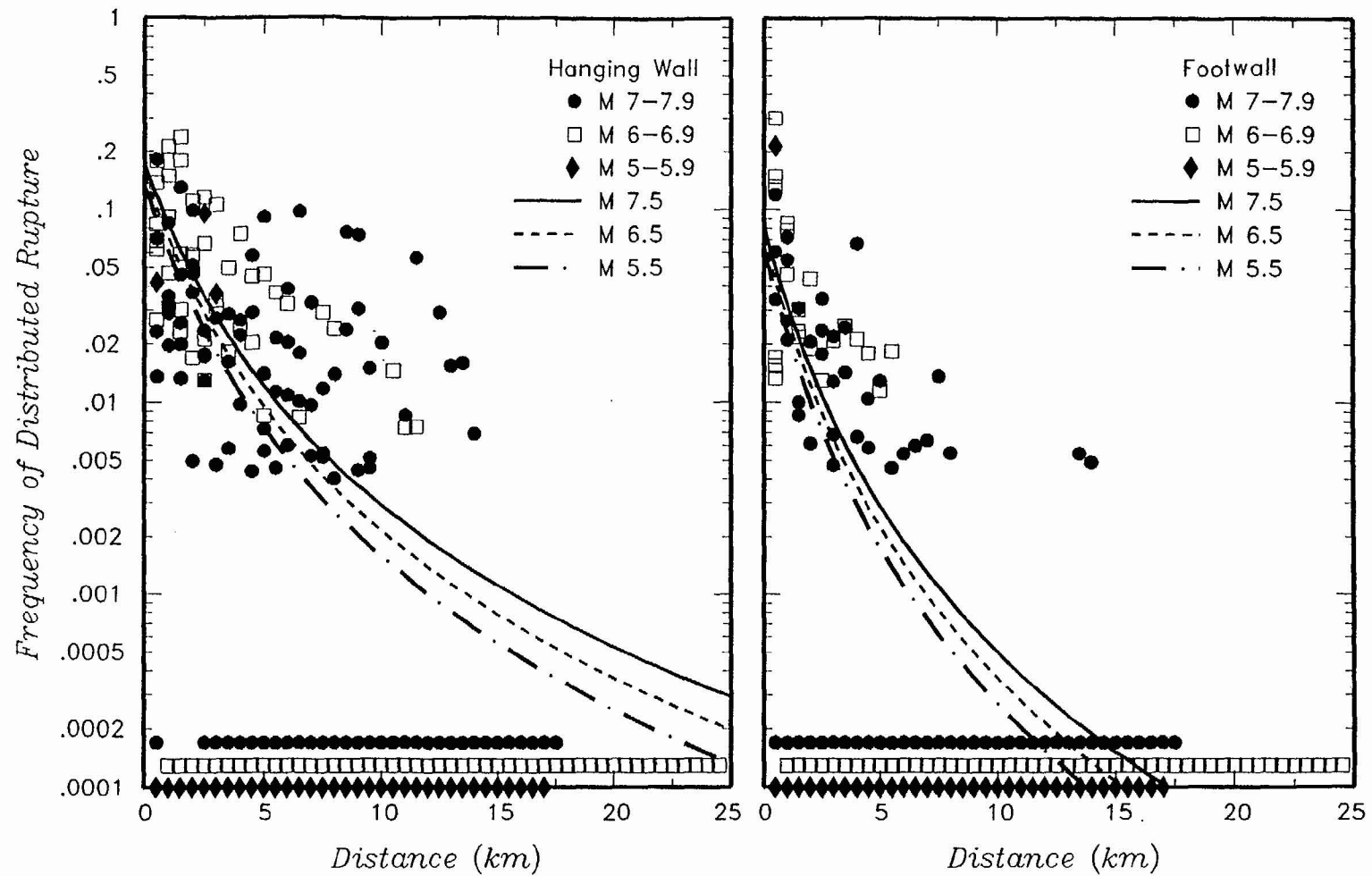


Figure SBK-16 Probability of induced distributed slip as a function of distance from the rupture and hanging wall/footwall location computed from the data presented in S.K. Pezzopane and T.E. Dawson (USGS, written communication, 1996). Curves show logit regression fits to data.

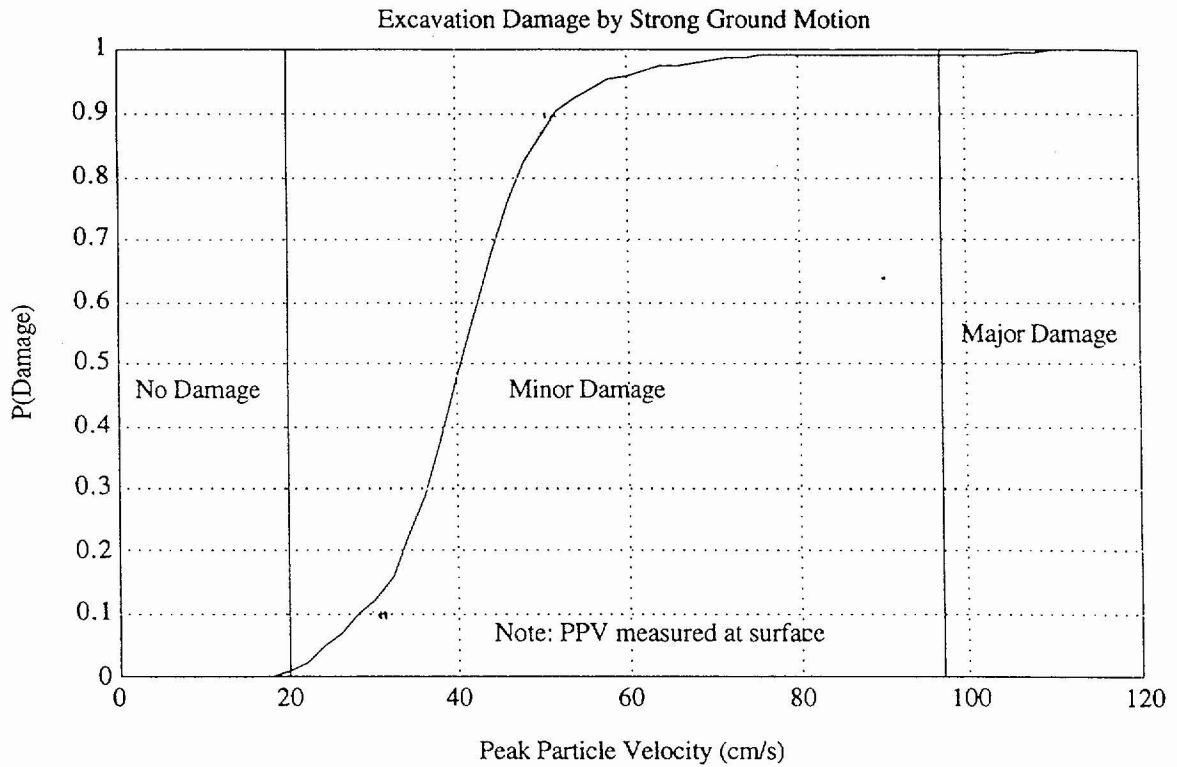


Figure SBK-17 Probability density function (sketched) for probability of initiating joint or fault displacement in an underground excavation. PDF is based on data summarized in Figure 2, page 2 of Brady (1990).

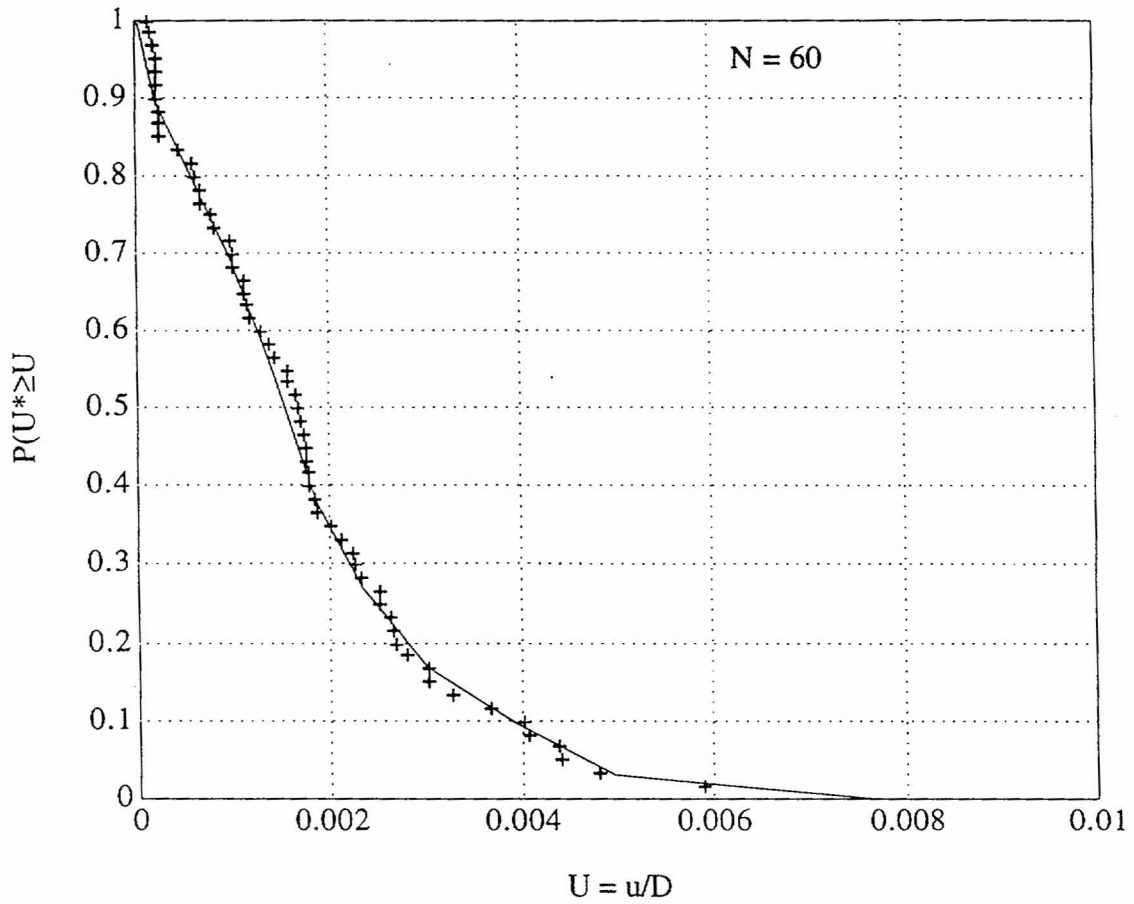


Figure SBK-18 Cumulative Probability Function $P(U/D_m)$. See Section 3.3.1.3 for discussion of derivation and use. Crosses represent data points from Yucca Mountain faults, solid line is a sketched fit to the data values.

APPENDIX SBK-1 SUMMARY OF SEISMICITY REPORTS

Our decisions and weightings for the particular locations of background source regions and the behavior of seismicity were based on published reports on seismicity in the southern Great Basin. These reports have varied in their focus and scope: There are periods of time for which minor sequences are discussed in some detail, whereas other time periods are covered only by being represented in the historical earthquake catalog. Detailed reports of the seismicity in selected regions near Yucca Mountain began with the Nuclear Testing program in the 1960s, in particular, with reports on the explosion-triggered seismicity in the Pahute Mesa area (Hamilton *et al.*, 1969a).

Meremonte and Rogers (1987) have compiled a catalog of historical earthquakes in the southern Great Basin from 1868 through 1978. This established the historical catalog to the time of the installation of the southern Great Basin regional seismic network in 1978; Meremonte and Rogers (1987) provide a full bibliography of sources for that historical compilation. In the 1930s, instrumental records of small- to moderate-sized earthquakes in the southern Great Basin were compiled for the first time by the Californian Institute of Technology; prior to that, catalog entries were primarily based on felt reports.

From 1910 through 1939, all entries in the 100 km catalog are $M > 3$, and all but one of these events is located west of Yucca Mountain. These earthquakes generally are associated with the northwest-trending Death Valley-Furnace Creek (DVFC) fault zone. From 1940 through 1949, with the increase in instrumental recording and a corresponding decrease in the magnitude detection threshold, earthquakes were located throughout the 100-km region. During this time period, the region adjacent and within DVFC fault zone is the dominant source of seismic energy release. The largest event between 1940 and 1949 was an $M 4.8$ in 1944.

King *et al.* (1971) provide maps and some discussion of notable earthquakes within 100 km of the central Nevada Test Site (NTS) from 1950 through 1971. Many of the earthquakes reported by King *et al.* (1971) are not assigned magnitudes and are considered to be smaller than $M 3$. Several $M 4$ events are reported for the NTS, including several felt events, during

this 20-year period. The most significant earthquake during this time period was the August 5, 1971, M 4.5 Massachusetts Mountain event. Portable instruments were deployed in the epicentral area of the Massachusetts Mountain sequence: 612 aftershocks were counted in the 72 hours following the earthquake (King *et al.*, 1971). They note that the 1971 Massachusetts Mountain event took place near the location of an M 4.3 earthquake in 1957, although the locations of the two earthquakes are clearly separated in their published maps. From 1971 through the late-1970s, earthquakes were reported in monthly reports for the Atomic Energy Commission by the Earth Sciences Laboratories, a division of NOAA (Las Vegas, Nevada). The other significant earthquake sequence in the 1970s was the February, 1973, Ranger Mountains swarm. This sequence was unusual in that it produced eight earthquakes greater than M 3.5 during a three-week period, including two events greater than M 4. Also, the seismicity was distributed over a 10 x 10 km area (Earth Sciences Laboratories, 1973).

In the region south and east of the Massachusetts Mountain earthquake and within the 100-km region, approximately 75 percent of an estimated total moment release of 4.1×10^{23} dyne-cm (estimated from the historical catalog) is represented by the Massachusetts Mountain and Ranger Mountain sequences. Only 5 percent of the total moment release is from the pre-1971 period. Another 12 percent is accounted for in a cluster in January 1993. In the 10-year period 1980 through 1990, the moment release rate for this region was about 2×10^{21} dyne-cm/yr. The 1993 cluster occurred during a general increase in seismicity in the Rock Valley fault zone following the Little Skull Mountain earthquake, although this small sequence was east of the Rock Valley system.

In 1978, the USGS installed a regional analog telemetered seismic network and began reporting on the seismicity in the southern Great Basin for Yucca Mountain Site Characterization. These reports covered the years 1978 through 1991 (Rogers *et al.*, 1981, 1983; Harmsen and Rogers, 1987; Harmsen, 1991, 1993a). Seismicity reports from 1992 to the present have been generated by the University of Nevada Reno Seismological Laboratory (von Seggern and dePolo, 1995; von Seggern *et al.*, 1996, von Seggern and Smith, 1997). A report by Rogers *et al.* (1987a) on the relationship of the seismicity to the regional tectonic framework summarized the initial years of comprehensive seismic monitoring with the regional network. That study included detailed discussions of the seismicity and focal

mechanisms of specific source regions, descriptions of the development of the various magnitude scales in use, an analysis of the regional stress field, and proposed models of regional deformation. Conclusions regarding the seismicity and tectonic framework of the Yucca Mountain region from the Rogers *et al.* (1987a) are summarized as follows (Priestley, written communication, 1991).

- Seismic activity in the southern Great Basin is generally expressed in clusters of earthquakes distributed in an east-west belt between latitude 36 and 38 degrees north, referred to here as the southern Nevada seismic zone (Figure 7-1). The earthquake clusters are diffusely distributed around mapped faults, covering areas larger than the surface projections of the rupture (Figure. 7-2). Most events are not readily associated with the surface traces of known faults. These clusters may align with local structural grain; composite and single-event focal mechanisms suggest that nodal planes correlate with regional stress directions.
- Earthquakes tend to distribute in vertical tubular-shaped clusters rather than along planar fault zones. Rogers *et al.* (1987a) interpret this geometry to represent activity at the intersections of faults. These vertically distributed, localized clusters of seismicity stretch to 10 to 15 km deep. Most seismicity is within the upper 15 km of the crust, but some earthquakes may occur below 15 km. The depth distribution of seismicity is bimodal, with maxima at 1.5 and 9 km, and a minimum of activity at 4 km.
- Focal mechanisms and hypocenter alignments indicate that right-lateral slip on northerly trending faults is the predominant mode of stress release near the site (Figures 7-3, 7-4, and 7-5). Subordinate faulting on east-northeast (left-lateral) and northeast (normal) faults has been observed, as has oblique slip on structures of intermediate orientation with the appropriate dip angles. The inferred principal stress orientations are NW for the extensional (minimum compression) axis, and angles between NE and vertical for the maximum compressional axis (Harmsen and Rogers, 1986). The style of faulting determined from the focal mechanisms is not a function of depth.
- The comparison of energy release maps for the pre-1978 and post-1978 periods show that, averaged over decades, the seismically active zones appear to be releasing moment at about the same rates. Rogers *et al.* (1991) show that the historical rate of occurrence of the largest earthquakes (M 7) in the central Nevada seismic belt west and northwest of Yucca Mountain is larger by an order of magnitude than would be expected from geologic evidence. Wallace (1987) notes evidence that the occurrence of active periods lasting hundreds to thousands of years is followed by quiescent periods of 10,000 to 30,000 years. On a larger

distance but shorter time scale, Bufe and Topozada (1981) describe a period of relative quiescence encompassing both California and western Nevada from 1960 to 1980. The current active period for M 6 encompasses the same large region, as characterized by Bufe and Topozada (1981).

- Yucca Mountain lies within a region of relatively low historic seismic energy release.
- Focal mechanisms indicate that the maximum (P-axis) and minimum (T-axis) compressive stresses are roughly horizontal, although there is more variation in the P-axis, implying a preponderance of strike-slip faulting mechanisms. The T-axis has a consistent orientation throughout the region.
- Regional stress orientations indicate north-south and east-west orientations for high angle fault planes, with dextral slip on the north striking and sinistral slip on the east-west-striking surfaces. Normal and oblique slip are preferred on fault surfaces with orientation intermediate to these directions.

Gross and Jaume (1995) compiled a historical catalog of the southern Great Basin and discussed intensity based magnitude scales (Modified Mercalli) and levels of shaking experienced at Yucca Mountain in the historical period. After compiling a list of events within 200 km of Yucca Mountain, they concluded that the strongest shaking experienced at Yucca Mountain in historic time has been during the 1992 Little Skull Mountain earthquake. They also determined a revised location for the M 6.1, 1916 earthquake, the largest event within the 100km region, by comparing waveforms recorded during the Little Skull Mountain earthquake with a heliocorder record of the 1916 event from the Reno Seismograph Station. The revised location suggests that the event may have taken place in the Death Valley fault zone. Von Seggern and Brune (1997) relocated two M 3.5 earthquakes from 1948 that previously were reported as being located at Yucca Mountain. The initial locations of these two events were constrained by first-motion data at California seismic stations. The waveforms and S minus P times at the regional stations operating in 1948 were more consistent with a source near the Rock Valley fault zone rather than one at Yucca Mountain. By comparing waveforms from Little Skull Mountain aftershocks and heliocorder records from the Caltech station for one more well-located 1948 Rock Valley area event, they concluded that the two 1948 events most likely occurred in the Rock Valley area and not at Yucca Mountain. Von Seggern and Brune (1997) concluded that events were most likely part of one localized earthquake sequence in the Rock Valley area. Nevertheless, the quality

of locations for earthquakes in the Yucca Mountain area in the 1940s would be expected to be poor at best because of the lack of station coverage.

A report by Rogers *et al.* (1987b) initiated some controversy by concluding that the attenuation in the southern Great Basin was lower than that in California. Therefore, earthquake magnitudes would be lower for an equivalent amplitude recorded at the same distance in the California region. This meant that the Ao curve of Richter (1958) was not appropriate for Nevada. These conclusions have a direct effect on recurrence estimates, moment-magnitude scales, and estimates of moment release rate for the southern Great Basin. In contrast, Chavez and Priestly (1985) and Savage and Anderson (1995) concluded that the Richter curve was in fact applicable to Nevada. In support of these results, von Seggern and Smith (1997), from an analysis of three-component digital seismograms, have shown that the Richter curve is generally appropriate for the southern Great Basin, in contrast to the Rogers *et al.* (1987b) study. They note that the Hanks and Kanamori (1979) moment magnitude relationship is acceptable for the Basin and Range province, and that at small magnitudes, moment-magnitude relations determined from the modern three-component digital records are not consistent with the Rogers *et al.* (1987b) results. Chavez and Priestly (1985) also determined a moment-magnitude relationship that was different from the Hanks and Kanamori (1979) relation, at intermediate magnitudes, for the western Great Basin.

Other published reports on the seismotectonics of the southern Great Basin have applied the historical seismicity data set to constrain models of regional deformation. Gombert (1991b) developed regional strain models that incorporated slip rates on active faults and comparisons with regional seismicity, then tested these models using a boundary element method. They concluded that the seismicity is associated with the local strain field near more active faults and that Yucca Mountain was geometrically situated such that strain accumulation in the Yucca Mountain block was minimal. Also, they interpreted the general lack of seismicity at Yucca Mountain as reflecting the presence of an isolated block or zone of low strain accumulation. In another study, Harmsen and Rogers (1986) analyzed the stress field from a set of regional focal mechanisms. The presence of both strike-slip and dip-slip mechanisms in particular localities was explained as most likely resulting from an axially symmetric stress field, in which the intermediate and maximum compressive stresses are nearly equal (Harmsen and Rogers, 1986). They suggested that because no large earthquakes were present

in the data set, that movement along a variety of fault plane orientations was accommodated by an ample number of small, preferably oriented faults.

Rogers *et al.* (1991) proposed a model in which right-lateral strike-slip faulting on north-striking planes is indicative of north-south crustal shortening. Anderson *et al.* (1993) suggest a crustal shortening mechanism for deformation in the Lake Mead area, consistent with the model proposed by Rogers *et al.* (1991). Interpreting models of regional deformation from the focal mechanism database is problematic because of the limited number of small earthquakes that account for only a small portion of moment release; the record of historical seismicity does not span the complete seismic cycle of faults in the region, which can be on the order of 10s to 100s of thousands of years in most cases.

REFERENCES

See reference list that follows main SBK text.

APPENDIX SBK-2 SUMMARY OF SEISMICITY

This appendix presents a discussion of the seismicity in the Nevada Test Site (NTS) region. The discussion focuses on specific issues regarding the behavior of earthquake sequences, earthquake clusters, and focal mechanisms and issues related to observations of earthquake triggering. The observations of the behavior of earthquake activity contributed to the weightings we assigned to background source zones, thickness of the seismogenic crust, relationship between seismicity and mapped Quaternary faults, and the problem of discriminating between true tectonic earthquakes and earthquakes triggered or potentially triggered by underground nuclear testing. This appendix includes some of the team's interpretations of the distribution of historical seismicity.

Northern Nevada Test Site

The northern region of the NTS includes the Timber Mountain caldera, Pahute Mesa, Rainier Mesa, and Yucca Flat. These areas have been the focus of considerable seismic activity, either directly or indirectly associated with nuclear testing. In contrast, most of the seismicity that extends across the south part of the NTS, within and adjacent to the Rock Valley, Mine Mountain, and Cane Springs fault zones (including the 1992 M 5.6 Little Skull Mountain earthquake), and activity around the southern boundary of the Timber Mountain caldera is, we believe, most likely tectonic in origin. We draw this conclusion primarily because this area is somewhat distant from the testing areas.

Determining what earthquake activity is related to underground nuclear explosions (UNEs), either through cavity collapse or the stresses induced by the explosions, is problematic. A study to determine the relative number of artificial and induced seismic events in the testing area suggests that the natural seismicity of the region reflects the background activity generally found in the southern Basin and Range province (Vortman, 1991). In 1979 and 1983, several swarms of micro-seismicity apparently unrelated to the UNEs occurred in the region. Two sequences that occurred during the period of active testing took place in the vicinity of Dome Mountain and Thirsty Canyon (Rogers *et al.*, 1981, 1987a). Focal mechanisms indicate primarily right-lateral strike-slip faulting on north-trending structures and normal faulting on northeast-trending structures (Rogers *et al.*, 1987a).

Southern Nevada Test Site

The south part of the NTS is a seismically active region relative to some other areas in the southern Great Basin. Most of the seismicity that stretches across the south part of the NTS, within and adjacent to the Rock Valley, Mine Mountain, and Cane Springs fault zones (including the 1992 M 5.6 Little Skull Mountain earthquake), and activity around the southern boundary of the Timber Mountain caldera, is not in areas of underground nuclear testing. Some of the activity near the eastern NTS boundary, particularly the 1971 Massachusetts Mountain earthquake and 1973 Ranger Mountain swarms, may have been triggered following the initiation of testing in the Yucca Flat area; however, there seem to be considerable numbers of small earthquakes related to natural tectonic strain release (Gomberg, 1991a, b). The largest event in this region is the 1992 ML 5.6 Little Skull Mountain earthquake, which most likely was triggered by a larger regional earthquake (Anderson *et al.*, 1993a, b).

Focal mechanisms from Rogers *et al.* (1987a) indicate sinistral slip on northeast structures and (or) dextral slip on northerly striking structures in the southern Great Basin. A prominent concentration of seismicity that includes the 1992 Little Skull Mountain earthquake occurs within a wide northeast-trending zone centered on the Rock Valley fault zone. This area includes the 1970 M 4.5 Massachusetts Mountain earthquake, the 1973 Range Mountains sequence, the 1992 M 5.6 Little Skull Mountain earthquake (Harmsen, 1993; Meremonte *et al.*, 1995; Smith *et al.*, 1997), the 1993 Rock Valley sequence (Shields *et al.*, 1995), and other relatively minor earthquake clusters and alignments. Also, spatial patterns in the seismicity within this wider Rock Valley zone extend both north along the Mine Mountain system (Rogers *et al.*, 1987) and south subparallel to the South Specter Range fault.

A general lack of seismicity characterizes the vicinity of Yucca Mountain. An analysis of the earthquake detection threshold for the Southern Great Basin Seismic Network (SGBSN) suggests that this zone of quiescence is real (Gomberg, 1991b). An experiment in high-resolution monitoring of seismicity at the potential site by Brune *et al.* (1992) confirms the existence of the quiescent zone. Modeling of the strain field in southern Nevada by Gomberg (1991a) suggests that this area is not accumulating significant strain, and that

Yucca Mountain is an isolated block within the structural framework of the southern Great Basin.

Northern Amargosa Valley-Sarcobatus Flat

The northern Amargosa Valley-Sarcobatus Flat encompasses the areas west and northwest of the Bare Mountain fault, 25 to 90 km from the site. Seismicity in the northern Amargosa Valley is diffusely distributed in the vicinity of Beatty, Nevada, and the Bullfrog Hills mining district. In Sarcobatus Flat, earthquakes have occurred in four clusters since the advent of instrumental monitoring (Rogers *et al.*, 1983, 1987a). These clusters are spaced roughly 10 to 20 km apart in a northerly trend along the length of the valley. Focal mechanisms for the three southern clusters suggest dextral slip along north- to north-northeast-trending structures.

Northern Death Valley Region

Seismicity along the Furnace Creek fault zone in northern Death Valley is diffusely distributed over an area much larger than the mapped surface traces of the primary fault system. A concentration of activity extends northeast from northern Death Valley at the north end of the Furnace Creek fault through the Gold Mountain-Mount Dunfee region. The largest event in this area in the modern era was an ML 4 event at Gold Mountain. A cluster of events occurred in a northeast alignment near Mount Dunfee in 1983. A composite focal mechanism from several of these earthquakes suggests left-oblique normal faulting on a northeast-striking fault plane (Rogers *et al.*, 1987a). The seismicity appears to be occurring at a low rate for such a high-slip system of faults, suggesting that the moment release in the region is concentrated on the main structures.

Explosions and Seismicity Triggered by Non-Tectonic Events

Seismicity analyses attempt to distinguish between underground nuclear explosions (UNEs), their collapses and aftershocks, chemical explosions associated with testing and mining, seismicity associated with the filling and subsequent changes in level of Lake Mead, and the natural seismicity in the region. The historical catalog of southern Great Basin earthquakes for the period 1868 to 1978, compiled by Meremonte and Rogers (1987a), labels seismic events that are attributed to UNEs. The triggering of earthquakes by UNEs presents a difficulty in interpreting the distribution of seismicity within the context of a seismotectonic framework for the NTS area.